RIL 2022-03
INL/EXT 17 40928, Rev. 1

U.S.NRC
United States Nuclear Regulatory Commission
Protecting People and the Environment

A SIMULATION-BASED DYNAMIC ANALYSIS APPROACH FOR MODELING PLANT RESPONSE TO FLOODING EVENTS

Date Published: February 2022

Prepared by:
Z. Ma
C. L. Smith
S. R. Prescott

Idaho National Laboratory
Battelle Energy Alliance
Idaho Falls, Idaho 83415

Joseph Kanney, NRC Project Manager

Research Information Letter
Office of Nuclear Regulatory Research

This report was prepared as Idaho National Laboratory Report INL/EXT 17 40928, Rev.1 to document research funded the U.S. Nuclear Regulatory Commission's Office of Regulatory Research under NRC Agreement Number NRC-HQ-60-14-D-0029. The report has been re-published as an NRC Research Information Letter (RIL).

Disclaimer

ABSTRACT

This report presents an exploratory research to develop possible approaches to investigate plant response to flooding events. Dynamic analysis approaches that depict scenarios through simulation methods were investigated in the project. A framework to perform a simulation-based dynamic flooding analysis (SBDFA) was developed. Four main tasks, flood hazard analysis, flood fragility analysis, plant response modeling, and three-dimensional (3-D) simulations and plant response model quantification, under the SBDFA framework were discussed. As a proof-of-concept demonstration, this project focuses on the plant response modeling with the 3-D simulation-based dynamic analysis approach for external flooding events. A previous local intense precipitation (LIP) event that occurred in a pressurized water reactor (PWR) plant was reviewed and used as the case study in this project. General plant responses to an external flood are discussed for both external plant response and internal plant response stages. An external flooding event tree was developed to assess the flood damages states due to the external flood event for the external plant response stage, while an internal event, at-power probabilistic risk assessment (PRA) model was used as the base to model the internal plant response stage. Event-modeled risk assessment using linked diagrams (EMRALD), a state-based PRA modeling tool, was utilized to incorporate time-related interactions from both 3-D physical simulations and stochastic failures into traditional PRA logic models. An example state-based PRA model was developed by converting a simplified traditional transient event tree and the associated fault trees and basic events. 3-D simulation models were developed using the 3-D simulation software Neutrino to simulate the flooding scenarios and communicate with the PRA model. The results from the 3-D simulation models and the state-based PRA model were compared with the traditional PRA model using Systems Analysis Programs for Hands on Integrated Reliability Evaluations (SAPHIRE). Insights and lessons learned from the project are documented for future research and applications.

CONTENTS

FIGURES

TABLES

ACKNOWLEDGMENTS

The authors wish to thank Dr. Joseph Kanney of the U.S. Nuclear Regulatory Commission (NRC) for his management support and technical inputs. We acknowledge Nathan Siu, Fernando Ferrante, Suzanne Dennis, Mehdi Reisi Fard, Kevin Coyne and other staff of the NRC for their detailed review and insightful comments during the development of this document. We acknowledge the contributions of Ramprasad Sampath of Centroid PIC to the development of 3-D simulation models for this project. Steven Prescott of Idaho National Laboratory (INL) was a key contributor to this project by providing the EMRALD support and 3-D simulation support. The support from other INL personnel, David Sharp for the development of 3-D plant models and Heather Rohrbaugh for the editorial review, are greatly appreciated.

ACRONYMS

AB	auxiliary building
AEP	annual exceedance probability
AFW	auxiliary feedwater
AMS	annual maximum series
ARI	annual return interval
CCF	common cause failure
CCCG	common cause component group
CCS	containment cooling system
CCW	component cooling water
CDF	core damage frequency
CSR	containment spray recirculation
CST	condensate storage take
DB	diesel generator building
EMRALD	event-modeled risk assessment using linked diagrams
EPR	external plant response
EPRI	Electric Power Research Institute
ET	event tree
FB	fuel building
FDS	flood damage state
FW	feedwater
FT	fault tree
GEV	generalized extreme value
HPI	high pressure injection
HPR	high pressure recirculation
IE	initiating event
INL	Idaho National Laboratory
IPR	internal plant response
LERF	large early release frequency
LIP	local intense precipitation
LOSP	Loss of Offsite Power
LPI	low pressure injection
LSHR	long term secondary heat removal
MFW	main feedwater

NOAA	National Oceanic and Atmospheric Administration
NRC	Nuclear Regulatory Commission
OTC	once through cooling
PDS	partial duration series
PFHA	probabilistic flood hazard assessment
PORV	power-operated relief valve
PRA	probabilistic risk assessment
PWR	pressurized water reactor
RCS	reactor coolant system
RPS	reactor protection system
RWST	refueling water storage tank
RB	reactor building
RISMC	risk-informed safety margin characterization
SAPHIRE	Systems Analysis Programs for Hands on Integrated Reliability Evaluations
SBDFA	simulation-based dynamic flooding analysis
SDC	shutdown cooling
SPAR	standardized plant analysis risk
SSC	structures, systems, and components
TB	turbine building
U.S.	United States

1. INTRODUCTION

1.1 Background and Objectives

All nuclear power plants must consider external flooding risks, such as local intense precipitation (LIP), riverine flooding, flooding due to upstream dam failure, and coastal flooding due to storm surge or tsunami. These events have the potential to challenge offsite power, threaten plant systems and components, challenge the integrity of plant structures, and limit plant access. Recent lessons learned from Fort Calhoun (2011), Vermont Yankee (2013), and St. Lucie (2014) flooding events [1], as well as the Fukushima seismic/tsunami-initiated nuclear accident (2011) [2], show that applicants and licensees must evaluate the potential impact of these events to fully ensure plant safety and to meet the regulatory requirements. The regulatory basis governing flood hazards assessment is provided in the appropriate sections of 10 CFR Part 50, Part 52 and Part 100 [3-5]. The regulatory criterion for protection of structures, systems, and components (SSCs) important to safety against natural phenomena is provided in 10 CFR Part 50 Appendix A, General Design Criterion (GDC) 2:

> *"Structures, systems, and components important to safety shall be designed to withstand the effects of natural phenomena such as earthquakes, tornadoes, hurricanes, floods, tsunami, and seiches without loss of capability to perform their safety functions. The design bases for these structures, systems, and components shall reflect: (1) Appropriate consideration of the most severe of the natural phenomena that have been historically reported for the site and surrounding area, with sufficient margin for the limited accuracy, quantity, and period of time in which the historical data have been accumulated, (2) appropriate combinations of the effects of normal and accident conditions with the effects of the natural phenomena and (3) the importance of the safety functions to be performed."*

Historically, meeting the above requirements involved deterministically derived theoretical extreme flooding scenarios with conservative assumptions (e.g., probable maximum precipitation, flood, hurricane, windstorm, and storm surge). A direct link between the likelihood and magnitude of such events is not usually available and it does not include a wider sense of the hazard with respect to the various flooding elevations and risk contribution for scenarios that may be more frequent/less intense, as well as those that may exceed the deterministically derived limits. Probabilistic treatment of flood hazard phenomena would provide quantitative estimates of such events, as well as a wider spectrum of potential likelihood with varying flooding event intensity (in terms of probability or frequency of exceedance) and thus contribute to a better treatment of the risk-informed assessment of flooding hazards. Further, improvements in modeling of flood hazard likelihood and intensity will serve to also improve scenario-based risk analysis since these are a key part of scenario representation.

This research project is part of the Nuclear Regulatory Commission (NRC) Probabilistic Flood Hazard Assessment (PFHA) Research plan in support of development of a risk-informed analytical approach for flood hazards for both new and operating facilities as well as design standards at new facilities [6, 7]. The PFHA plan aims to build upon recent advances in deterministic, probabilistic, and statistical modeling of extreme precipitation events to develop regulatory tools and guidance for NRC staff regarding PFHA for nuclear facilities. The tools and guidance developed will support and enhance NRC's capacity to perform thorough and efficient reviews of license applications and license amendment requests. They will also support risk-informed reactor oversight activities such as evaluating the risk-significance of inspection findings.

In general, the key elements in the analysis of risk from any external event are:

- Hazard analysis
- Plant SSC response, fragility, and vulnerability analysis
- Plant response and accident sequence analysis (including manual actions)
- Consequence analysis

A hazard analysis estimates the frequency of occurrence of different intensities of an external event. Typically, the output of a hazard analysis is a hazard curve giving exceedance frequency versus hazard intensity. Since there is normally uncertainty in the parameter values and in the mathematical model of the hazard, the effects of uncertainty are often represented through a family of hazard curves with a probability distribution assigned to the family of curves, representing the relative likelihood of one hazard curve relative to the others.

The analysis of plant SSC response translates the hazard input into responses of structures, piping systems, and equipment. The fragility or vulnerability of a structure or equipment is the conditional frequency of failure given a value of the response parameter. In some external event analyses, the response and fragility evaluation are combined, and the fragility is expressed in terms of a global parameter of the hazard (e.g., tornado wind speed).

The analysis of plant response and accident sequences traditionally consists of developing event trees and fault tress in which the initiating event can be the external hazard itself or a transient or loss-of-coolant accident (LOCA) initiating event induced by the external event. Various failure sequences that lead to core damage, containment failure, and a specific release category are identified and their conditional frequencies of occurrence are calculated. The unconditional frequency of core damage or of radionuclide release for a given release category is obtained by integrating over the entire range of hazard intensities.

The steps outlined above have to date been implemented almost exclusively by frequency analysis combined with system event and fault trees in a model. While this approach has demonstrated for some external events (e.g., seismic events and loss of offsite power), flooding events present some unique and challenging aspects:

- The performance of flood protection features may be a function of flooding levels and associated effects (e.g., hydrostatic and hydrodynamic forces, floating debris impact)
- The degree of flooding may influence the rate of random or common cause failures (CCFs)
- The planned response to flooding events at many nuclear power plants (NPP) relies heavily on procedures and manual actions (both for flood protection and mitigation).
- The feasibility and reliability of manual actions can be impacted by the flooding (e.g., water levels) and associated effects (e.g., wind, lightning)
- The duration of the flooding event (i.e., from the time that a flood warning is received, or a flood procedure is entered to the time that flood waters recede from the site) can be quite long and onsite conditions may change throughout the event.
- Forecasting for certain types of flooding events (e.g., local intense precipitation) may not be highly reliable for the extreme events that may challenge flood protection features and procedures.

In summary, the details of the flooding event become very important to representing component or system behavior and reliability of procedures and manual actions, which is difficult to capture in static models such as event trees and fault trees. Dynamic analysis approaches that depict scenarios through simulation methods offer an alternative for representing flooding processes and highly time-dependent nature of flooding response. In general, simulation-based dynamic methods become useful compared to static methods when one or more of the following attributes of system complexity are present in a problem:

- Temporal – the system configuration/state is time dependent
- Spatial – the spatial information is important to the problem and the system model cannot be simply treated as a 0-dimensional entity
- Mechanics – multi-physics phenomena exist in the problem
- Topology – multi-state systems/components (different levels of performance versus the success/failure binary states) and network systems (causal links among the system constituents)

While the details of scenarios are important for both static and dynamic modeling methods, dynamic methods are useful when complexities such as time, space, and physical phenomena behavior start to drive the scenarios. Capturing these kinds of "dynamics" via static basic events, fault trees, or event trees becomes challenging. A simulation-based dynamic modeling approach provides a more natural framework to represent, understand, and visualize the problems and scenarios related to flooding.

The objective of this project is to investigate dynamic analysis approaches to model plant response to flooding events. The focus of this project is the plant response to a LIP event, but the results could inform anticipated follow-on work for other flooding scenarios such as river or dam failure events. Both margins analysis and probabilistic risk assessment (PRA) approaches are considered in the project. The results and lessons learned from this project could be utilized in the future development of regulatory guidance on assessing plant response to flooding events.

1.2 Scope

The purpose of this project is to investigate simulation-based dynamic analysis approaches that model plant response to flooding events. As a proof-of-concept demonstration, this project focuses on the plant response modeling with a three-dimensional (3-D) simulations-based dynamic analysis approach for flooding events. The flood hazard analysis and flood fragility analysis are briefly discussed as part of the framework but are not analyzed in detail for this project.

1.3 Outline

Section 2 of this report provides an overview of the general framework of the SBDFA approach. Section 3 discusses the flood hazard analysis. Section 4 presents an overview of the flood fragility analysis. Section 5 introduces the general plant response modeling process to flooding events. EMRALD (Event-Modeled Risk Assessment using Linked Diagrams), a state-based PRA modeling tool that could incorporate time-related interactions from both 3-D time-dependent physical simulations and stochastic failures into traditional PRA logic models, is introduced in this section. Section 6 applies the SBDFA approach to an LIP event as a case study by developing 3-D simulation models and EMRALD dynamic models. The EMRALD dynamic models are quantified and compared with the traditional PRA model using Systems Analysis Programs for Hands on Integrated Reliability Evaluations (SAPHIRE) [8]. Section 7 provides the insights obtained from the project. Section 8 provides a summary of the report.

2. FRAMEWORK OF SIMULATION-BASED DYNAMIC FLOODING ANALYSIS

2.1 Overview

In support of this project, Idaho National Laboratory (INL) investigated approaches to model plant response to external flooding events. Simulation-based dynamic analysis approaches were specifically explored and used in the project to represent probabilistic flooding hazards and highly time-dependent flooding response. From a bigger picture, external flood risk assessment (either with the traditional static approach or the dynamic approach studied in this project) constitutes an important input to risk-informed decision makers along with other traditional engineering analyses for external flood-related issues. After the problem defining stage, a LIP event (or other types of external flood event, which could be either single type flood event or a combining flood event such as storm surge and river flooding) can be assessed for its risk significance by performing either the static event tree/fault tree analysis or the simulation-based dynamic flooding analysis (Section 2.2). When the risk assessment is verified and validated (Section 2.3), the analysis results can be used along with other traditional analyses and principals to provide valuable risk insights to the decision makers (Section 2.4). This general process is illustrated in Figure 2-1.

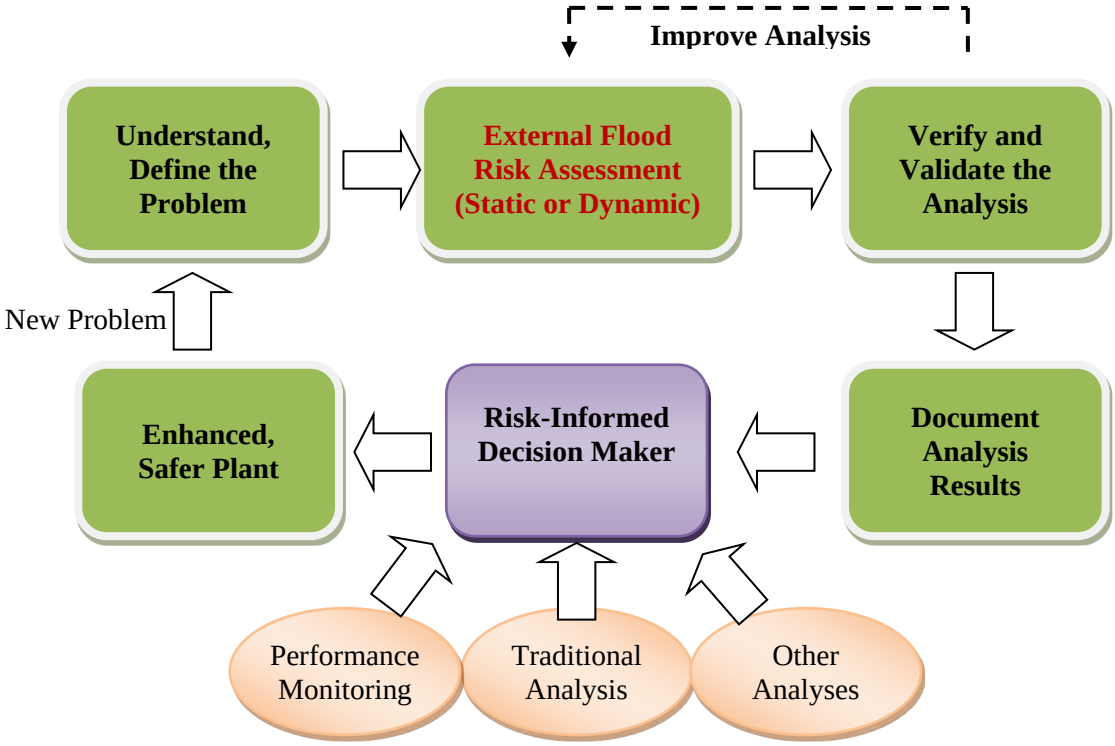

Figure 2-1. External flood risk assessment in risk-informed decision-making process.

Part 8 of the ASME/ANS PRA Standard, RA-Sb-2013 [9], establishes technical requirements for the Level 1 and large early release frequency analysis of the external flood hazard group while at-power. Three technical elements are defined in the standard for an external flood PRA: External Flood Hazard Analysis (XFHA), External Flood Fragility Evaluation (XFFR), and External Flood Plant Response Model and Quantification (XFPR). While the requirements in the standard are more relevant to a traditional PRA instead of the simulation-based dynamic approaches that are investigated in this project,

the requirements were reviewed and applied to this analysis as proper. Also, the PRA Standard addresses an at-power PRA while plants are often not at power throughout an external flood event. Special considerations should be given on low power and shutdown modes other than at-power mode.

2.2 Simulation-based Dynamic Flooding Analysis

Figure 2-2 presents the general framework to perform a simulation-based dynamic flooding analysis. There are four main tasks under this framework to perform a simulation-based dynamic flooding analysis: (1) external flood hazard analysis, (2) external flood fragility analysis, (3) external flood plant response modeling, and (4) 3-D simulations for safety margin analysis or PRA quantification. These tasks would be similar to those required to perform a traditional PRA analysis except that 3-D simulations and dynamic approach are introduced in this project. For each task, several subtasks must be performed to accomplish the task. As a proof-of-concept demonstration, this project focuses on the plant response modeling and 3-D simulations for PRA analyses. The flood hazard analysis and flood fragility analysis are included but are not analyzed in detail for this project.

Task 1 – Perform External Flood Hazard Analysis

This task evaluates the frequency of occurrence of external floods as a function of magnitude based on site-specific, up-to-date information. The output of this task is a hazard curve (or a family of hazard curves) giving occurrence frequency versus hazard intensity (or magnitude). The frequency of external flooding at the site should be based on a site-specific analysis that reflects recent available site-specific information. Uncertainties in the parameter values and in the mathematical model of the hazard should be properly accounted for and propagated to obtain a family of hazard curves including a mean hazard curve. A probability distribution is assigned to the family of curves to represent the relative likelihood of one hazard curve relative to the others. This task includes the following sub-tasks:

Task 1.1 Identify all relevant flood-causing mechanisms (including combinations of mechanisms) and associated effect for the plant studied. Identify mechanisms associated with coexistent hazards (e.g., high wind concurrent with storm surge, or seismic induced dam failure). Perform screening process as appropriate.

Task 1.2 Collect and characterize site-specific (and regional) flood hazard data. Use appropriate measures such as flood elevation, flood event duration, and associated effects (e.g., hydrostatic and hydrodynamic forces, wind waves, wave runup) for the characterization.

Task 1.3 Develop hazard curves with uncertainties characterized and propagated for each not screened out flood mechanism or group of mechanisms.

While traditional flood analysis usually uses point estimate or grouped bins as the external flood initiating event frequency, the simulation-based dynamic approach uses sampling and simulations to assess the full spectrum of the flood hazard curves and other hydrological and hydraulic characteristics (e.g., precipitation rate and flow rate).

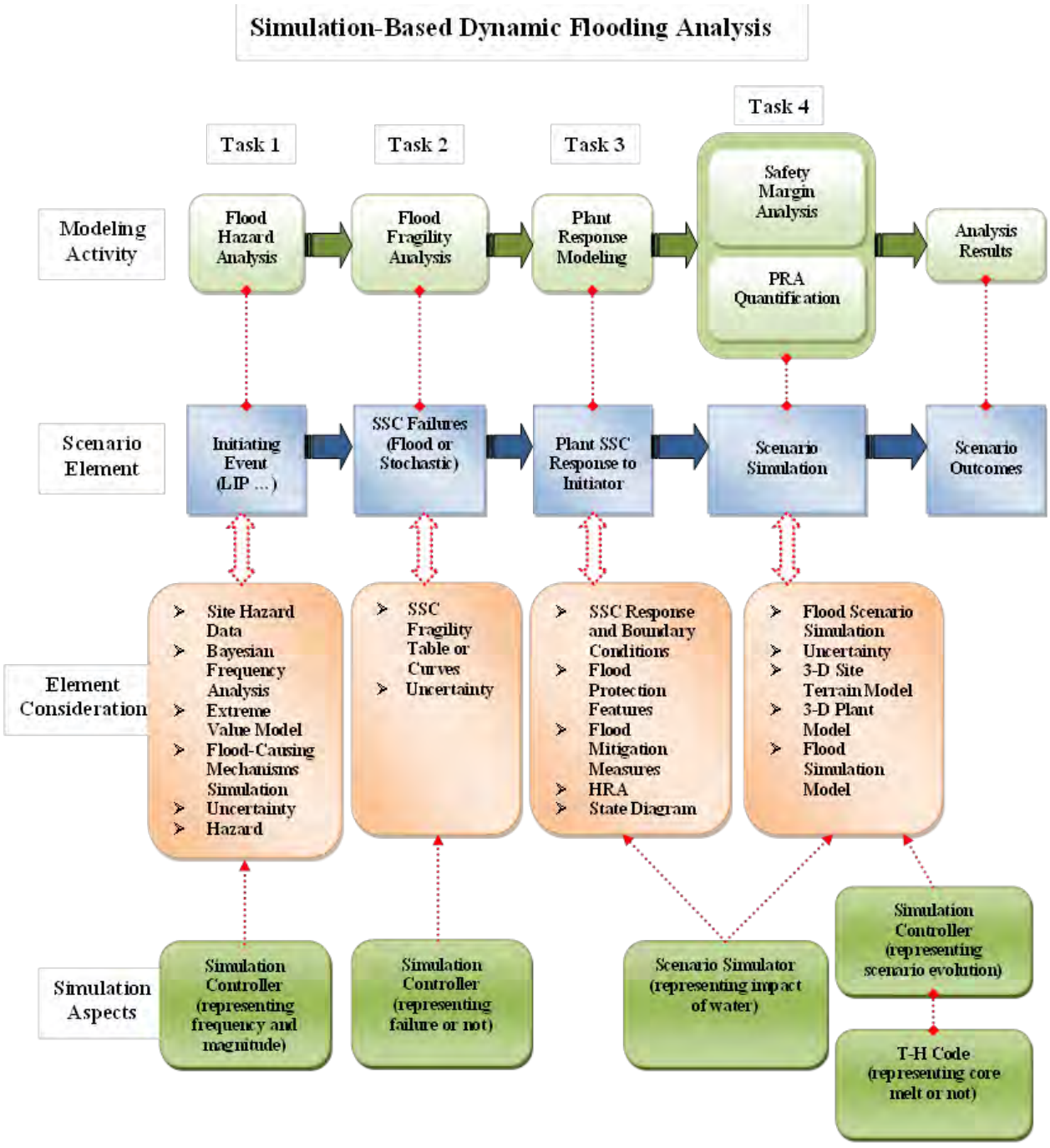

Figure 2-2. Simulation-based dynamic flooding analysis (SBDFA) framework.

Task 2 – Perform External Flood Fragility Analysis

This task evaluates the fragility of plant SSCs as a function of the magnitude of the external flood using proper engineering method for the postulated failure. The SSCs that are susceptible to the effects of external floods and whose failure contributes to core damage or large early release are identified. Their failure probabilities as a function of the magnitude of the external flood are estimated. The output of this task is a table or tables of SSCs that are included (or excluded for) in the plant response model, as well as their failure probabilities as a function of the magnitude of the external floods (e.g., fragility tables, failure models based upon flooding characteristics, or probabilistic curves). The structures and equipment considered in the evaluation includes equipment located at low elevations, intake, and ultimate-heat-sink equipment. The flood-caused failure mechanism may be immersion of equipment or other flow-induced phenomena. This task includes the following sub-tasks:

Task 2.1 Identify plant SSCs (including flood protection features such as permanent and temporary flood barriers and equipment) that are susceptible to the effects of external floods. Use the internal events PRA model as the basis to develop an external flood SSC list. Add to the list those SSCs that are not modeled in the internal events PRA model but are required in the flood analysis. Perform screening evaluation as needed.

Task 2.2 Conduct plant walkdown to support the fragility evaluation, focusing on SSC condition (e.g., potential degradation) and configuration, potential physical interactions between SSCs, flood propagation pathways, and potential flood impacts to SSCs due to flood height, flood event duration, and flood associated effect.

Task 2.3 For each flood mechanism, identify relevant SSCs failure mechanisms (e.g., inundation and structural failure) and failure modes (e.g., fail-to-start and spurious operations), evaluate plant-specific SSCs flood susceptibilities, and develop SSCs fragilities for identified failure modes.

Unlike the concept of critical flood height used in traditional flooding analysis, the SSCs fragilities could be associated with various flood heights and various inundation rates in simulation-based dynamic flood analysis so that different SSCs failure probabilities could be defined for different inundation levels and different flood flow rates.

Task 3 – Develop External Flood Plant Response Model

This task develops a plant response model that addresses the initiating events and failures caused by the effects of external flooding that can lead to core damage or large early release. The model reflects external flood-caused failures as well as non-flood caused unavailabilities and human actions that give rise to significant accident sequences or significant accident progression sequences. The plant response model should capture the important dependencies among external flood-caused failures (e.g., spatial or environmental dependencies). Common-cause failure (CCF) analysis is particularly important for external-flood hazards. The model should properly consider the special impact from external floods on the feasibility and reliability of manual actions. This task includes the following sub-tasks:

Task 3.1 Identify potential flood hazard scenarios that could lead to a plant initiating event such as plant trip or loss of offsite power. Identify initiating events caused by external flood hazards or coexistent hazards.

Task 3.2 Identify those plant SSCs and their failure modes that are important to risk and would be affected by the flooding to be included in the response model. This task would be performed efficiently together with the identification process in Task 2.1.

Task 3.3 Identify flood propagation paths, flood protection features, and flood mitigation features by performing a walkdown and reviewing drawings and procedures. Assess the reliability of flood protection and mitigation for the identified flooding scenarios.

Task 3.4 Perform scenario-specific human reliability analysis to investigate the feasibility and reliability of operator actions that may be dependent upon the flood progressing.

Task 3.5 Develop external flood plant response model by integrating the external flood hazard, fragility, and plant response analyses. The model could use the at-power, internal event PRA model as the basis for system logic which should be revised properly to account for external flood-caused SSC failures, SSC unavailability and failures not caused by the external flood event, and human errors associated with the plant response. The plant response model should incorporate the plant-specific flood mitigation features, flood protection features, time-dependent operator actions, and CCFs in the model. The cliff edge effect should be considered and incorporated properly into the response model.

In this task, either traditional static modeling approach or dynamic approach could be used. However, the traditional event tree/fault tree approach in a static PRA model could be difficult to represent component or system behavior and reliability of manual actions during an ever-progressing flood event. In contrast, dynamic analysis approaches can be used to depict flood scenarios through simulation methods, which can better illustrate the SSCs performance and their responses along with the flooding event progresses. Probabilistic simulation of components and mechanistic analysis can be coupled together to represent the flooding event and determine which (if any) components fails, when they fail, what caused their failure, what impact these failures have on associated systems, and what impact system failures have on the overall plant. A state-based PRA modeling tool, EMRALD, was utilized in the project to incorporate time-related interactions from both stochastic failures and 3-D physical simulation results into traditional PRA system logic models.

Task 4 – Perform 3-D Simulations and Plant Response Model Quantification

This task develops a 3-D external flood simulation model, revises the state-based PRA model from Task 3, and performs 3-D simulations and plant response model quantification. In a traditional flood PRA analysis, this task is not needed, and the plant response model quantification part of this task can be combined into Task 3. This task includes the following sub-tasks:

Task 4.1 Develop a 3-D terrain model that represents the topography of the plant area.

Task 4.2 Develop or obtain an applicable 3-D plant model upon the terrain model for the simulation.

Task 4.3 Develop a 3-D external flood simulation model that integrates the previous developed 3-D terrain and plant models.

Task 4.4 Revise the state-based PRA model developed from Task 3 by incorporating 3-D simulation elements into the logic. Perform 3-D simulations and quantify the state-based PRA model. Uncertainty analyses should be performed to assess aleatory variability and epistemic uncertainty contained in all relevant analyses. For example, the uncertainty in modeling the possible occurrence of a flood event in space and time while accounting for site-specific factors, in selecting appropriate data, models, and methods to be used in the analyses, in modeling the SSC fragilities to a flood event, and in modeling the plant response model (propagation paths, flood scenarios, reliability estimation of flood protection and mitigation features and manual actions, etc.) for a flood event.

Under this task, a safety margin analysis other than a PRA quantification analysis can be performed. To perform a safety margin analysis, the factors and controls that determine safety margin are identified and characterized. SSCs robustness is assessed through quantified margins. The defense-in-depth capabilities are evaluated. While the 3-D simulation model and the state-based PRA model are used to simulate and measure plant responses for various hazard parameters inputs, mechanistic codes such as RAVEN/RELAP-7 [10-12] are coupled to the PRA model for the plant response function to evaluate the

impact of external flood hazards on the reactor core. This type of analysis could be a future research by coupling thermal hydraulic code such as RELAP-7 with the state-based PRA model.

2.3 External Flooding Analysis Validation

Validation of the flooding analysis and model should be performed to increase the confidence in their accuracy and creditability to be used in the risk-informed decision-making process. Several general approaches could be used for the validation of models and methods. One is to perform independent peer review of the analysis and use expert judgment to check the analysis assumptions, inputs, data, structure, and outputs: whether the model structural assumptions are proper, whether the assumed statistical distribution for the data is appropriate (by using goodness of fit tests and other techniques), whether the selection and use of the data in the analysis is proper, etc. Another approach is to compare the analysis results with the actual flood data, if they are available, or with traditional PRA model outputs. When conducting the validation through the comparison of the simulation model results with actual flood data, the same boundary conditions as seen in an actual event will be set up in the simulation model. The simulation model should then provide reasonable representation of the event (for example, the Fukushima tsunami event from 2011 could be simulated and the site "flooding footprint" compared between the simulated results and the actual flood recorded by the Japanese). This comparison is one part of an overall validation approach to the dynamic method. Other validation efforts should include those that validate the physical simulations, mechanistic analysis, and 3-D simulation code used in the flooding analysis.

2.4 Input to Risk-Informed Decision Making

It is expected that after developing and validating the external flooding analysis, the results from the model would provide important insights and inputs to the risk-informed decision maker. The dynamic analysis approaches depict flood scenarios through simulation methods and provide an alternative for representing highly time- and space-dependent external flood events and assessing the risk contributions from the events. The inclusion of the site-specific meteorological and geographical data in the 3-D flood scenario simulation, as well as the inclusion of the hydrological and hydraulic characteristics of the flood event in the dynamic model, will provide realistic evaluation of the time-dependent plant response model, reduce the uncertainties, and provide invaluable insights to the risk-informed decision making regarding external flood hazards. The results can be used to support risk-informed reactor oversight activities such as evaluating the risk-significance of operating events or inspection findings. Further, these simulation results provide a natural way to visualize different potential scenarios and outcomes since the analysis models themselves are 3D based.

3. EXTERNAL FLOOD HAZARD ANALYSIS

The external flood hazard analysis task evaluates the frequency of occurrence of external floods as a function of magnitude based on site-specific, up-to-date information. The output of this task is a hazard curve (or a family of hazard curves when considering uncertainty) giving occurrence frequency versus hazard intensity. The frequency of external flooding at the site should be based on a site-specific analysis that reflects recent site-specific information. Uncertainties in the parameter values and in the mathematical model of the hazard should be properly accounted for and propagated to obtain a family of hazard curves, including a mean hazard curve. A probability distribution is assigned to the family of curves to represent the relative likelihood of one hazard curve relative to the others.

The hazard analysis should identify all of the external flood mechanisms (including combinations of mechanisms) and associated effects that are applicable to the site. A non-inclusive list that is categorized under the external flood hazard analysis includes LIP, river and stream flooding, dam and levee failure, tsunami, hurricane, waves, storm surge, seiche, high tide, snow, and coastal erosion. For each flood mechanism, appropriate measures such as flood elevation, flood event duration, and parameters related to associated effects should be characterized. Multiple sets of flood scenario parameters (or one set of bounding flood scenario parameters) are developed for later plant response analysis.

While traditional flood analysis usually uses point estimate or group bins as the external flood initiating event frequency, the simulation-based dynamic approach uses sampling and simulations to assess the full spectrum of the flood hazard curves and other hydrological and hydraulic characteristics (e.g., precipitation rate and flow rate). It is noted that flooding hazards may display multiple "stair stepping" effects that can be captured more readily when using a full spectrum approach for the hazard (i.e., frequency versus magnitude) to represent the initiating event. For example, as the flood height increases, many different "cliff edge" effects may be realized as an increasing number of components are damaged from the flood waters. While binning of the initiating event is possible, binning may miss this non-linear behavior unless the binning resolution is reduced to the point of capturing the "stair step" impacts. This binning may limit the usefulness of the approach depending on the plant-specific impacts. Capturing these non-linear effects may be important to the realism of the modeling and to addressing uncertainties in the analysis. By simulating the initiating event(s) directly, one can avoid simplifications in the static model. The simulation approach can represent directly, not just the frequency/magnitude, but also physical phenomena related to the flood such as the inundation rate, debris, hydraulics, etc. Further, by representing different flooding hazards via simulation, one integrated model can be used to represent different magnitude events (with their respective frequencies) thereby capturing flooding effects such as precipitation, river, hurricane, etc., in a streamlined fashion, since a single model is used for a spectrum of the hazard possibilities. This integrated fashion overcomes the challenge of binning or discretizing the static model where clones of the event trees, fault trees, and basic events are used typically to represent the different aspects of the flood hazard.

As stated in Section 1, this project does not perform a complete external flood hazard analysis. The following subsections present a case study for a LIP event that is focused on estimating the precipitation frequency with precipitation height for long return periods based on the existing data. It is important to note that this case study is for *demonstration purpose only*. The use of the extrapolation methods related to hazard curves in this study does not imply the acceptance of such methods by the NRC, nor the discussions in the study being interpreted as guidance for such extrapolation. Other important characteristics of flood events such as flood event duration (e.g., warning time and period of inundation) and parameter defining associated effects (e.g., debris, dynamic loads, and sedimentation) are not discussed in this report, but should be included in a full external flood hazard analysis.

3.1 NOAA Precipitation Frequency Estimates

Site-specific historical external flood data (LIP in this case study) could be obtained from data sources such as the National Oceanic and Atmospheric Administration (NOAA) Atlas 14 [13]. The historic data should be assessed and characterized to develop hazard curves that represent the frequency of exceeding a relevant parameter of interest, such as flood height, considering the flood-causing mechanisms that could affect the plant. The hydrological and hydraulic characteristics of the flood event (precipitation rate, soil moisture and infiltration, surface water flow rate, accumulation water level, flood duration, hydrostatic and hydrodynamic forces, debris impact forces, etc.) should be evaluated properly as part of the external flood hazard analysis.

Without collecting regional- and plant-specific information and performing a detailed flood hazard analysis, applicable data from the NOAA Atlas 14 was used for this study. Specifically, the NOAA Precipitation Frequency Data Server (http://hdsc.nws.noaa.gov/hdsc/pfds/index.html) [14] provides NOAA Atlas 14 precipitation frequency estimates for interested location by either clicking the interact map or directly entering the latitude and longitude of the location (Figure 3-1). There are two time series types in the NOAA Precipitation Frequency Data Server that NOAA performed for frequency analyses: annual maximum series (AMS) and partial duration series (PDS). AMS-based precipitation frequency estimations can be used directly as source data points in the Extreme Value Theory or Generalized Extreme Value (GEV) model [15] and the OpenBUGS [16] script to perform Bayesian inference for GEV distribution parameters and rare frequency estimation (see Section 3.2). If PDS-based estimations are selected from the NOAA Precipitation Frequency Data Server, according to Section 4.6.4 of the NOAA Atlas 14, the average recurrence interval (ARI) values should be converted to annual exceedance probability (AEP) before applying it to the OpenBUGS script, using the following equation:

$$AEP = 1 - \exp\left(-\frac{1}{ARI}\right) \quad (1)$$

Table 3-1 shows the NOAA AMS-based precipitation frequency estimates for an U.S. nuclear power plant. The AEP ranges from one in 2 years to one in 1000 years. The estimations include 17 durations: 15-minutes, 30-minutes, 1-hour, 2-hour, 3-hour, 6-hour, 12-hour, 1-day, 2-day, 3-day, 4-day, 7-day, 10-day, 20-day, 30-day, 45-day, and 60-day. For each duration, NOAA provides the mean precipitation value in the first row and the 5% and 95% values (within the parentheses) in the second row for the corresponding AEP.

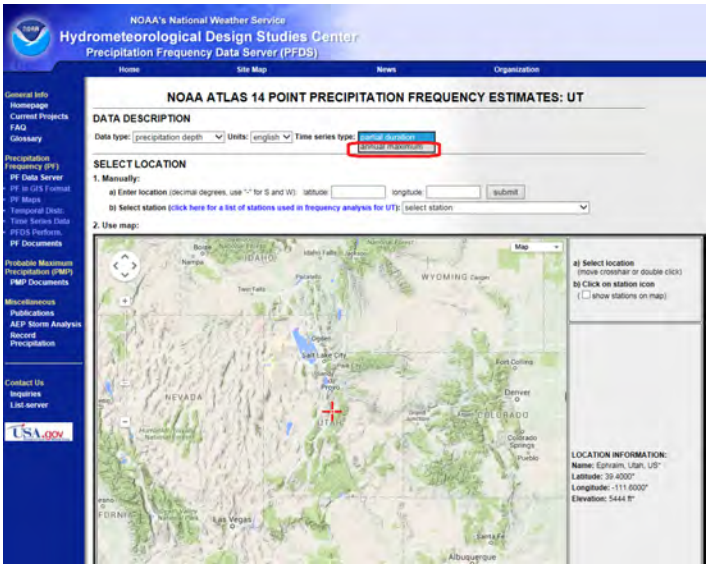

Figure 3-1. NOAA Atlas 14 point precipitation frequency estimates.

Table 3-1. NOAA precipitation frequency estimates with 90% confidence intervals (in inches).

Duration	Annual Exceedance Probability (1/years)								
	1/2	1/5	1/10	1/25	1/50	1/100	1/200	1/500	1/1000
5-min	0.595	0.746	0.865	1.03	1.15	1.28	1.41	1.59	1.73
	(0.478-0.744)	(0.598-0.936)	(0.689-1.09)	(0.791-1.34)	(0.869-1.52)	(0.934-1.73)	(0.989-1.97)	(1.07-2.28)	(1.14-2.51)
10-min	0.871	1.09	1.27	1.5	1.69	1.88	2.07	2.33	2.54
	(0.700-1.09)	(0.875-1.37)	(1.01-1.59)	(1.16-1.95)	(1.27-2.23)	(1.37-2.54)	(1.45-2.88)	(1.57-3.33)	(1.66-3.68)
15-min	1.06	1.33	1.54	1.83	2.06	2.29	2.53	2.85	3.1
	(0.853-1.33)	(1.07-1.67)	(1.23-1.94)	(1.41-2.38)	(1.55-2.72)	(1.67-3.09)	(1.77-3.51)	(1.92-4.07)	(2.03-4.49)
30-min	1.61	2.03	2.35	2.8	3.14	3.49	3.85	4.34	4.72
	(1.30-2.02)	(1.63-2.54)	(1.88-2.96)	(2.16-3.64)	(2.37-4.14)	(2.54-4.72)	(2.70-5.36)	(2.93-6.21)	(3.10-6.85)
60-min	2.15	2.7	3.12	3.68	4.11	4.55	4.99	5.57	6.02
	(1.72-2.68)	(2.16-3.38)	(2.48-3.93)	(2.83-4.77)	(3.10-5.41)	(3.31-6.13)	(3.48-6.91)	(3.75-7.95)	(3.95-8.73)
2-hr	2.68	3.36	3.88	4.57	5.08	5.6	6.12	6.8	7.31
	(2.17-3.32)	(2.71-4.18)	(3.11-4.85)	(3.53-5.87)	(3.85-6.63)	(4.10-7.49)	(4.30-8.42)	(4.60-9.62)	(4.83-10.5)
3-hr	2.96	3.74	4.32	5.09	5.67	6.25	6.83	7.59	8.17
	(2.41-3.66)	(3.03-4.63)	(3.48-5.37)	(3.96-6.51)	(4.32-7.37)	(4.60-8.33)	(4.82-9.36)	(5.16-10.7)	(5.42-11.7)
6-hr	3.43	4.4	5.17	6.21	7.02	7.85	8.7	9.85	10.7
	(2.81-4.20)	(3.60-5.41)	(4.20-6.38)	(4.88-7.92)	(5.39-9.09)	(5.83-10.4)	(6.20-11.9)	(6.76-13.8)	(7.18-15.3)
12-hr	3.87	5.14	6.19	7.68	8.9	10.2	11.5	13.4	15
	(3.20-4.71)	(4.23-6.27)	(5.07-7.58)	(6.12-9.82)	(6.91-11.5)	(7.64-13.5)	(8.31-15.7)	(9.32-18.9)	(10.1-21.2)
24-hr	4.4	6.03	7.38	9.33	10.9	12.6	14.4	17	19
	(3.66-5.31)	(5.00-7.29)	(6.09-8.96)	(7.49-11.9)	(8.56-14.1)	(9.55-16.7)	(10.5-19.6)	(11.9-23.7)	(12.9-26.8)
2-day	5.14	7.07	8.63	10.8	12.6	14.4	16.4	19.1	21.2
	(4.31-6.15)	(5.91-8.48)	(7.17-10.4)	(8.73-13.6)	(9.91-16.0)	(11.0-18.9)	(12.0-22.0)	(13.4-26.4)	(14.5-29.6)
3-day	5.72	7.68	9.26	11.5	13.2	15.1	17.1	19.8	21.9
	(4.82-6.82)	(6.45-9.17)	(7.73-11.1)	(9.29-14.3)	(10.5-16.8)	(11.5-19.6)	(12.5-22.8)	(13.9-27.2)	(15.0-30.5)
4-day	6.22	8.15	9.7	11.9	13.7	15.5	17.4	20.1	22.2
	(5.26-7.38)	(6.86-9.69)	(8.13-11.6)	(9.67-14.8)	(10.8-17.2)	(11.9-20.1)	(12.8-23.2)	(14.2-27.6)	(15.3-30.9)
7-day	7.4	9.31	10.8	13	14.7	16.5	18.4	21	23
	(6.30-8.73)	(7.90-11.0)	(9.14-12.9)	(10.6-16.0)	(11.7-18.4)	(12.7-21.2)	(13.6-24.3)	(14.9-28.6)	(15.9-31.8)
10-day	8.43	10.4	12	14.2	16	17.8	19.7	22.3	24.4
	(7.20-9.90)	(8.87-12.3)	(10.2-14.2)	(11.7-17.4)	(12.8-19.9)	(13.8-22.8)	(14.6-25.9)	(15.9-30.2)	(16.9-33.5)
20-day	11.4	13.9	15.9	18.6	20.6	22.8	25	27.9	30.2
	(9.79-13.2)	(11.9-16.2)	(13.5-18.6)	(15.3-22.5)	(16.7-25.5)	(17.8-28.8)	(18.7-32.6)	(20.1-37.5)	(21.2-41.3)
30-day	13.8	16.9	19.3	22.4	24.8	27.2	29.6	32.8	35.3
	(12.0-16.0)	(14.6-19.6)	(16.5-22.5)	(18.5-27.0)	(20.1-30.4)	(21.3-34.2)	(22.2-38.4)	(23.7-43.9)	(24.8-48.1)
45-day	16.9	20.7	23.6	27.2	29.9	32.6	35.3	38.7	41.2
	(14.7-19.5)	(18.0-24.0)	(20.3-27.4)	(22.6-32.5)	(24.3-36.4)	(25.6-40.8)	(26.5-45.4)	(28.0-51.4)	(29.1-55.9)
60-day	19.6	24	27.2	31.3	34.2	37.1	39.8	43.3	45.8
	(17.1-22.6)	(20.9-27.7)	(23.5-31.5)	(26.0-37.1)	(27.9-41.4)	(29.2-46.1)	(30.0-51.0)	(31.4-57.2)	(32.4-61.9)

3.2 GEV-Model Precipitation Frequency Estimates

The historical data itself is usually sufficient in developing hazard intensity for observed return periods but cannot be used directly for hazard with longer return periods. As Table 3-1 demonstrates, NOAA provides precipitation frequency estimates for up to 1 in 1,000 years based on the observed data. To estimate the hazard for longer return periods (e.g., 10,000 years or longer), some approaches such as the GEV model [14] can be used.

The GEV is a single family of limiting distribution that combines three other limit distributions: Gumbel, Frechet, and Weibull. It has the following cumulative distribution functional form:

$$G(z) = \exp\{-\left[1 + \xi\left(\frac{z-\mu}{\sigma}\right)\right]^{-1/\xi}\} \quad (2)$$

where ξ is a shape parameter, μ is a location parameter, and σ is a scale parameter. The shape parameter ξ determines the distribution type and the tail behavior. $\xi = 0$ corresponds to the Gumbel distribution, which is unbounded and has exponential tail. $\xi > 0$ corresponds to the Fréchet distribution, which has lower bound and long tail. $\xi < 0$ corresponds to the Weibull distribution, which has an upper bound and short tail (Figure 3-2).

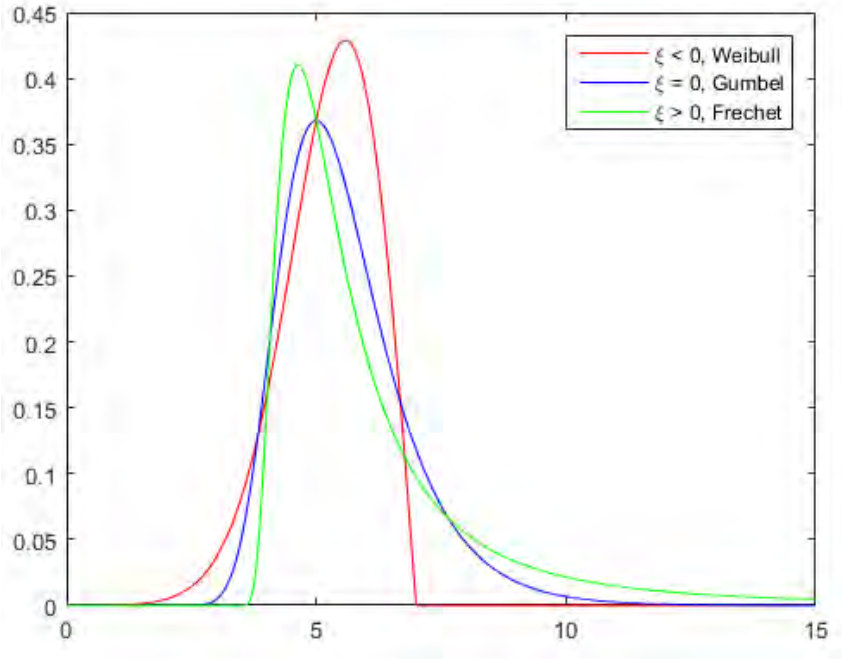

Figure 3-2. Generalized extreme value distribution family.

The inverse distribution function, or quantile function, is often used to calculate the extreme values:

$$z_p = G^{-1}(1-p) = \mu - \frac{\sigma}{\xi}\{1 - [-\log(1-p)]^{-\xi}\},\ \xi \neq 0 \quad (3)$$

The return level z_p is exceeded by the annual maximum in any particular year with the annual exceedance probability p, when the measuring time is in year. Or one can say that the return level z_p is exceeded, on average, once during the return period $1/p$.

The GEV model shown in Eq. (2) was applied to the NOAA precipitation data in Table 3-1 for the 24-hour duration using OpenBUGS. Table 3-2 shows the GEV model calculation results (mean, 5%, and 95% values) for both observed return periods (up to 1,000 years) and longer return periods (up to 1,000,000 years) for the 24-hour duration, along with the NOAA data (for the observed return periods

only) obtained from the NOAA Precipitation Frequency Data Server. Note that additional uncertainties including those in the observed data, competing predictive (aleatory) models, and physical limits of the phenomena are not considered in this study. It should also be noted that the use of the GEV model here does not mean it (and other extrapolation methods) is accepted by the NRC. The discussions in this section should not be interpreted as guidance for such extrapolation.

Table 3-2. NOAA estimated and GEV model calculated precipitation frequencies for 24-hour duration.

Precipitation Amount (inches)		Annual Exceedance Probability (1/years)								
		1/2	1/5	1/10	1/25	1/50	1/100	1/200	1/500	1/1000
NOAA Data	Mean	4.40	6.03	7.38	9.33	10.90	12.60	14.40	17.00	19.00
	5%	3.66	5.00	6.09	7.49	8.56	9.55	10.50	11.90	12.90
	95%	5.31	7.29	8.96	11.90	14.10	16.70	19.60	23.70	26.80
GEV Calculated	Mean	4.29	6.12	7.47	9.36	10.90	12.55	14.34	16.93	19.08
	5%	4.12	6.02	7.39	9.27	10.80	12.46	14.25	16.83	18.92
	95%	4.45	6.22	7.56	9.45	10.99	12.65	14.43	17.04	19.25
	Difference on Mean	-2.6%	1.5%	1.2%	0.3%	0.0%	-0.4%	-0.4%	-0.4%	0.4%

Precipitation Amount (inches)		Annual Exceedance Probability (1/years)								
		5E-4	2E-4	1E-4	5E-5	2E-5	1E-5	5E-6	2E-6	1E-6
GEV Calculated	Mean	21.41	24.80	27.60	30.65	35.07	38.74	42.71	48.49	53.29
	5%	21.15	24.34	26.95	29.74	33.75	37.03	40.55	45.60	49.74
	95%	21.68	25.26	28.27	31.57	36.41	40.48	44.94	51.49	57.00

Table 3-2 shows that for those observable return periods (the upper section of the table), the mean precipitation values predicted from the GEV model are very close to the NOAA data (less than 3% difference). However, the GEV model results have a smaller uncertainty ranges than the NOAA data. For example, for AEP of 1 in 100 years, the NOAA data has a mean value of 12.60 inches, with 5% and 95% values being 9.55 inches and 16.70 inches, respectively. The GEV model estimates a mean value of 12.55 inches, only 0.4% below the NOAA data, but the 5% and 95% values are 12.46 inches and 12.65 inches, respectively, a much narrower range that estimated in the NOAA table. The cause of the narrow uncertainty range estimated from the GEV model is that while the NOAA data are estimated from thousands of scattered, observed “raw” precipitation measuring data, the GEV model uses the NOAA estimated mean precipitation values as “real” data for the input of the model.

The narrow uncertainty range in the GEV model estimations could present a problem in later task when sampling is needed for Monte Carlo simulation of the precipitation frequencies and rates. One potential approach to address this problem is to use the NOAA 5% or 95% precipitation values as the input data in the GEV model, and then use the output of the GEV model as approximate 5% or 95% values for the GEV estimations. Table 3-3 shows these new lower bound (i.e., based upon 5% points) and upper bound (i.e., based upon 95% points) values from the GEV model using the NOAA corresponding uncertainty range values as the input data. This approach provides a better approximation of uncertainty ranges for the desired return periods. For those observable return periods, the GEV estimated uncertainty ranges are close to those from the original NOAA data. For example, for AEP of 1 in 100 years, the GEV model

now estimates the 5% and 95% values to be 9.50 and 16.64 inches, respectively, comparable to the corresponding NOAA uncertainty ranges of 9.55 inch and 16.70 inches.

Table 3-4 and Table 3-5 provide the estimations from the GEV model for the 1-hour and 2-hour durations, respectively. The case study in this report is a 2-hour rain fall event.

Table 3-3. GEV model calculated precipitation frequencies with revised uncertainty values for 24-hour duration.

Precipitation Amount (inches)		Annual Exceedance Probability (1/years)								
		1/2	1/5	1/10	1/25	1/50	1/100	1/200	1/500	1/1000
NOAA Data	Mean	4.40	6.03	7.38	9.33	10.90	12.60	14.40	17.00	19.00
	5%	3.66	5.00	6.09	7.49	8.56	9.55	10.50	11.90	12.90
	95%	5.31	7.29	8.96	11.90	14.10	16.70	19.60	23.70	26.80
GEV Calculated	Mean	4.29	6.12	7.47	9.36	10.90	12.55	14.34	16.93	19.08
	Lower Bound	3.57	5.11	6.15	7.49	8.49	9.50	10.52	11.88	12.93
	Upper Bound	5.02	7.43	9.27	11.92	14.16	16.64	19.39	23.50	27.03

Precipitation Amount (inches)		Annual Exceedance Probability (1/years)								
		5E-4	2E-4	1E-4	5E-5	2E-5	1E-5	5E-6	2E-6	1E-6
GEV Calculated	Mean	21.41	24.80	27.60	30.65	35.07	38.74	42.71	48.49	53.29
	Lower Bound	13.99	15.42	16.51	17.62	19.11	20.25	21.41	22.97	24.16
	Upper Bound	30.95	36.84	41.89	47.53	55.98	63.24	71.34	83.50	93.94

Table 3-4. GEV model calculated precipitation frequencies with revised uncertainty values for 1-hour duration.

Precipitation Amount (inches)		Annual Exceedance Probability (1/years)								
		1/2	1/5	1/10	1/25	1/50	1/100	1/200	1/500	1/1000
NOAA Data	Mean	2.15	2.70	3.12	3.68	4.11	4.55	4.99	5.57	6.02
	5%	1.72	2.16	2.48	2.83	3.10	3.31	3.48	3.75	3.95
	95%	2.68	3.38	3.93	4.77	5.41	6.13	6.91	7.95	8.73
GEV Calculated	Mean	2.12	2.73	3.14	3.69	4.11	4.53	4.97	5.57	6.04
	Lower Bound	1.71	2.19	2.49	2.83	3.07	3.29	3.50	3.76	3.94
	Upper Bound	2.62	3.41	3.99	4.78	5.43	6.12	6.85	7.91	8.78

Precipitation Amount (inches)		Annual Exceedance Probability (1/years)								
		5E-4	2E-4	1E-4	5E-5	2E-5	1E-5	5E-6	2E-6	1E-6
GEV Calculated	Mean	6.52	7.17	7.69	8.22	8.94	9.51	10.09	10.89	11.51
	Lower Bound	4.11	4.33	4.47	4.61	4.79	4.91	5.03	5.17	5.27
	Upper Bound	9.72	11.07	12.18	13.37	15.09	16.50	18.03	20.22	22.03

Table 3-5. GEV model calculated precipitation frequencies with revised uncertainty values for 2-hour duration.

Precipitation Amount (inches)		Annual Exceedance Probability (1/years)								
		1/2	1/5	1/10	1/25	1/50	1/100	1/200	1/500	1/1000
NOAA Data	Mean	2.68	3.36	3.88	4.57	5.08	5.60	6.12	6.80	7.31
	5%	2.17	2.71	3.11	3.53	3.85	4.10	4.30	4.60	4.83
	95%	3.32	4.18	4.85	5.87	6.63	7.49	8.42	9.62	10.50
GEV Calculated	Mean	2.64	3.40	3.91	4.57	5.07	5.58	6.10	6.79	7.33
	Lower Bound	2.15	2.75	3.11	3.53	3.82	4.08	4.32	4.62	4.82
	Upper Bound	3.25	4.22	4.93	5.89	6.66	7.47	8.34	9.57	10.57

Precipitation Amount (inches)		Annual Exceedance Probability (1/years)								
		5E-4	2E-4	1E-4	5E-5	2E-5	1E-5	5E-6	2E-6	1E-6
GEV Calculated	Mean	7.88	8.62	9.19	9.77	10.56	11.17	11.79	12.63	13.28
	Lower Bound	5.01	5.24	5.40	5.55	5.74	5.86	5.98	6.13	6.23
	Upper Bound	11.64	13.17	14.41	15.73	17.63	19.17	20.81	23.16	25.08

4. EXTERNAL FLOOD FRAGILITY ANALYSIS

This task evaluates the fragility of plant SSCs as a function of the magnitude of the external flood using proper engineering method for the postulated failure. The SSCs that are susceptible to the effects of external floods and whose failure contributes to core damage or large early release are identified. Their failure probabilities as a function of the magnitude of the external flood are estimated. The output of this task is a table or tables of SSCs that are included (or excluded for) in the plant response model, as well as their failure probabilities as a function of the magnitude of the external floods (e.g., fragility tables, failure models based upon flooding characteristics, or probabilistic curves). An example of fragility curve with failure probability versus flood intensity is shown in Figure 4-1.

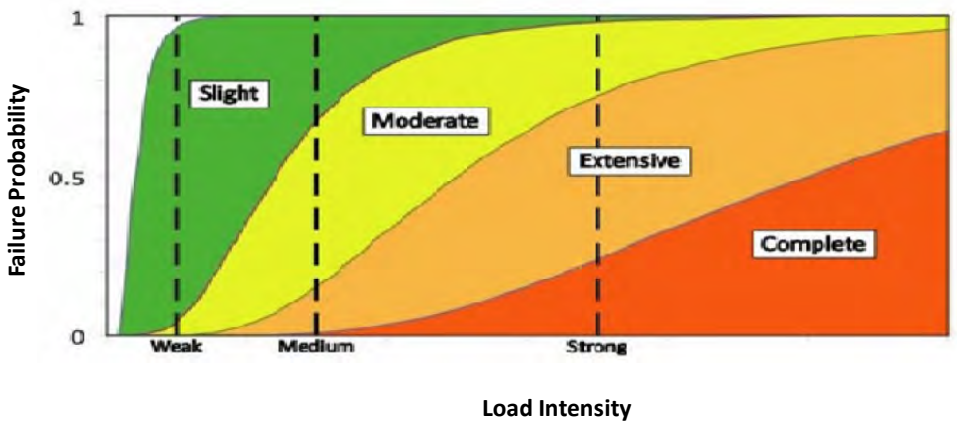

Figure 4-1. Example of a fragility curve.

In the external flood fragility analysis, the plant SSCs, including flood protection features such as permanent and temporary flood barriers and equipment, that are susceptible to the effects of external floods should be identified with an external flood SSC list. The internal events PRA model can be used as the basis to develop the list. Then those SSCs that are not modeled in the internal events PRA model but are required in the flood analysis are added to the list. The structures and equipment located at low elevations, intake, and ultimate- heat-sink equipment should be included in the list. Screening evaluation can be performed to reduce the number of SSCs that need detailed fragility analysis. The fragility analysis should be performed for each flood mechanism or combinations of mechanisms. The analysis should identify all relevant SSC failure mechanisms (e.g., inundation, structural failure, or other flow-induced phenomena) and failure modes (e.g., fail-to-start and spurious operations), evaluate plant-specific SSC flood susceptibilities and develop SSC fragilities for identified failure modes.

Plant walkdown is usually conducted in the task to support the fragility evaluation. The walkdown should focus on SSC condition (e.g., potential degradation) and configuration, potential physical interactions between SSCs, flood propagation pathways, and potential flood impacts to SSCs due to flood height, flood event duration, and flood associated effect.

Unlike the concept of critical flood height used in traditional flooding analysis, the SSC fragilities could be associated with various flood heights and various inundation rates in simulation-based dynamic flood analysis so that different SSC failure probabilities could be defined for different inundation levels and different flood flow rates.

As stated in Section 1, this project did not perform a detailed plant-specific flood fragility analysis. Instead, existing PRA database and plant information, including external flood related analyses, are reviewed and used to provide SSC flood fragilities for plant response model and 3-D simulations.

It should be noted that the purpose of the above discussions is to demonstrate a possible flooding fragility modeling aspect that could be incorporated into the dynamic simulation approach. They should not be taken as guidance for performing fragility analyses.

5. PLANT RESPONSE MODELING

The plant response modeling task develops a plant response model that addresses the initiating events and failures caused by the effects of external flooding that can lead to core damage or large early release. The model includes external flood-induced initiating events and other failures, non-external flood-induced unavailability (such as random failures, unavailability due to test or maintenance), and human actions associated with plant flood response that can cause significant accident sequences or significant accident progression sequences. The plant response model evaluates the characteristics of an external flood initiating event (for example, a LIP event with precipitation rate of *x inch per hour*, or a dam failure with a discharge of *x cubic feet per second* at the site); identifies the SSCs and human actions that participate in plant responses to the flood and thus accident sequences; examines the adverse impacts caused by the external flooding, which includes external flood-induced initiating events (for example, a general transient that shuts down the plant, a loss of offsite power, or a loss of service water) and other failures; and assesses accident sequences based on the plant configurations and responses including the plant flood protection features and flood mitigation measures, the external flood-induced initiating events, other external flood-induced failures, and non-external flood-induced failures.

The plant response to an external flood event can be divided into two stages: external plant response (EPR) stage and internal plant response (IPR) stage. During the EPR stage, the plant flood protection features, including both as-designed features (site drain system, water-tight doors and penetration seals, drain systems within buildings, etc.) and temporary features (portable pumps, sandbag barriers, etc.), perform their functions and prevent risk-significant SSCs from flood damages. If the flood protection features fail to perform the functions and the manual actions (e.g., installation of portable pumps and floodgates, construction of barriers) are not effective due to insufficient warning times or ineffective measures, the plant would be in undesirable conditions of flood damage state (FDS) with the external flood-induced initiating event and other risk-significant SSC failures. The plant response enters the next stage, IPR stage, which would evaluate plant mitigation measures along with the manual actions to maintain key safety functions and prevent core damage and large early release. While an internal event, at-power PRA model usually exists prior to the external flood analysis, and can be used as the basis, modified as appropriate, to model the IPR stage for key safety functions and core damage frequency (CDF)/large early release frequency (LERF) analysis, EPR stage modeling may involve new, site-specific, and flood mechanism-specific analysis for the plant.

EMRALD [17-19] was utilized in this project to represent plant responses to highly spatial- and time-dependent flooding events by integrating simulation and time elements into the system logic models. Advanced 3-D modeling and simulations can be conducted using EMRALD and the associated 3-D simulation software. By using simulation methods, the performance of SSCs and the plant responses with the flooding event can be explicitly illustrated. 3-D physical simulations, Monte Carlo simulations of components, and mechanistic analysis are coupled together to represent the flooding event and to determine which SSCs fail, when they fail, what caused their failure, what impact these failures have on associated systems, and what impact system failures have on the overall plant. The state-based PRA model uses “states” to represent and track the conditions of the SSCs in the model. A set of states is represented at any given moment within the mission time. The set of current states could change over the time until a terminal state is reached. The state-based PRA model could be developed from scratch or converted from an existing traditional PRA model.

Section 5.1 presents general plant responses to an external flood, as well as a typical external flooding event tree that can be used to assess the flood damages states due to the external flood event for the External Plant Response stage. Section 5.2 describes a portion of a traditional, typical internal event PRA model that is evaluated for the Internal Plant Response stage. Section 5.3 provides an overview of the state-based PRA modeling approach. Section 5.4 describes how the traditional PRA model in previous section is translated into the state-based PRA model for the case study of this project.

5.1 External Plant Response

The plant response to an external flood event can be divided into two stages: External Plant Response and Internal Plant Response (Figure 5-1). During the External Plant Response stage, the plant flood protection features, including both as-designed flood protection features (site drain system, water-tight doors and penetration seals, drain systems within buildings, etc.) and temporary flood protection features (portable pumps, sandbag barriers, etc.), perform their functions and prevent risk-significant SSCs from flood damages. If risk-significant buildings have no structural damage or loss of function from the flood and its associated effects (e.g., loss of ultimate heat sink due to debris clogging), and the site drain system, building flood barriers, or other flood protection features perform their functions successfully (with the cliff-edge effect considered) and keep water out of risk-significant SSCs, the plant would be in a safe condition with no or minimal impact from the flood. However, if any risk-significant building suffers structural damage, or the as-designed flood protection features are degraded while temporary flood protection features are not effective to prevent water invading risk-significant buildings, the plant risk-significant SSCs as well as the key safety functions would be challenged. With the plant being in undesirable conditions of flood damage state with the external flood-induced initiating event (general transient, loss of offsite power, loss of intake, etc.) and other risk-significant SSC failures, Internal Plant Response would try to maintain the key safety functions to prevent core damage from occurring with various mitigation measures that are available.

An internal event, at-power PRA model usually exists before performing external flood analysis. The modeling of Internal Plant Response stage can use the internal events PRA as the basis, modified as appropriate, for CDF and LERF analysis, which will be discussed in Section 5.2. However, the modeling of External Plant Response stage needs new site-specific and flood mechanism-specific analysis for the target plant.

Figure 5-2 provides an example event tree that can be used to assess the plant responses (external stage) and flood damage stages in an external flood event. The event tree evaluates the plant responses during the External Plant Response stage, examines external flood vulnerabilities for each risk-significant building or area, and determines the flood damage states due to degraded or ineffective flood protection features. Specifically, the following capabilities are questioned for the whole duration of a flood event: what are the SSCs that are susceptible to the effects of external flood? Will the structural integrity of the buildings remain intact? Will the flood associated effects such as debris and sedimentation prevent risk-significant SSCs from performing their functions? Will the site drain system be functional? If the site drain system fails, will the flood barriers (e.g., conduits, seals, doors, hatches, and pipe/ventilation penetrations) prevent water from entering the building and challenge risk-significant systems and components? And if flood barriers fail to prevent water invasion, will other flood protection features, including the drain systems within the building and temporary features such as portable pumps and temporary barriers, provide effective protection for risk-significant systems and components before they are damaged by flooding? If neither the as-designed flood protection features nor the temporary features could prevent water entering the buildings and challenging/damaging risk-significant systems and components, the plant is in the flood damage states with the external flood-induced initiating events (general transients, loss of offsite power, loss of intake structure, etc.) and flood-induced component failures that may occur in different buildings as one flood event could challenge several buildings and components in the same time. The event tree sequences will be transferred to proper internal plant response event trees (e.g., IPR-TRANS for flood-induced general transient initiating event) along with the set of component failures caused by the flood.

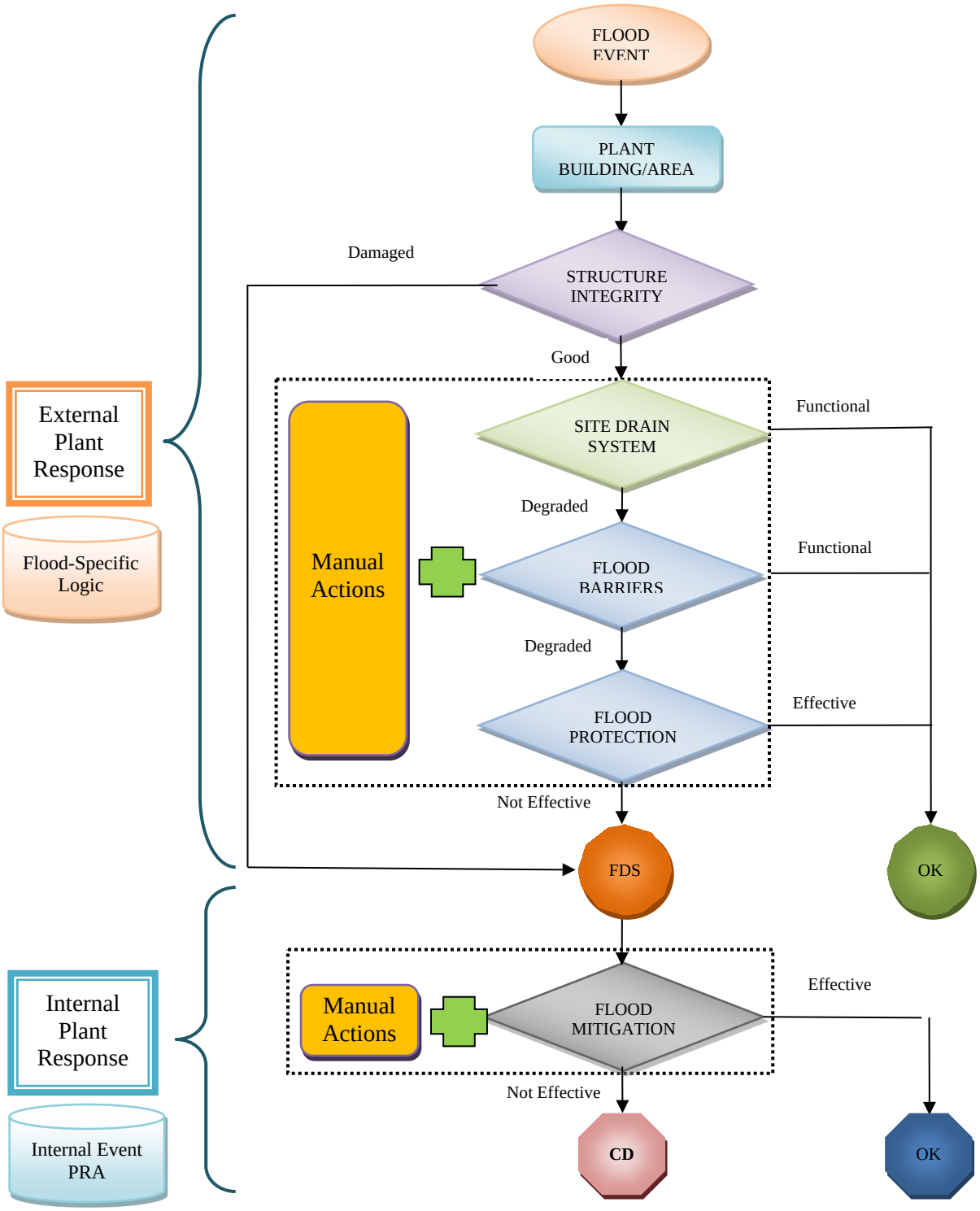

Figure 5-1. Plant response to an external flooding event.

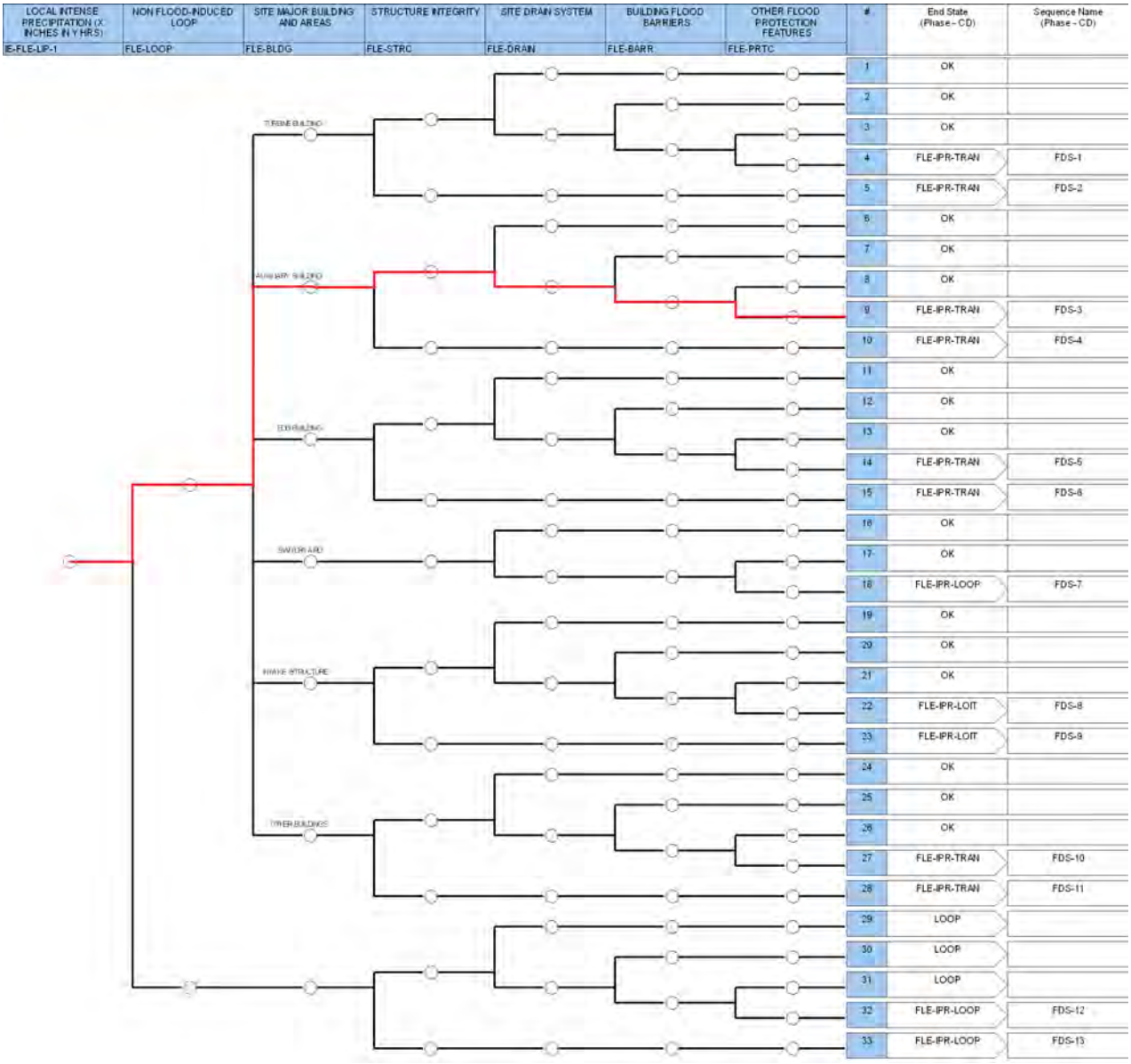

Figure 5-2. External flood event tree - external plant response stage.

The external flood event tree has the following top events that represent the external plant responses and assess plant flood damage states during a postulated LIP event. The event tree could be revised as needed for other external flood mechanisms such as riverine, seiche, storm surge, tsunami, and dam failures, or a combination of the flood mechanisms.

IE-FLE-LIP-1 A local intense precipitation event with X inches rainfall within Y hours has occurred. Following the prefix convention guidelines in the SPAR-ICM Model Maker's Guideline [20], FLE- is used as prefix for external flood events.

FLE-LOOP This top event represents whether a loss of offsite power has occurred before or during an external event. The loss of offsite power may not be induced by the flooding of the switchyard, which is examined in other sequences.

FLE-BLDG This top event examines each of the site risk-significant buildings and areas that would be challenged by the external flood event. Depending on site-specific features, the site

buildings and areas to be evaluated should include turbine building, auxiliary building, EDG building, switchyard, intake structure, and other risk-significant buildings/areas, such as reactor building and control building.

FLE-STRC This top event represents whether the risk-significant buildings suffer structural damage of loss of function due to the flood and the associated effects such as debris and sedimentation.

FLE-DRAIN This top event represents whether the site drain system is successful to perform its function and prevent water accumulation that would challenge flood barriers of the buildings.

FLE-BARR This top event represents whether the flood barriers (water-tight doors, penetration/conduit seals, etc.) are successful to prevent water adversely entering the buildings and challenge risk-significant systems and components.

FLE-PRTC This top event represents whether other plant flood protection features (including the drain system within the building as well as temporary features such as portable pumps and temporary barriers) are successful to prevent risk-significant systems and components from flood damage.

When an external flooding event such as a local intense precipitation occurs at a nuclear plant site, one important aspect of the plant condition is whether a non-flood induced loss of offsite power has occurred during the flood event. If a non-flood induced loss of offsite power has not occurred, the flooding impact on structural integrity for each risk-significant buildings (turbine building, auxiliary building, diesel generator building, intake structure, reactor building, and control building, etc.) is examined. If the structural integrity of the building is compromised, the risk-significant systems and components located in the building would be challenged. The sequences are transferred to internal plant response event trees (for example, FLE-IPR-LOIT for loss of intake structure, FLE-IPR-TRAN for loss of other building integrity). If the building maintains its structural integrity as well as its function intact, the plant would be in a stable and safe condition when the site drain system successfully performs its function, or the building flood barriers can keep water out of the building, or other flood protection features are effective to prevent risk-significant systems and components from flood damage even when water enters the building. Otherwise, the sequences will be transferred to internal plant response event trees (for example, FLE-IPR-LOIT, FLE-IPR-TRAN, or FLE-IPR-LOOP for the flooding of switchyard that causes a loss of offsite power).

On the other hand, if there is a non-flood induced loss of offsite power that occurs before or during the flood event, when the building structural integrity is intact, the site drain system, flood barriers, and other flood protection features are functional and effective to prevent flood damage to risk-significant systems and components, the sequences are transferred to regular, internal event LOOP event tree. There is no flood-induced failures, but non-flood induced random unavailability should be evaluated through the internal event PRA model. If the building structural integrity is lost, or the flood protection features, including the site drain system and flood barriers, are degraded and ineffective, water finds its pathway to enter risk-significant buildings and challenge risk-significant systems and components. The sequences are transferred to the internal plant response event tree, FLE-IPR-LOOP, along with the set of failed risk-significant systems and components.

Note that the above external plant response event tree shows an example overall plant response model during the external response stage of an external flood event. The event tree should be revised as necessary to address external flood event characteristics, site-specific considerations, and plant-specific response strategies. For example, multiple buildings might be impacted by the flood event. For the case study in this project, a local intense precipitation occurs at a site that has degraded site drain system and degraded flood barriers. Thus, a significant amount of water enters the Auxiliary Building that would

cause a shutdown of the plant and threaten risk-significant SSCs within the building and the plant safety. Sequence 9 depicts the external plant response stage of the event and is transferred to FLE-IPR-TRAN for internal plant responses.

5.2 Internal Plant Response

When the flood protection features fail to perform their functions and protect the risk-significant SSCs from flood-caused damages during the external plant response stage, the internal plant response stage would start to deal with the undesirable conditions of flood damage state by evaluating plant mitigation measures and maintaining key safety functions. An internal event, at-power PRA model usually exists and could be used as the basis, modified as appropriate, of the internal plant response for key safety functions and CDF/LERF analyses. The following key safety functions and associated acceptance criteria are from a typical internal event PRA model and can be used for internal plant response to external flood:

- Reactivity control: subcriticality be rapidly achieved and subsequently maintained.
- Reactor coolant system (RCS) pressure control: pressure control is established by requiring that the peak RCS pressure does not exceed the pressure limit corresponding to the service limit stress of the ASME Boiler and Pressure Vessel Code for Level C (“emergency condition”) events.
- Early decay heat removal/ RCS Inventory Control: successful early decay heat removal for core cooling and RCS inventory control is established by requiring that the core remains covered with water. It is assumed that this requirement will be met if the mitigative system’s success criteria are achieved.
- Long Term Heat Removal: Following the success of the core cooling function, heat must be removed from the containment. Containment heat removal is considered a success if the containment pressure is kept below the pressure at which loss of containment integrity is estimated to occur.

It is assumed that core damage would occur if any of these key safety functions are not met. The reactor protection system (RPS) provides reactivity control by inserting enough negative reactivity through control rods to shut down the reactor. RCS power-operated relief valves (PORVs) and safety relief valves (SRVs) provide RCS pressure control. Feedwater (FW) systems (auxiliary feedwater (AFW) or main feedwater (MFW) and high-pressure injection (HPI) system provide early decay heat removal and inventory control. AFW/MFW, low pressure injection (LPI) system in the shutdown cooling (SDC) mode, HPI system in recirculation mode (HPR), and containment spray recirculation (CSR) provide long-term decay heat removal. Figure 5-3 shows the main mitigation systems, along with operator actions needed, that are used to maintain the key safety functions and prevent core damage.

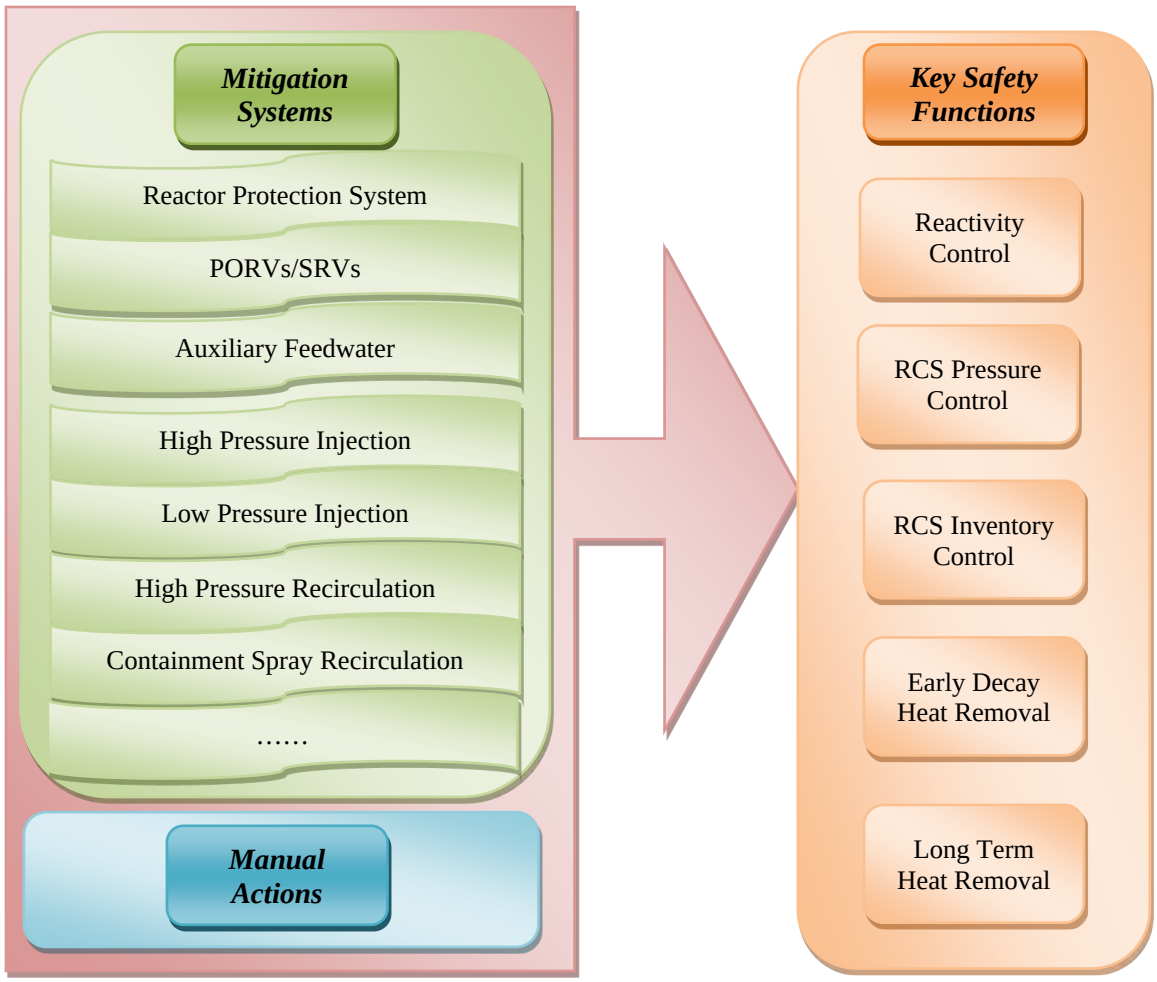

Figure 5-3. Internal plant response to external flood – flood mitigation to maintain key safety functions.

For an external flood-induced transient initiating event, successful internal plant response requires successful reactivity control, early decay heat removal and inventory control, and long-term decay heat removal. If the reactor fails to trip following the external flood-induced transient event, the sequence goes to the anticipated transient without scram sequences that questions the RCS system pressure, secondary cooling, emergency boration, and reclose of the PORVs and SRVs. Successful operations of secondary cooling by AFW or MFW can place the reactor in a stable condition if there is no PORVs opened and the long-term makeup can be provided to the water source of AFW, condensate storage take (CST). However, if a PORV opens and fails to reclose, HPI is required to provide makeup flow to the RCS. If HPI succeeds, then long-term cooling provided by SDC or HPR or CSR is required.

If secondary cooling is unavailable or the long-term makeup to CST fails, once through cooling (OTC) (i.e., feed and bleed cooling) can provide successful decay heat removal. For the operation of OTC, PORVs are open to remove the decay heat while HPI provides makeup flow to replenish the lost RCS inventory.

Figure 5-4 shows an example external flood-induced transient event tree that can be used to evaluate internal plant responses to an external flood event. The example event tree is based on a typical pressurized water reactor (PWR) SPAR model and should be revised to reflect plant-specific design and operation information as needed. The event tree has the following top events arranged in the approximate order in which they would be expected to occur following an external flood-induced transient event.

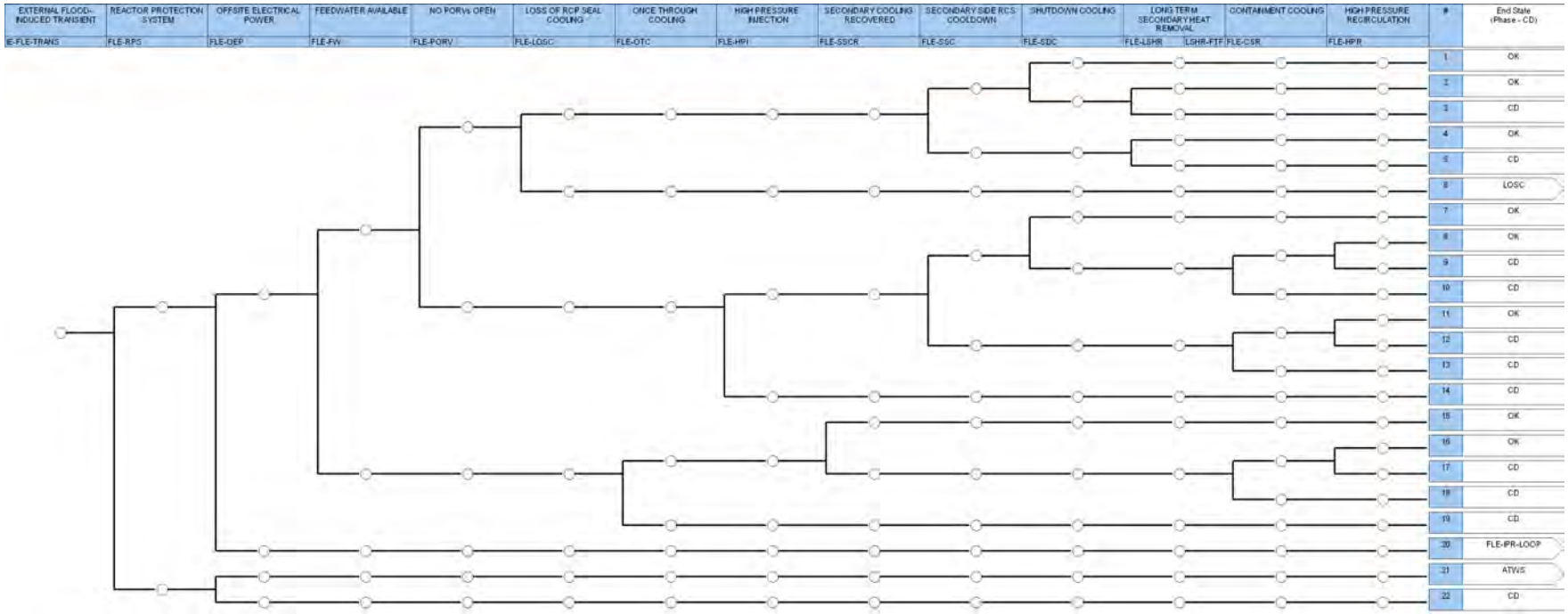

Figure 5-4. External flood-induced transient event tree (FLE-TRANS) – internal plant response stage.

IE-FLE-TRANS	External flood-induced transient event.
FLE-RPS	This top event represents the success or failure of the RPS to insert enough negative reactivity by the control rods to shut down the reactor.
FLE-OEP	This top event represents the success or failure of the offsite electrical power supply.
FLE-FW	This top event represents the success or failure of feedwater (MFW and AFW). Main feedwater trips given a reactor trip; however, main feedwater can still be available with successful restart and can provide flow to the steam generators for decay heat removal. Either the loss of MFW or isolation of MFW will require the AFW system to provide flow to the steam generators. Success implies automatic actuation and operation of the AFW system to supply sufficient cooling water to at least one steam generator.
FLE-PORV	This top event represents the success or failure of the power operated relief valves. Success requires that (1) no PORVs opened given the transient or (2) all opened PORVs reclosed once RCS pressure is lower than the relief pressure set points for the PORVs or the operator closes the PORV block valve(s).
FLE-LOSC	This top event represents the success or failure of RCP seal cooling from the component cooling water (CCW) system. Success requires the CCW to provide sufficient cooling the reactor coolant pumps (RCPs) to eliminate the potential of a RCP seal LOCA. Failure to provide cooling to the RCP seals leads to a potential RCP seal LOCA.
FLE-OTC	This top event represents the success or failure of once through cooling (i.e., feed and bleed) given secondary cooling is unavailable. Success requires PORVs open to remove decay heat from the RCS and HPI provide makeup flow to the RCS.
FLE-HPI	This top event represents the success or failure of the high-pressure injection system to provide makeup water to the RCS. Success implies automatic actuation and operation of the HPI system. The pumps take suction from the refueling water storage tank (RWST) and provide flow to the RCS cold legs. The HPI system provides sufficient water to keep the core covered.
FLE-SSCR	This top event represents the success or failure of secondary cooling recovery. Success requires recovery of either AFW or MFW to supply water to the steam generators. Success also requires the PORVs to close after successful OTC operations.
FLE-SSC	This top event represents the success or failure of cooling down the RCS to the point when shutdown cooling can be initiated. Success requires opening the turbine bypass valves or the atmospheric dump valves to lower the RCS temperature and pressure to the shutoff head of the LPI pumps for shutdown cooling.
FLE-SDC	This top event represents the success or failure of shutdown cooling. Success implies the RCS pressure and temperature are within the requirements to allow the RCS hot leg (to LPI pump suction) suction valves to be opened and provide a suction source to the LPI pumps. The shutdown cooling heat exchangers will slowly cool down the reactor. This system requires an operator action to open the RCS hot leg valves that provide the suction source for the pumps and align the pump discharge through the shutdown cooling heat exchangers. Success also requires the charging system to provide flow from one-of-three pumps from the RWST to the RCS to provide make-up flow during shutdown cooling.

FLE-LSHR This top event represents the success or failure of condensate storage tank refill. Success requires an operator to refill the CST using the refill pumps from the backup storage tank. This top event also includes the once through cooling as a backup to failing to refill the CST.

FLE-CSR This top event represents the success or failure of containment cooling. Success requires the containment spray pumps to take suction from the containment sump and cool the water down by running it through the shutdown cooling heat exchangers. The cooled water is then sprayed into containment to lower the containment pressure and temperature. The CSR system will keep the sump water cool enough to provide a net positive suction head for the HPI pumps.

FLE-HPR This top event represents the success or failure of high-pressure recirculation. Success requires the HPI pumps to take suction directly from the containment sump and deliver the water to the RCS. HPR will provide long-term cooling for the reactor given the HPI system was successful in supplying early makeup water to the reactor. Also, the continued operation of the CSR system is required to cool down the sump water. HPR is required if shutdown cooling cannot be established. The decay heat will be removed from the containment sump by the shutdown cooling heat exchangers or containment air coolers.

This example of the internal plant response event tree was used in Section 5.4 to develop a simplified event tree in which two sequences were used for the state-based PRA model and simulations as the case study of this project.

Note that when an internal event PRA model is used as the basis for the external flood plant response model, the internal event model should be modified as necessary. For example, the external flood PRA should include both external flood-induced SSC failures and non-flood induced unavailability and failures. The mission time of the external flood PRA model should be defined based on the time during which SSCs are required to perform their functions for the flood event duration, which may be different from the mission time defined in the internal event PRA model. The effect of external flood impact on the performance shaping factors for human actions should be evaluated in human reliability analysis. The failure modes of interest in the external flood model may be different from those in the internal event model for some SSCs (e.g., spurious actuations or instrument malfunctions caused by the external flood and the associated effects).

5.3 Overview of State-Based PRA Modeling

5.3.1 Basic Concepts

With previous sections using event trees to describe plant external and internal plant responses during an external flood event, this section describes the use of EMRALD in this project to model plant responses to flooding events that integrates simulation and time elements into the logic models. Advanced 3-D modeling and simulations can communicate with the state-based PRA model, with the time-related simulation results being incorporated into and accounted for in the state-based PRA model. Simulation methods can explicitly illustrate the SSCs performance and their responses along with the flooding event progresses. 3-D physical simulations, Monte Carlo simulations of components, and mechanistic analysis are then coupled together to represent the flooding event and determine which SSCs fail, when they fail, what caused their failure, what impact these failures have on associated systems, and what impact system failures have on the overall plant. The state-based PRA model could be developed from scratch or converted from an existing traditional PRA model.

The state-based PRA modeling technique uses a state model of the components and systems that allows for time-based plant responsive behaviors and dependencies. The states of components and systems represent and track their status (i.e., whether they are failed or still performing their functions at the moment). When a simulation starts, the model is in a set of initial states of components and systems. The component and system states may be changed driven by their predefined event and action attributes. The event attribute of a state is a condition-based item that will execute its defined actions such as transit to another state when the condition is met. Some examples of the events in a state include changing state when the associated state is in the list of current states, running the timer as time passed, and evaluating the logic of a system when it is defined. The action attribute of a state represents the immediate action it will take once it enters the state. Examples of such immediate actions include generating a new state, moving to another state, and changing the value of a variable of the model. At any given moment within the mission time or simulation time, the model is in a set of current states of components and systems that would change over time until a terminal state is reached when the component and system states are evaluated, and would determine which key state (for example, core damage, large early release, or small early release) this iteration, or run, of the model reaches. With millions of such simulation runs, the core damage frequency or other proper risk metrics can be obtained.

The definitions of some basic terms in the state-based PRA modeling technique are provided below based upon INL/EXT-14-33211 [17].

State:

- ***Standard State*** - a logical representation for the condition of a component, system, or human action.
- ***Start State*** - a state that is to be placed in the current state list when the model begins a simulation.
- ***Key State*** - a state that is to be tracked for final probability calculations. All “End States” from a traditional PRA model should have a corresponding “Key State.”
- ***Terminal State*** - a state when a simulation ends.

Event: A condition-based item that when met executes its assigned actions. (6 Types)

- ***Timer*** – executes when set time has passed.
- ***Fail Rate*** – executes when the sampled time (based on the failure rate) has passed.
- ***State Change*** – executes when the associated state is in the list of current states.
- ***System Logic*** – executes if the defined logic for a set of components is met (like evaluating a fault tree in PRA without probabilities).

- ***Variable Condition*** – executes if a variable meets the user defined condition.
- ***3-D Simulation*** – executes if the associated 3-D component fails.

Action: immediate action to be performed when entering a state.

- ***Transition*** – start or move to a new state or states. It is probabilistic if it contains more than one state.
- ***Change Value*** – change the value of a variable.
- ***3-D Sim Action*** – send a message to the 3-D simulator.
- ***ExtCode*** – process current states and run an external application then process results to determine any state changes.
- ***Reset Time*** – move back to a given time, sampling and process events again.

State Group: a group of states that together define the valid states of a component or system. Only one of these states can be in the "Current States" list at any given time. Each of these states must have a success or failed flag indicating if the component is in an "OK" or "Failed" condition.

Variables: named values that can be set by "Actions" or evaluated by "Events" (3 types).

- ***3-D Simulation Variable*** – value for the associated component in the 3-D simulation.
- ***Local Variable*** – available for all to read but only "Actions" in a "State" associated with that component can change the value.
- ***Global Variable*** – available for all to read the value and "Actions" to set it.

Figure 5-5 presents a simple flow of state processing in a state-based model. When a simulation starts, the initial states of components and systems of the model are loaded into the "Current States" list. Under the main process loop, any immediate actions for each new state are added to the "Current States" list. If any of the current states is a terminal state, then the simulation is done. Otherwise all the events for the current states will be evaluated. If an event occurs, its associated action will be executed. If any actions create new states, the simulation will return to the main process loop with the new states to be processed. If there are no events to be executed or no new states created, the simulation will go to the next timer event, execute the associated event actions, and return to the main process loop to process any new states.

The rest of this section will describe how the components, systems, and accident sequences are modeled in a state-based PRA.

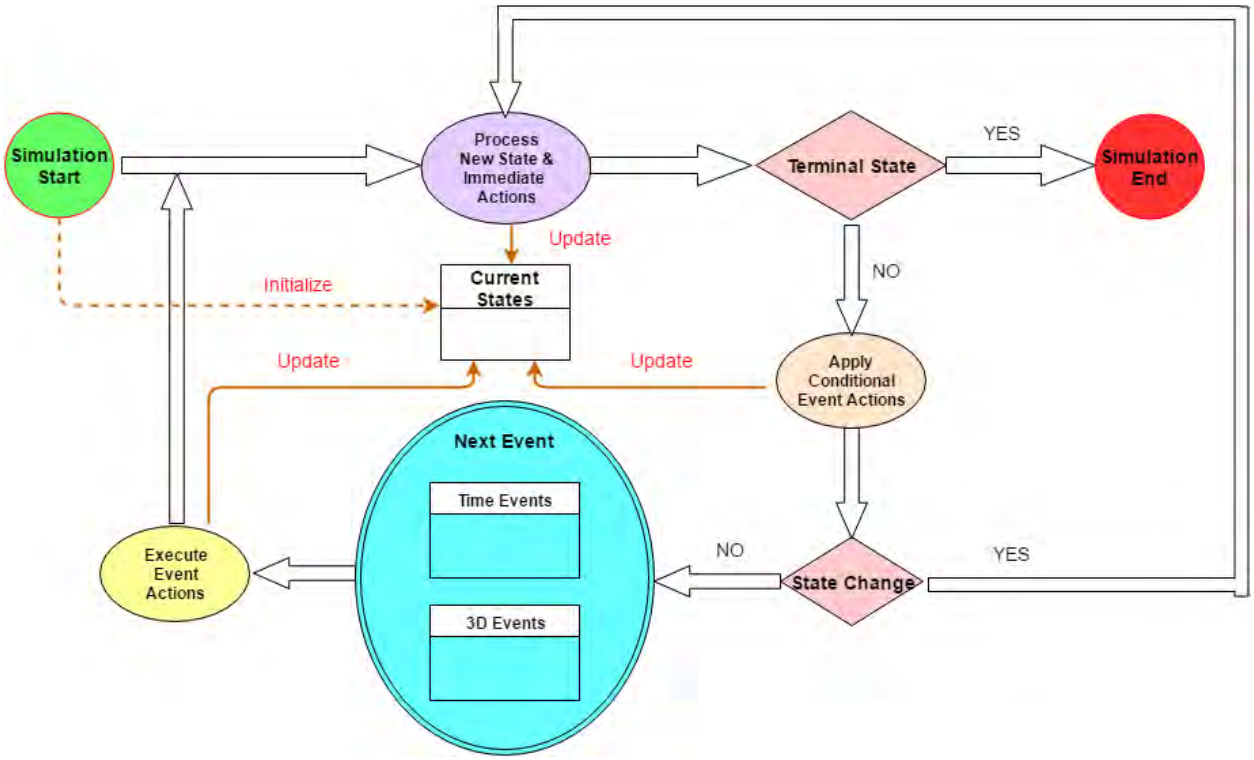

Figure 5-5. Simple flow of state processing in a state-based model.

5.3.2 State-Based Component Modeling

The condition of a component is usually defined by a group of states such as Standby (or Off), Active (or On), and Failed (or Unavailable). The transition from one state to another state is determined by the Events of the initial state. Figure 5-6 displays an example of a state group diagram for a pump component, E-PUMP-B, which is represented by three states (Standby, On, Failed) in the group. The start state of the pump is Standby (top-left node of Figure 5-6). When simulation starts, the Standby state will transit to either the On state or the Failed state depending on whether the pump starting is successful or not, which is determined by the Monte Carlo sampling results with the input of the pump fail-to-start probability. If the pump starts successfully, it moves to the On state (top-right node of Figure 5-6). In the On state, the Fails_To_Run event produces a time-based reaction by sampling the pump fail-to-run probability and moves to the Failed state. The 3D_Sim_Flooded event is included in the state diagram model for the pump to represent a failure path due to the flooding event. When the PRA model receives a message from 3-D flooding simulations that the pump is failed (for example, as the flooding height exceeds the pump failure height), the pump moves to the Failed state. If the pump does not fail due to either the stochastic failure (fail-to-run probability) or the flood-caused failure (3-D flood simulation physics) through the mission time, the pump state is flagged as a success state designated by the **[1]** before the state name. Otherwise, either Fails_To_Run or 3D_Sim_Flooded event will move the pump to the Failed state (bottom node of Figure 5-6), and the pump state is flagged as a failed state designated by the **[0]** before the state name. The success or failed flag allows for an evaluation of the pump by other parts in the model.

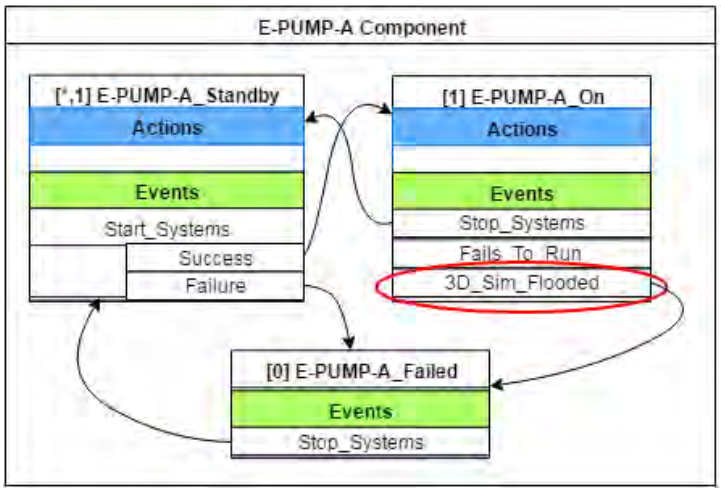

Figure 5-6. Example of a component (i.e., a pump) state diagram.

Besides the normal components modeled in traditional PRA (such as pumps, valves, and tanks), human actions and flood protection features such as flood barriers could be modeled in a similar way with their failure probabilities estimated in human reliability analysis and Task 2, External Flood Fragility Analysis, respectively.

5.3.3 State-Based System Logic Modeling

After all component states are modeled for the components in a system, the system can be modeled using a logic diagram of the components and a system state group diagram. The system logic diagram (left side of Figure 5-7) is similar to a fault tree in traditional PRA model that depicts the system logic and evaluates the failure probability of the fault tree top gate. However, differences exist between the state-based system logic modeling and the traditional fault tree modeling. For example, the basic events in a traditional fault tree are component and failure mode specific, while the basic events in a state-based system logic diagram are component-specific only because the failure modes are already represented within the component state groups. In a traditional fault tree, two different basic events C-PMP-A-FS and C-PMP-A-FR are included in the logic to represent fail-to-start and fail-to-run of pump A in system C, respectively. In the state-based system logic diagram, the basic event would be C-PMP-A to represent the status of pump A. The failure modes of pump A, fail-to-start and fail-to-run, will be represented in the component state group diagram in previous section. The other difference between the state-based system logic model and the traditional fault tree model is that instead of Boolean calculation and using mean probabilities of basic events, the state-based system logic model uses the Monte Carlo simulations on the component level and the logic of the system diagram to estimate the system overall success or failure probability. However, it should be noted that both the static and dynamic approaches have the capability to use and sample from the uncertainty distributions related to parameters such as failure rates and probabilities.

The system state group diagram (right side of Figure 5-7) defines the conditions of a system through a group of states, such as Active and Failed. The Evaluate_CCS_FT event in the system Active state of Figure 5-7 will evaluate the logic of the system diagram along with the component state results (success or failed, which is evaluated through the Monte Carlo simulations and 3-D simulations) for all the components in the logic. The system is then flagged as either success or failed with a designation of **[1]** or **[0]** before the system state name, respectively. The system state flag allows for an evaluation of the system by other parts of the model (for example, an electrical system that becomes flooded may not provide power, a **[0]** state, to other components depending on that power source).

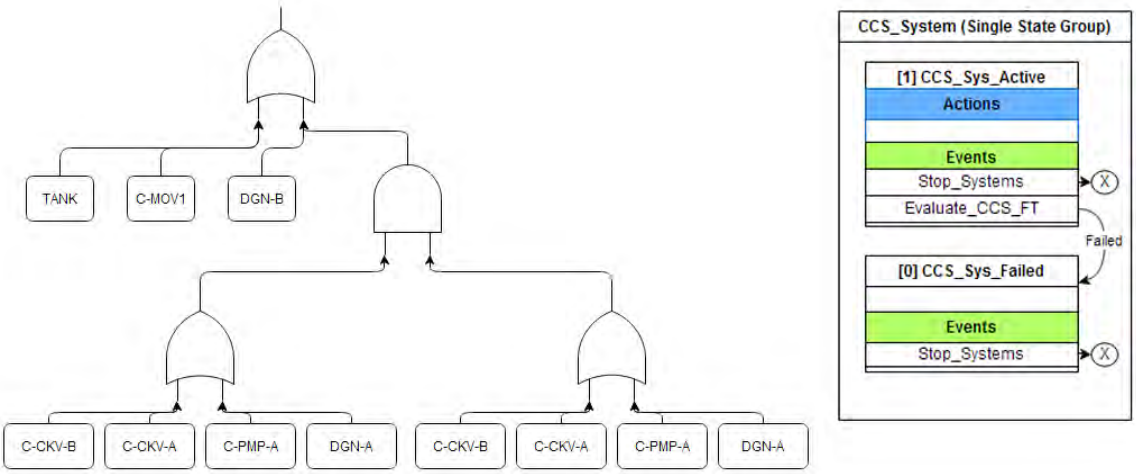

Figure 5-7. Example of a system logic diagram (left) and state diagram (right).

5.3.4 State-Based Accident Sequence Modeling

Unlike traditional PRA model that uses event tree to graphically represent accident sequences, there is no such explicit model in state-based PRA to sequentially depict the responses of the systems and operator actions to an initiating event in order to maintain key safety functions and prevent core damage and large early release. Instead, the accident sequences are implicitly represented in the plant state diagram with the flow paths between the start state, initiating event states, system or component states, and key/end states. As a simple example, the flow paths in Figure 5-8 imply two event trees: Loss of Offsite Power (LOSP) and External Flood. For each event tree, there are three accident sequences. Sequence 1 is with the occurrence of the initiating event (IE), either LOSP or External Flood, ECS system successfully performed its functions and mitigated the event. The end state of the sequence is OK. Sequence 2 is with the occurrence of the IE, ECS system failed but CCS) system successfully performed its functions. The end state of this sequence is small release. Sequence 3 is with the occurrence of the IE, both ECS and CCS systems failed and led to a large release.

It should be noted that while there is no explicit measure in state-based PRA model to represent accident sequences, the event tree technique could be used as a tool outside of the model to inform the development of the plant state diagram and the PRA model. Further, it should be noted that in this demonstration example for flooding, we did not integrate physics models related to the thermal-hydraulics of the scenario—a more complete model would incorporate other codes such as TRACE or RELAP into the simulation to determine the ultimate plant state for various scenarios.

It can be seen from the example in Figure 5-8 that other than the standard component/system states introduced in above sections, a plant state diagram would also include other special states, such as the Normal_Op state as the starting state for the simulation, the LOSP and External Flood states as the initiating event states, the Mission Time state that serves as the timer and finishes the simulation after the mission time has elapsed, the Small_Release and Large_Release states as the key states (or end states), and the Start_ and Stop_Systems states that start or stop to evaluate systems or components.

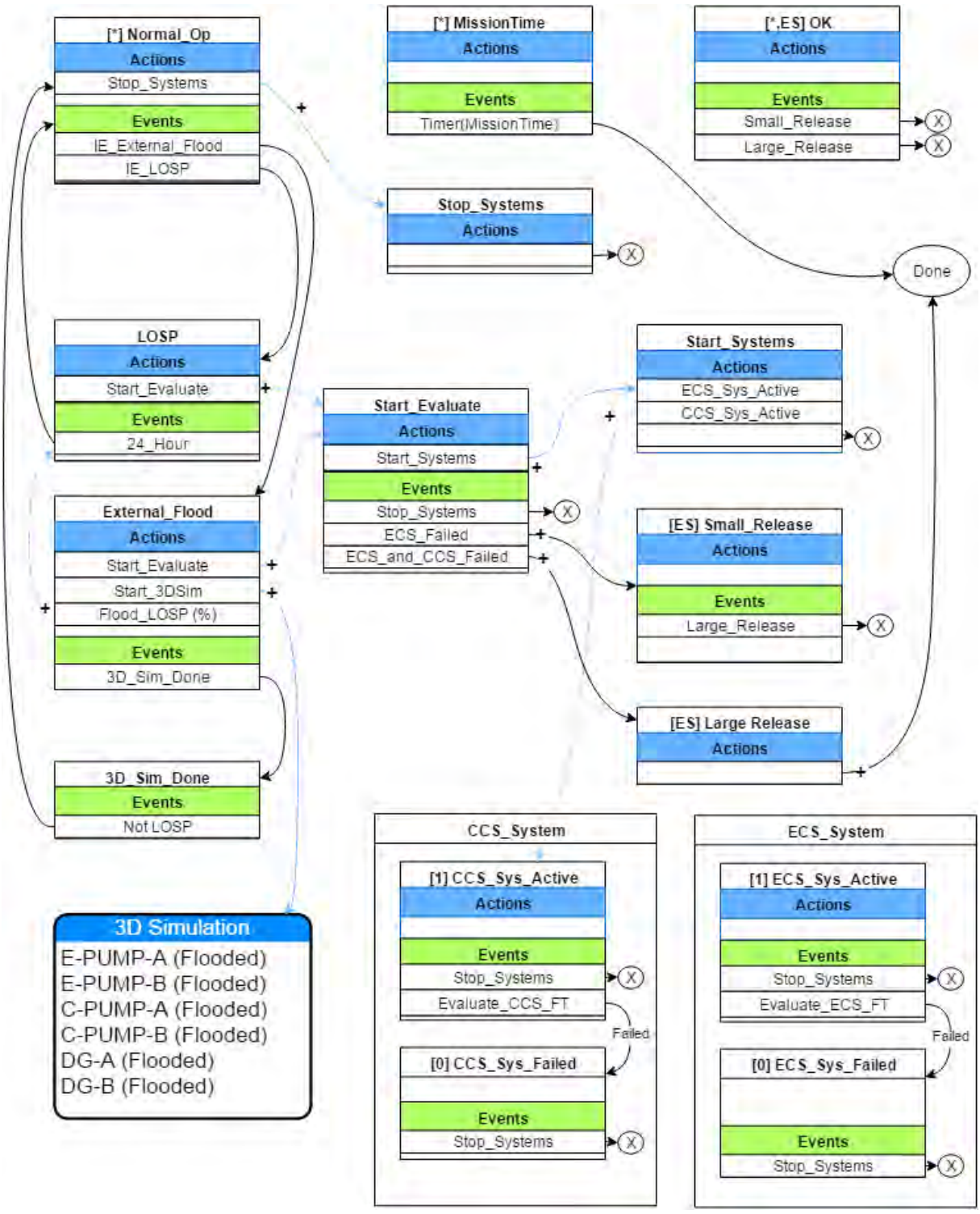

Figure 5-8. Example of a plant state diagram for the flooding case study.

5.4 Development of an Example State-Based PRA Model

An example state-based PRA model was developed for the project to demonstrate the capabilities of simulation for these types of risk analysis. The assumptions on the boundary conditions of the example model include:

- The plant site drain system is assumed to be in a degraded condition.
- The flood barriers to the plant auxiliary building (AB) that houses important engineering safety features are also assumed to be degraded.
- The local intense precipitation could enter the AB and threaten the safety injection pumps as well as other safety important systems and components in the building.
- The reactor would be shut down after the water height in safety injection pump rooms reaches abnormal level and triggers the alarm.

A simplified external flood-induced transient event tree was developed in Figure 5-9. Two specific accident sequences were selected for state-based PRA model. Sequence 3 is with the external flood-induced transient event occurred, feedwater is available to supply sufficient cooling water to steam generator (which can be represented by /FLE-FW, or /FW with the suffix FLE- being omitted for simplicity in later sections), no PORV is open (/PORV), secondary side RCS cooldown is successful so that shutdown cooling can be initiated (/SSC); however, shutdown cooling cannot be established to cooled down the reactor (SDC), and the long-term secondary heat removal is failed with the failure of condensate storage tank refill as well as the failure of the once through cooling as a backup (LSHR), core damage cannot be prevented (IE * /FW * /PORV * /SSC * SDC * LSHR). For Sequence 18, after the external flood-induced transient event occurred, feedwater is not available, if once through cooling (i.e., feed and bleed) is not functional, the core will be damaged (IE * FW * OTC). While Section 5.2 provides detailed descriptions and success criteria for all of the involved top events, below is a review of those failure top events:

FLE-SDC — This top event represents the success or failure of shutdown cooling. Success implies the RCS pressure and temperature are within the requirements to allow the RCS hot leg (to LPI pump suction) suction valves to be opened and provide a suction source to the LPI pumps. The shutdown cooling heat exchangers will slowly cool down the reactor. This system requires an operator action to open the RCS hot leg valves that provide the suction source for the pumps and align the pump discharge through the shutdown cooling heat exchangers. Success also requires the charging system to provide flow from one-of-three pumps from the RWST to the RCS to provide make-up flow during shutdown cooling.

FLE-LSHR — This top event represents the success or failure of condensate storage tank refill. Success requires an operator to refill the CST using the refill pumps from the backup storage tank. This top event also includes the once through cooling as a backup to failing to refill the CST.

FLE-FW — This top event represents the success or failure of feedwater. Success implies automatic actuation and operation of the AFW system to supply sufficient cooling water to at least one steam generator.

FLE-OTC — This top event represents the success or failure of once through cooling (i.e., feed and bleed) given secondary cooling is unavailable. Success requires PORVs open to remove decay heat from the RCS and HPI provide makeup flow to the RCS.

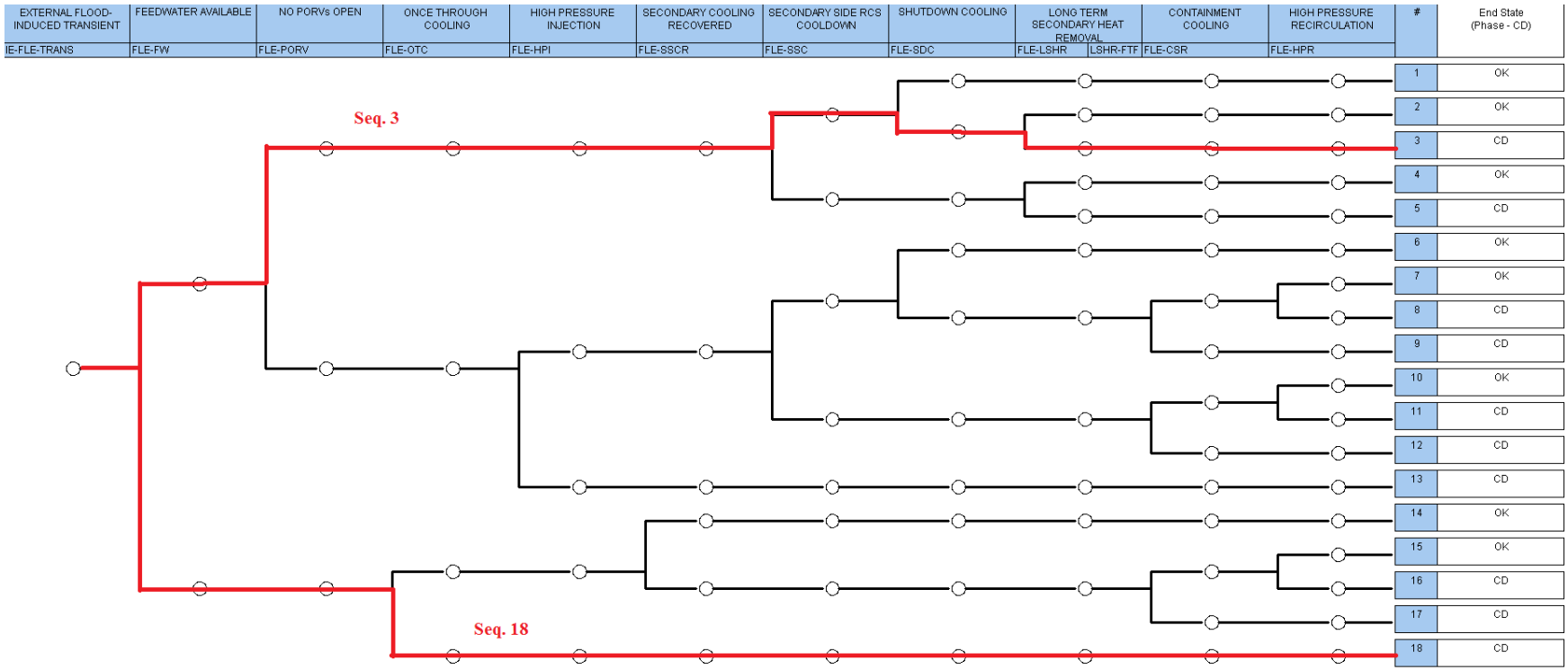

Figure 5-9. A simplified external flood-induced transient event tree.

The next step is to determine the components (including human actions) and system logic that need to be included in the state-based PRA model. This could be performed by reviewing and revising the corresponding fault trees in existing traditional PRA model. Since the basic events in traditional PRA model are component- and failure-mode-specific while those in state-based PRA system logic model are component-specific (with the component failure modes being included in the component state diagrams instead of system logic state diagrams), the fault trees in traditional PRA model have to be converted to be component-based for the state PRA model. Figure 5-10 presents an example for such conversion. Left side of Figure 5-10 is the traditional fault tree logic for failure of low-pressure injection motor-driven pump LPI MDP-1A (under the top event fault tree SDC). It is an "OR" logic of the following basic events:

LPI-MDP-FS-1A	LPI MDP-1A Fails to Start
LPI-MDP-FR-1A	LPI MDP-1A Fails to Run
LPI-MDP-TM-1A	LPI MDP-1A Unavailable due to T&M
LPI-MDP-CF-STRT	Common Cause Failure of LPI MDPs to Start
LPI-MDP-CF-RUN	Common Cause Failure of LPI MDPs to Run
LPI-XHE-XR-MDP1A	Operator Fails to Restore MDP-1A After T&M
LPI-MOV-OC-V3206	LPI MDP-1A Discharge MOV V3206 Fails to Remain Open
LPI-CKV-CC-V3106	LPI MDP-1A Discharge Check Valve V3106 Fails to Open
LPI-CKV-CF-PMPS	CCF of LPI Discharge Check Valves
HPI-MOV-OC-3659	ECCS Miniflow MOV V3659 Fails to Remain Open
HPI-MOV-OC-3660	ECCS Miniflow MOV V3660 Fails to Remain Open

The failure probabilities of the basic events are provided along with the events. For example, the failure probability for LPI MDP-1A fail-to start is 9.47E-4, the failure probability for LPI MDP-1A fail-to run is 3.62E-4, the unavailability of LPI MDP-1A due to test and maintenance is 7.12E-3, the common cause failure probability for both LPI pumps fail-to-start is 2.37E-5, etc.

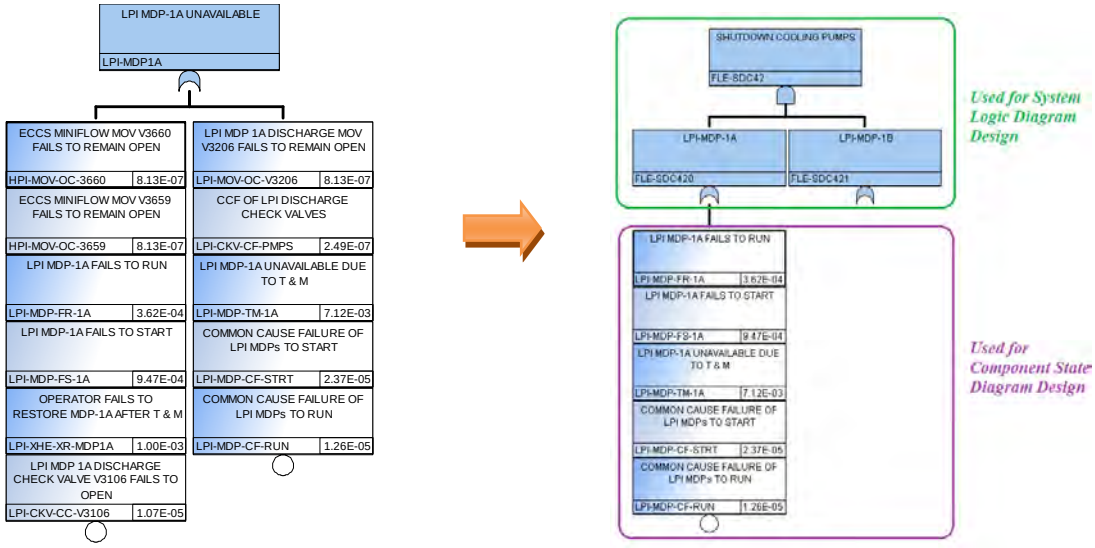

Figure 5-10. Converting traditional fault tree model (left) to state-based PRA model (right).

As a proof-of-concept project, the original fault trees were simplified by selecting a few types of components and failure modes to be modeled in the state-based PRA model. For the failure logic of LPI MDP-1A, the following basic events were chosen:

LPI-MDP-FS-1A	LPI MDP-1A Fails to Start
LPI-MDP-FR-1A	LPI MDP-1A Fails to Run
LPI-MDP-TM-1A	LPI MDP-1A Unavailable due to T & M
LPI-MDP-CF-STRT	Common Cause Failure of LPI MDPs to Start
LPI-MDP-CF-RUN	Common Cause Failure of LPI MDPs to Run

Right side of Figure 5-10 represents the simplified converted fault tree that can be used to develop corresponding system logic and component state diagrams in a state-based PRA model. The top part of it is used for system logic state diagram design with the component-based basic event (i.e., LPI-MDP-1A) (LPI-MDP-1B and the "AND" logic between MDPs 1A and 1B are not displayed in left side of Figure 5-10). The bottom part of the converted fault tree is used for component state diagram design as described in Section 5.3.2. The failure probabilities associated with different failure modes such as fail-to-start and fail-to-run are modeled in state-based PRA through the Monte Carlo sampling in appropriate component states, for example, sampling fail-to-start probability in the component Standby state, and sampling fail-to-run probability in the component On state.

After the related traditional fault trees being reviewed/revised and the list of component-based basic events being compiled, the components as well as the logic for the two sequences (Sequence 3 and Sequence 18) in Figure 5-9 were manually entered into a C# program-based code [21] for the state-based PRA model tool, EMRALD. Table 5-1 presents an overview of this example state-based PRA model. It includes two sequences (Sequence 3, IE-TRANS * SDC * LSHR, and Sequence 18, IE-TRANS * AFW * OTC), four main system logics (AFW for the FLE-FW top, OTC for the FLE-OTC top, SDC for the FLE-SDC top, and LSHR for the FLE-LSHR top), three transfer system logics from LSHR (HPR for high-pressure recirculation, CSR for containment cooling spray system, and CCS for containment cooling fan system), and about 70 components, which include motor-driven or turbine-driven pumps, heat exchangers, motor-driven valves, air-driven valves, check valves, tanks, human actions, and common cause failures. Refer to Appendix A for the details of the model (Figure A-1 shows the accident sequences, SSCs Modeled in the Example State-Based PRA Model.

Table A-1 shows the list of components and systems included in the model, Figure A-2 to Figure A-10 show the revised fault trees for the state-based PRA model).

Table 5-1. An overview of the example state-based PRA model.

<table>
<tr><th>Model Element</th><th>Total Number</th><th colspan="2">Details</th></tr>
<tr><td rowspan="2">Accident Sequences</td><td rowspan="2">2</td><td>Sequence 3</td><td>IE-TRANS * SDC * LSHR</td></tr>
<tr><td>Sequence 18</td><td>IE-TRANS * FW * OTC</td></tr>
<tr><td rowspan="7">System Logic</td><td rowspan="7">7</td><td rowspan="4">4 Main System Logics</td><td>SDC</td></tr>
<tr><td>LSHR</td></tr>
<tr><td>FW</td></tr>
<tr><td>OTC</td></tr>
<tr><td rowspan="3">3 Transfer System Logics</td><td>HPR</td></tr>
<tr><td>CSR</td></tr>
<tr><td>CCS</td></tr>
<tr><td>Component State Diagrams</td><td>70</td><td colspan="2">Components, human actions, CCFs</td></tr>
</table>

Two unique aspects were encountered during the developing of the state-based PRA model. One is the input of failure probabilities for different component failure modes. For the fail-to-start failure mode, as well as the unavailability due to test and maintenance and human errors, the failure probabilities should be entered into the EMRALD directly. However, for the fail-to-run failure mode the failure rates instead of failure probabilities should be entered. For these basic events, the simulation model will use the input failure rate and the time passed since the simulation starts to estimate a time-at-failure for the component.

The second aspect is the treatment of common cause failure of a component. Figure 5-10 (right side) and Figure A-2 to Figure A-10 put CCFs at the same component failure mode level with other independent failures. For example, both the independent failures (LPI-MDP-FS-1A and LPI-MDS-FR-1A) and the CCFs (LPI-MDP-CF-STRT and LPI-MDP-CF-RUN) are at the same level under the component LPI-MDP-1A (right side of Figure 5-10). This kind of treatment is difficult to be implemented in the state-based PRA model. Instead, the CCFs, LPI-MDP-CF-STRT, and LPI-MDP-CF-RUN are modeled in a separate, special component state diagram. Figure 5-11 provides an example of a CCF state diagram along with the state diagrams of the common cause component group (CCCG) members. The CCF state diagram (right side of Figure 5-11) is at the same level as the other component state diagrams and provides inputs to its CCCG members (Pump A and Pump B at the left side of Figure 5-11).

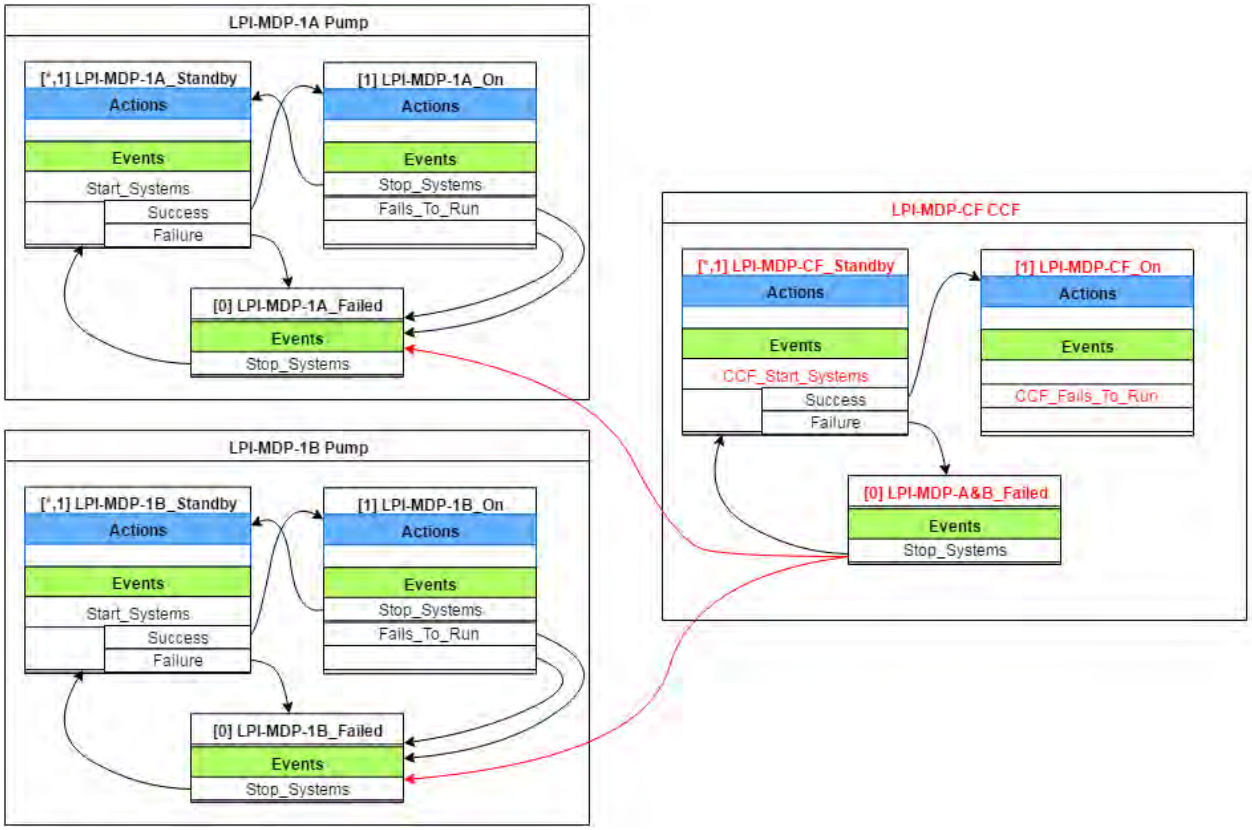

Figure 5-11. Example of a CCF state diagram (right) linking with component state diagrams (left).

During the development of the above example state-based PRA model, each of the seven system logic state models was tested with a minimum of 1,000,000 Monte Carlo simulation runs for debugging and benchmarking purpose. The simulation results of the state-based model were then compared with the SAPHIRE results for the same system logic and component data base. Table 5-2 presents the comparison results. It shows that the simulation results of the state-based system model are very close to those of the SAPHIRE model with the same system logic and component database, although for system logic with extremely low probability (e.g., LSHR system logic which has a failure probability of about 1E-9), the

simulation runs of the state-based system model might not be able to detect a failure even with hundreds of millions of simulation runs if using a naïve approach to the simulation.

Table 5-2. Benchmarking simulation results of the state-based system model with SAPHIRE results.

System	SAPHIRE	State-based System Model
AFW	1.3E-05	9.0E-06
OTC	2.7E-02	2.7E-02
SDC	5.5E-03	5.5E-03
LSHR (1)	1.1E-09	0
HPR	2.7E-04	2.4E-04
CSR (2)	6.3E-07	6.0E-07
CCS	5.5E-04	5.3E-04
Notes: (1) The LSHR fault tree was tested with 10 × 10,000,000 simulation runs. (2) The CSR fault tree was tested with 20,000,000 simulation runs.		

After the individual state-based system models were successfully tested, they were integrated to the state-based plant model (Figure 5-12), which was run with 25 × 10,000,000 simulations to check the sequence results with those from SAPHIRE. Note that the simulations at this stage are only for stochastic simulation with no plant physics such as the 3-D flooding simulation and not time-dependent considerations (e.g., time-based recovery actions, switching of standby components). Table 5-3 shows the comparison results between SAPHIRE and the state-based plant model. Accident Sequence 3 has an extremely low core damage frequency of about 5E-10 based on the SAPHIRE results. The state-based plant model shows a result of 0 for the sequence, meaning that it could not detect or verify the SAPHIRE results with the 250 million runs. Accident Sequence 18 has a higher CDF of 2.3E-7 per year based on the SAPHIRE results. The state-based plant model shows the same result of 2.3E-7 with millions of simulation runs.

Table 5-3. Benchmarking simulation results of the state-based plant model with SAPHIRE results.

Accident Sequence		SAPHIRE	State-based PRA Model
Seq. 3	IE-TRANS * SDC * LSHR	5.0E-10	0 (< 4E-9)
Seq. 18	IE-TRANS * AFW * OTC	2.3E-07	2.3E-07

The next stage of developing state-based PRA model is to incorporate 3-D simulation elements (flood initiating event, flood-caused failure events, and simulation related state/event) into current logic properly, to develop 3-D plant model and 3-D simulation model, and to link the 3-D simulation model to the PRA model. This stage of the state-based PRA model can start both the stochastic simulations and the 3-D flood simulations and monitor the component status from both the random failure side and the flood-caused failure side. When a monitored component fails in 3-D flood simulation, the change of status is fed back to the state-based PRA model and the component state is flagged with failure due to flood. Section 6 describes the process and results for such development.

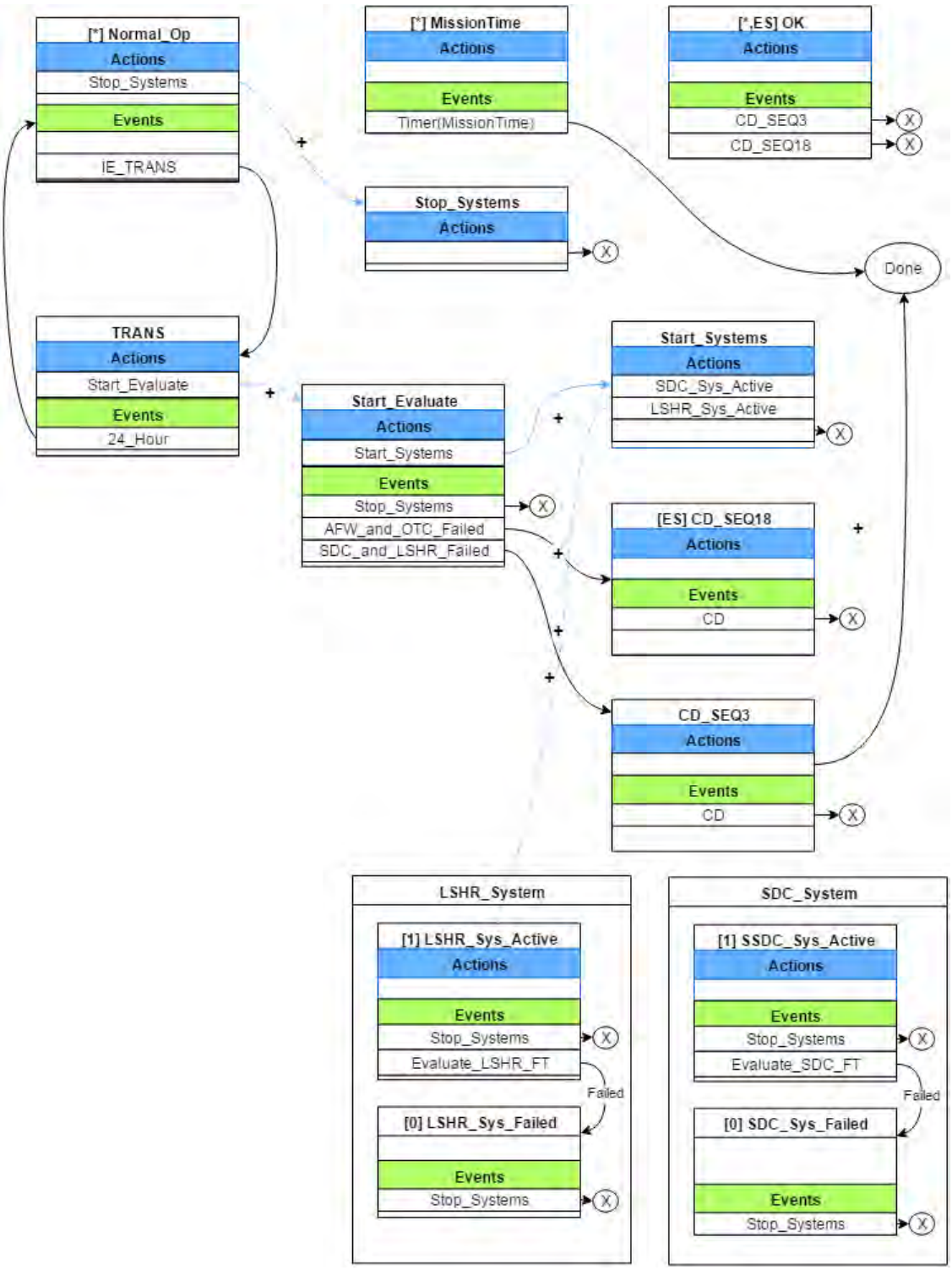

Figure 5-12. Plant state diagram of the example state-based PRA model (AFW and OTC systems are not shown in the diagram for simplicity reason).

6. 3-D SIMULATIONS AND PLANT RESPONSE MODEL QUANTIFICATION

This section presents the work performed for developing and quantifying integrated external flood plant response model. The integrated external flood plant response model incorporates 3-D flood simulations into the previously developed state-based PRA model (or EMRALD model) to represent the flooding scenarios and the plant response progress. A 3-D site terrain model was obtained for the interested plant with a web-based application that interacts with the Google Maps Elevation API [22]. A 3-D plant model was developed with available plant information such as layout drawings for a typical PWR plant. Flooding scenarios and pathways for the LIP case study were identified and characterized. 3-D simulation models were developed to emulate the flooding scenarios and communicate with the EMRALD model. The integrated external flood plant response model which accounts for both stochastic failures and flood-induced failures was quantified and compared with the corresponding SAPHIRE model.

6.1 3-D Site Terrain Model

To simulate the evolution of an external flooding event, a terrain map with the topography of the site area is needed. In this project, a web-based application, Web Terrain Mapper API, was used to obtain such information using the public available Google Maps Elevation API, which retrieves elevation levels from a set of points in a rectangular area anywhere on the surface of the earth (Figure 6-1). The input for the application includes the latitude and longitude of the left-bottom vertex of the selection rectangle, the width and height of the selection rectangle (in meters), and the resolution or scale (in meters). The output of the application is a visual representation of the defined area on a Google map and output the terrain map as a 3-D model.

Figure 6-1 shows an example usage of the terrain map application to retrieve the terrain map of a nuclear power plant site area. The results can be saved in .obj format and processed in 3-D software as in Figure 6-2.

Figure 6-1. Web Terrain Mapper API.

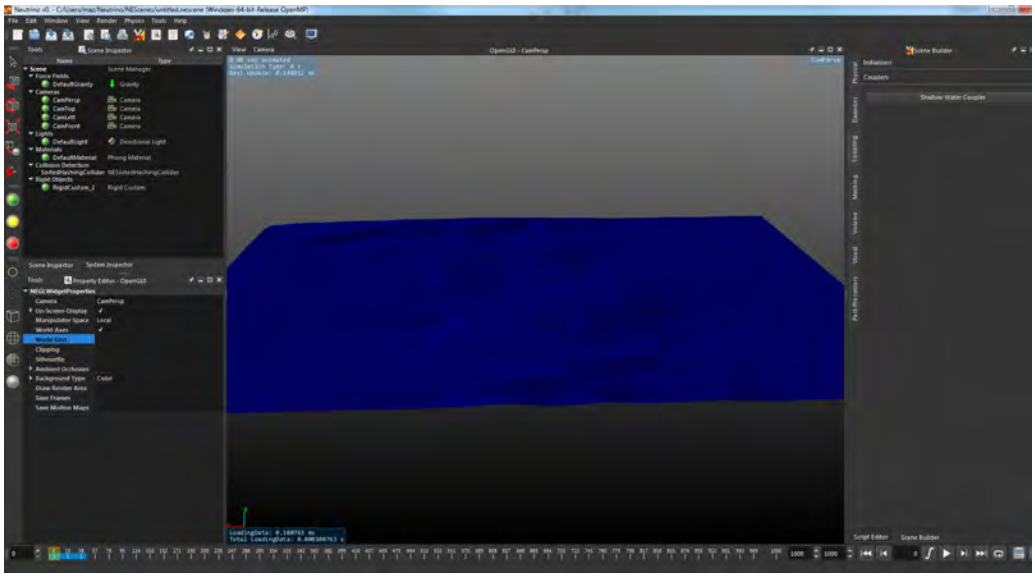

Figure 6-2. 3-D terrain map of an example nuclear plant site.

6.2 3-D Plant Model

To simulate the progression of a flooding event, a 3-D plant model must be developed using available plant information such as layout drawings. The level of details for the 3-D plant model could be varying as long as they are sufficient for the flooding scenarios to be simulated.

Figure 6-3 shows the 3-D model of a typical PWR that is used for the flood simulations in this project. The plant includes a Reactor Building, Fuel Building, Building C, Diesel Generator Building, Auxiliary Building, and Turbine Building. The external flooding event (caused by local intense precipitation) used in this scenario impacted Building C and two floor levels of the Auxiliary Building, which were modeled in much more details than other buildings.

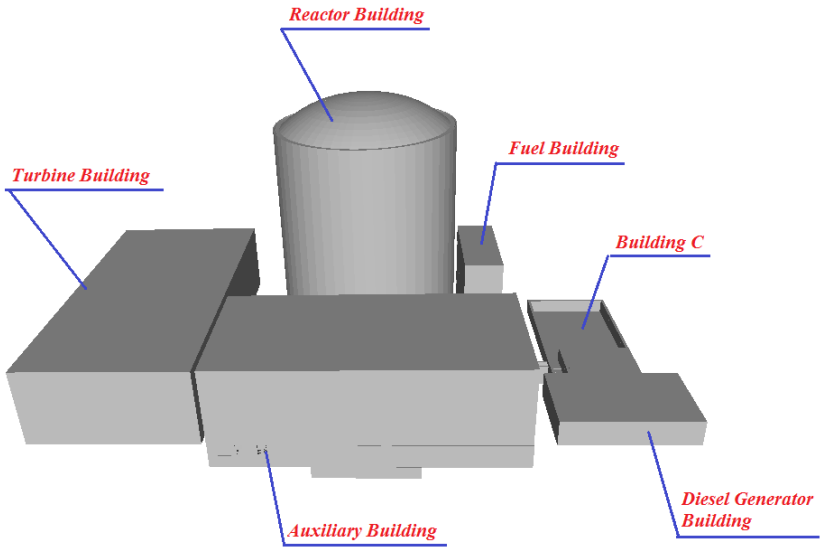

Figure 6-3. 3-D model of a typical PWR plant.

Figure 6-4, Figure 6-5, and Figure 6-6 show the detailed 3-D models of Building C, pipe tunnel, and Underground Levels 1 and 2 of the Auxiliary Building. In Figure 6-4, part of Building C has no roof. The rain fall on the building ground usually flows through the site drain system and does not accumulate in the building. However, if the site drain system is degraded, the water can accumulate and exceed the curb height to the pipe tunnel. The pipe tunnel is adjacent to the Auxiliary Building on its left side. There are numerous penetrations between Auxiliary Building and pipe tunnel. Although these penetrations are designed as flood barriers to prevent water invading from non-safety related structure (i.e., pipe tunnel) to safety related structure (i.e., Auxiliary Building), the flood seals might be degraded or even missed over the time when the plant was constructed and operated.

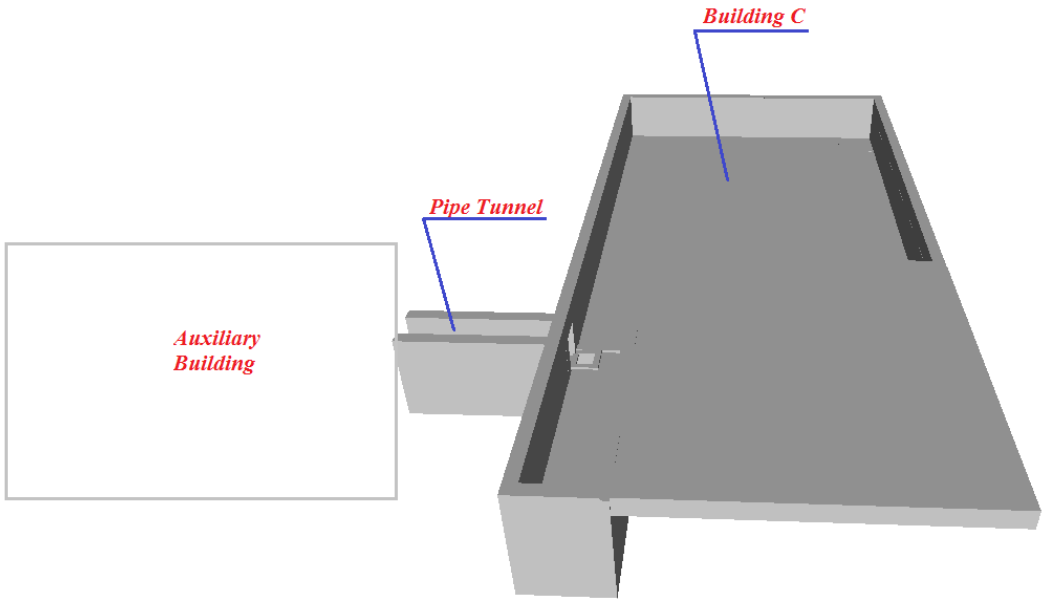

Figure 6-4. 3-D model of Building C and pipe tunnel.

Figure 6-5 shows Underground Level 1 of the Auxiliary Building with the Reactor Building on its top and pipe tunnel and Building C on its right. The central part of Underground Level 1 goes deeper to Underground Level 2 (Figure 6-6). Many risk-significant components are located in these two levels of the Auxiliary Building. For example, the following components are located in the area and also included in the example state-based PRA model:

Underground Level 1:

- Containment Spray Recirculation (CSR) heat exchangers which are also functioned as shutdown cooling (SDC) heat exchangers CSR-HTX-1A and CSR-HTX-1B
- Charging pumps CVC-PDP-1A, CVC-PDP-1B, and CVC-PDP-1C

Underground Level 2:

- Low pressure safety injection pumps LPI-MDP-1A and LPI-MDP-1B
- High pressure safety injection pumps HPI-MDP-1A and HPI-MDP-1B
- CSR pumps CSR-MDP-1A and CSR-MDP-1B.

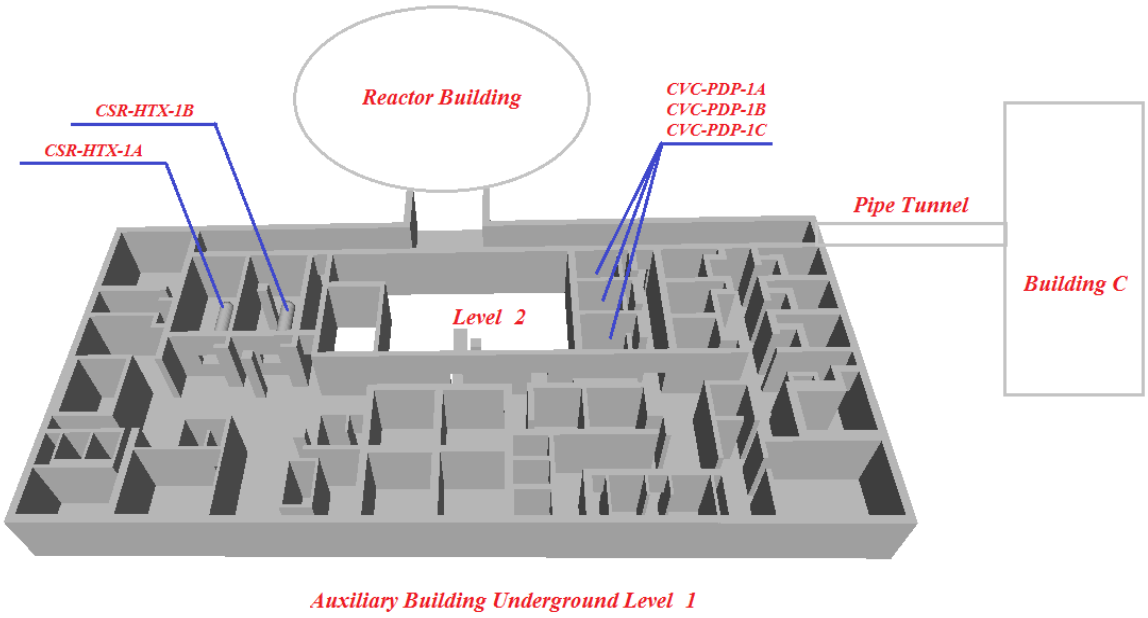

Figure 6-5. 3-D model of the Auxiliary Building Underground Level 1.

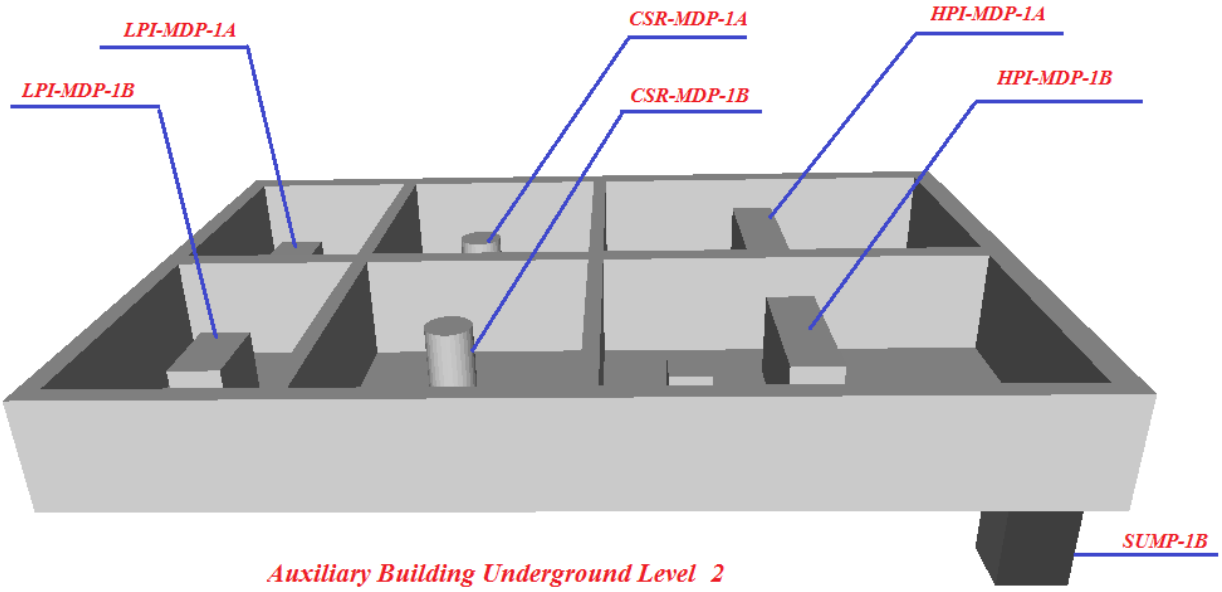

Figure 6-6. 3-D model of the Auxiliary Building Underground Level 2.

6.3 Flooding Pathway and Scenarios

The external flood event analyzed in this project is a local intense precipitation event combined with degraded site drain system and degraded flood barriers that occurred in a U.S. nuclear plant. For this project, the flood event was divided into four different stages based on the locations associated with the flooding: site and Building C, pipe tunnel that links Building C and Auxiliary Building, Underground Level 1, and Underground Level 2 of the Auxiliary Building.

Site and Building C

The external flood event analyzed in this project is a local intense precipitation event. All safety-related structures, such as the Reactor Building, Auxiliary Building, Fuel Building, and Diesel Generator Building, are designed with flood protection features including flood barriers to prevent water ingress from external flooding. For the site and non-safety-related structures, such as Building C part of which has no roof, the site drain system is designed to pull water away from the buildings and prevent water accumulation to cause damage. However, in a worse scenario, if the site drain system is degraded, the rainfall plus the backflow from degraded drain system could accumulate on the ground of Building C.

Pipe Tunnel between Building C and Auxiliary Building

When the water accumulates on the ground of Building C and exceeds the height of a curb of the manhole from Building C to the pipe tunnel, it starts to flow into the tunnel and accumulates in this lower section. If there is no outflow path from the pipe tunnel, the tunnel water level would increase continuously until it reaches the same water level as that of the Building C ground level. At this time, the water level would increase much slower due to the larger area of Building C.

Underground Level 1 of the Auxiliary Building

Figure 6-3 and Figure 6-4 show that the pipe tunnel is adjacent to the Auxiliary Building on its left side. There are numerous penetrations between the pipe tunnel and the Auxiliary Building. Although these penetrations are designed as flood barriers to prevent water invading from non-safety-related structures (i.e., pipe tunnel) to safety-related structures (i.e., Auxiliary Building), the flood seals might be degraded or even missed over the time when the plant was constructed and operated. With degraded flood barriers, the water accumulated on the tunnel side starts to flow through the degraded/opened penetrations into Underground Level 1 of the Auxiliary Building.

Underground Level 2 of the Auxiliary Building

After water intrudes through the pipe tunnel and degraded flood barriers into Underground Level 1 of the Auxiliary Building, it flows across the floor and is collected by the building drain system down to the two sumps of the emergency core cooling system (ECCS) safeguard pump rooms at Underground Level 2 of the Auxiliary Building. Figure 6-6 displays the one sump, Sump-1B, in the room of the HPI Pump 1B. The other sump, Sump-1A, is located at the corner of the LPI Pump 1A room (not displayed in Figure 6-6). Since the rooms house safety important components, an alarm would be announced in the Control Room if the water level in the sump reaches the predefined high value. The ECCS sump pumps would automatically start. However, since the inlet flow from the flooding Underground Level 1 is greater than the outlet flow by ECCS sump pumps, the water level in ECCS sumps would continue to increase. When the water level reaches a predefined high-high level, an alarm would prompt operators to close the drain valves and prevent ECCS pump damage from the flooding.

6.4 3-D Simulation Model

The 3-D simulation software Neutrino, developed by Neutrino Industries, has been used in previous INL projects [17-19] and was used in this project for LIP simulations. The Neutrino fluid solver is based on Smooth Particle Hydrodynamics [23] with a pressure solver to handle incompressible fluids. The fluid solver factors in accurate boundary handling and adaptive time stepping to help to increase accuracy and calculation speed. Neutrino can handle the memory requirements needed for large simulations while providing accurate fluid movement. The simulation network of Neutrino is flexible with a python-based expression system to accurately model the movement of the wave machine. Neutrino provides a variety of tools to measure parameters in a section of the fluid simulation, including flood height at a specific point; average pressure and average velocity in a certain area or volume; and flow rate across a certain area or volume. Also, the Neutrino solve engine and options are customizable.

3-D simulation models would combine the 3-D terrain model and 3-D plant models developed in previous sections. Figure 6-7 shows an overview of the site 3-D simulation model. Figure 6-8 shows the 3-D simulation model for the Auxiliary Building (both Underground Level 1 and Underground Level 2), Building C, and the tunnel that connects the two buildings.

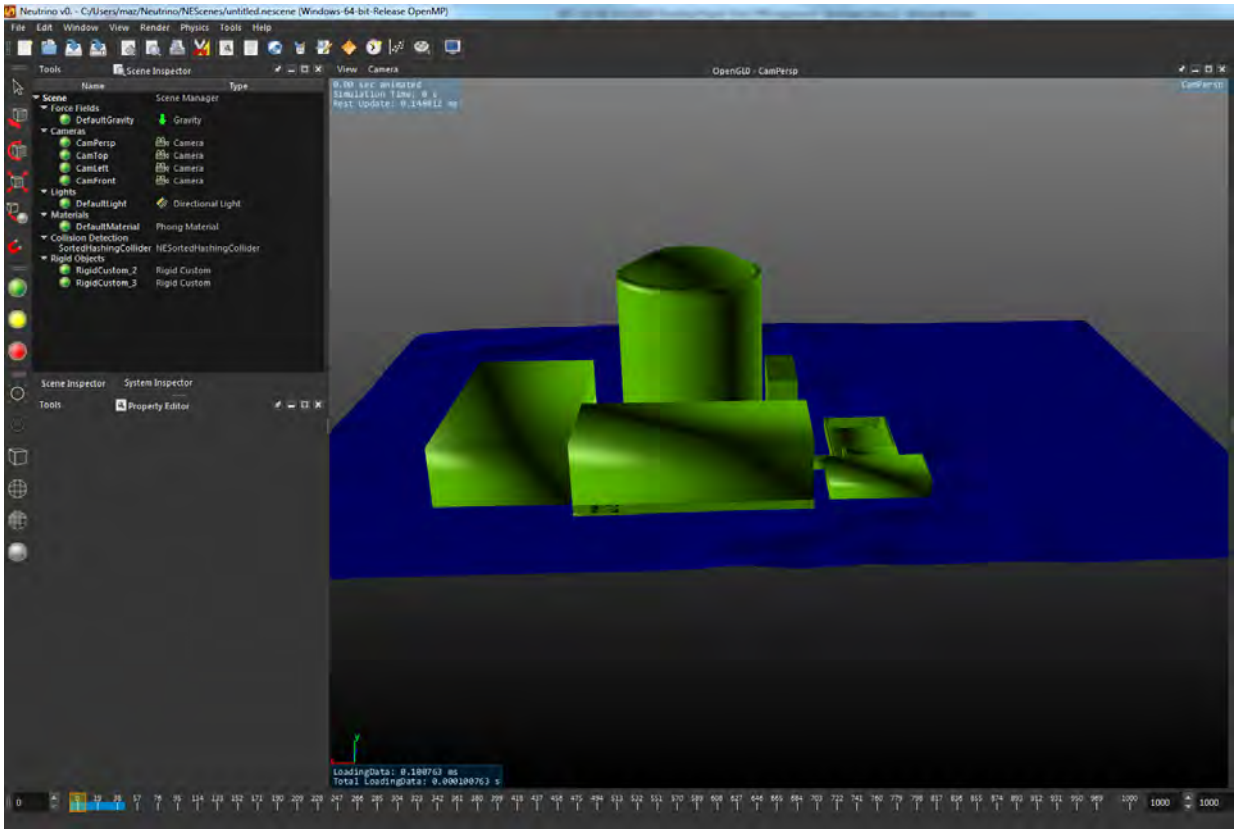

Figure 6-7. 3-D simulation model – overview of the site.

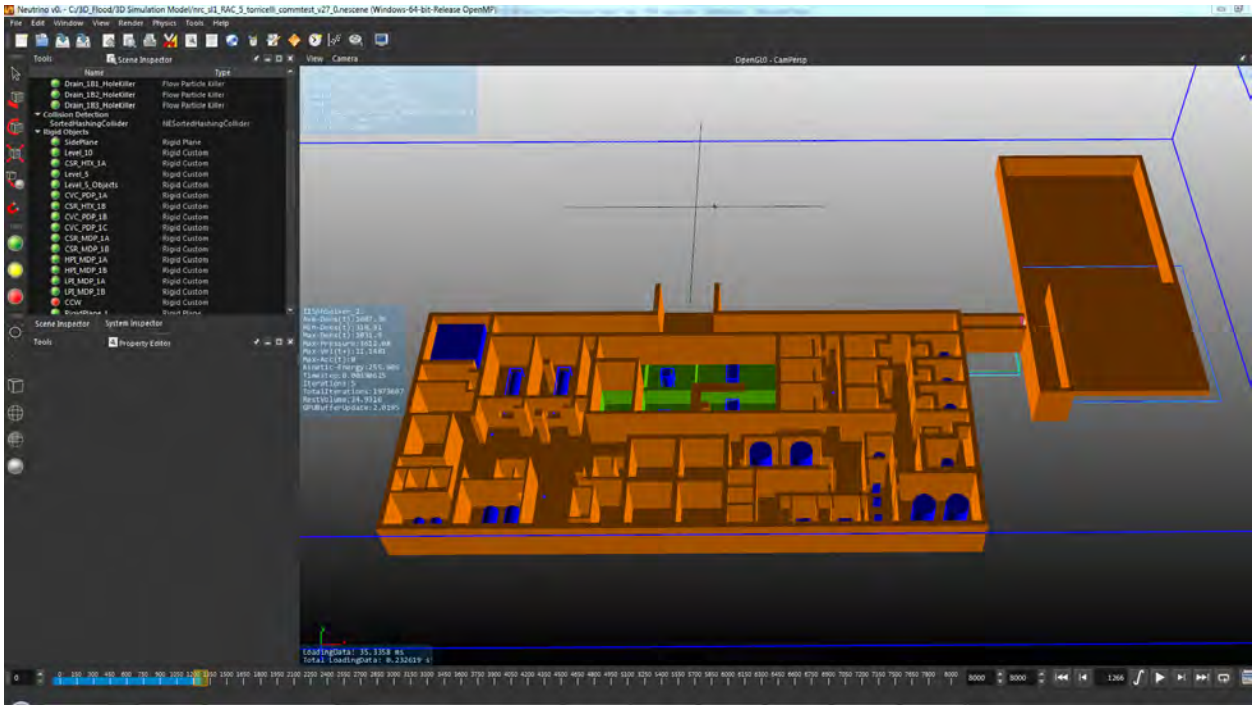

Figure 6-8. 3-D simulation models – Auxiliary Building, Building C, and Tunnel.

The flooding scenarios can be simulated using the above 3-D models with setup in Neutrino. One issue during the 3-D simulation setup relates with water flowing from one place to another place through an open hole. For example, when the water level in Building C exceeds the curb of the open hole, water starts flowing to the tunnel underneath the hole; when water accumulates in the tunnel and exceeds the level of the degraded conduit on the wall, water flows to Underground Level 1 of the Auxiliary Building through the conduit; after water flows into Underground Level 1 of the Auxiliary Building, it would flow to Underground Level 2 of the building by the floor drain system. To correctly simulate such kinds of water flowing path, the flow rate must be determined in Neutrino so that the same amount of water would be transported from one side of the open hole to the other side. This flow rate could be estimated by the Torricelli's Theorem with a Borda's mouthpiece:

$$\dot{V} = CA\sqrt{2gh} \tag{4}$$

Where:

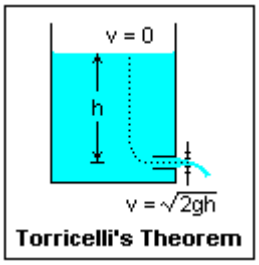

$\dot{V}$: volumetric flow rate that water enters RAB through the degraded conduit

C : discharge coefficient

A : opening conduit area

g: nominal gravitational acceleration

h: the pipe tunnel water level above the degraded conduit.

A new function called Torricelli Emitter was developed in Neutrino based on the Torricelli's Theorem. Appendix B presents the implementation of the function in Neutrino.

6.5 Revising EMRALD Model with 3-D Simulation Elements

To integrate the state-based PRA model with 3-D simulations, the example EMRALD model developed in Section 5.4 was revised to incorporate 3-D simulation elements (flood initiating event, flood-caused failure events, and simulation related state/event) into the logic. Changes were made on different levels of the EMRALD model: component state diagrams, system state diagrams, and plant state diagram.

Figure 6-9 shows an example of revising component state diagram LPI-MDP-1A to add the flood-induced failure event, 3-D_Sim_Flooded, to the diagram. The new component state diagram now consists of both the flood-induced failure event as well as other failure events that are not induced by the flood.

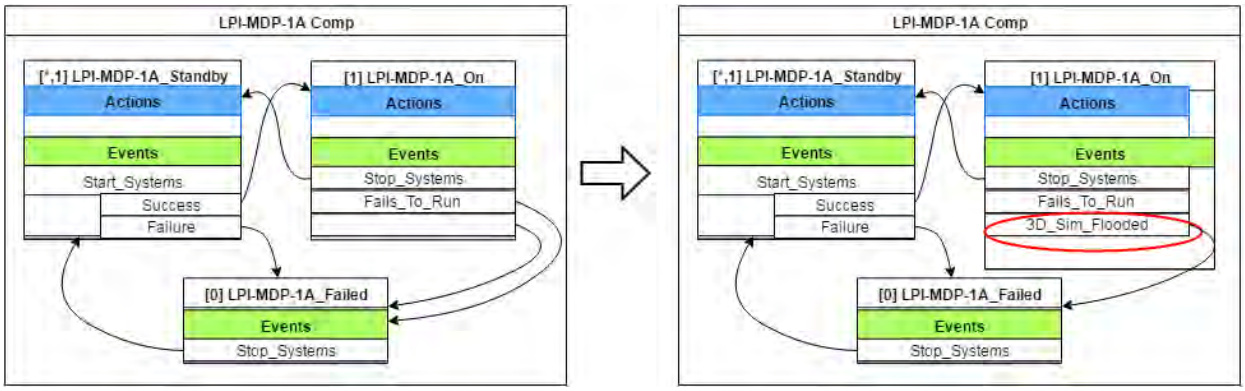

Figure 6-9. Component state diagram with flood-caused failure event.

Figure 6-10 presents the new plant state diagram that incorporates 3-D flood simulation elements. The external flood initiating event, IE-FLE-LIP, was added to the initiating event list. The 3-D simulation state was added to start 3-D simulations as required. The PRA model would communicate with the 3-D simulation models. When one or more modeled components are failed in 3-D simulations due to the flood, the result feeds back to the PRA model. The impacted component would be flagged as failed due to the flooding event. The flood-induced failures are then evaluated along with other random component failures and human action failures for the system logic and sequences with Monte Carlo simulation runs.

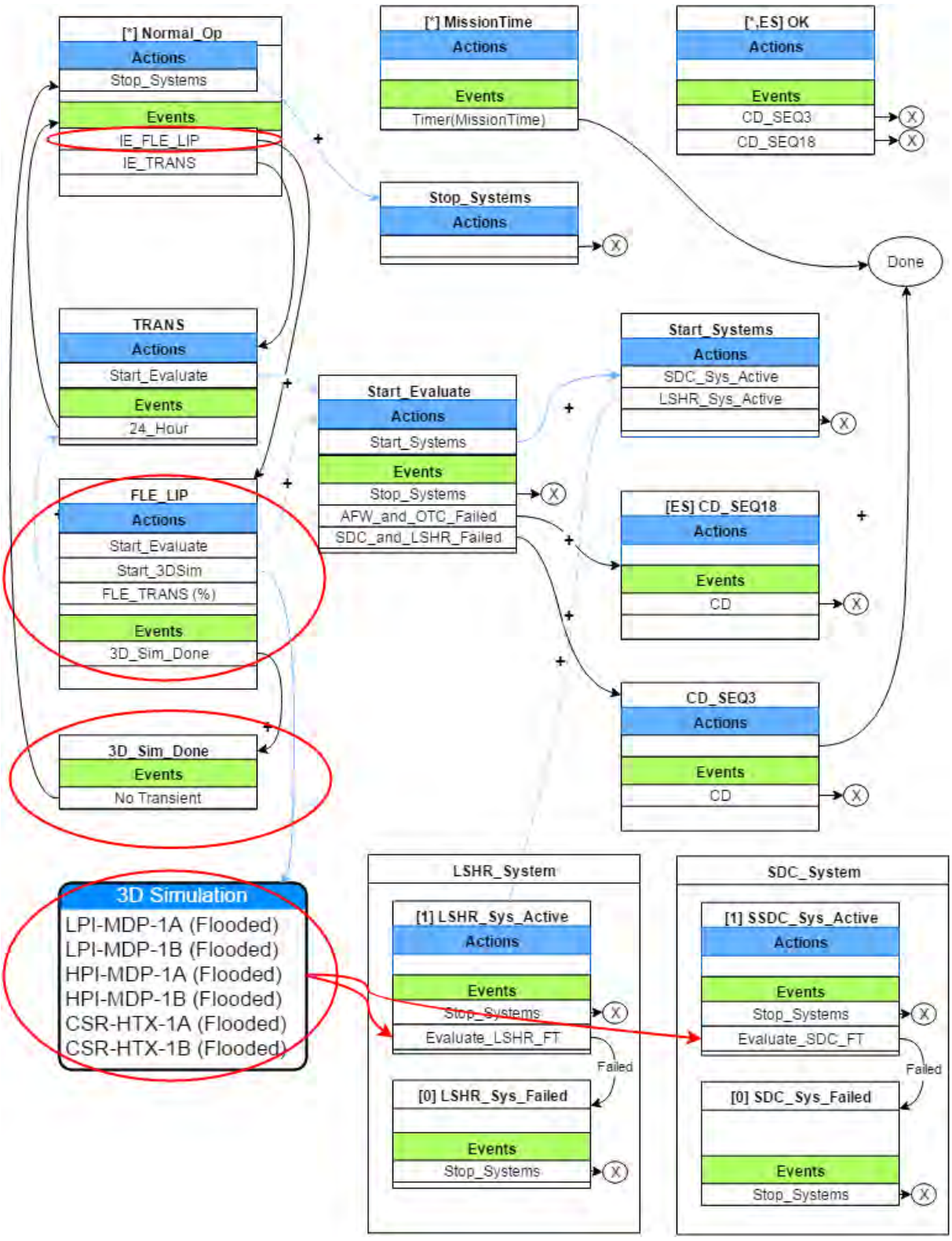

Figure 6-10. Plant state diagram with 3-D flood simulation elements.

6.6 Integrated EMRALD Model Quantification

6.6.1 Stochastic Layering

Initially the stochastic component failures were modeled concurrently with the flood-caused or 3-D simulation failures. However, to see the importance of random failures, one would need to run the 3-D simulations many more times than the failure rate of the system. For the state-based PRA model example described in Section 5, even if all the components subject to flood impact (refer to Section 6.2 for the component list) are failed in the 3-D simulation, the failure rate for Sequence 18 is still in the 1E-6 range. This means that unless the 3-D simulations are run more than 1,000,000 times it would not likely see the effects from random failures and hit the sequence failure (or core damage) end state. For this model, each simulation of a 2-hour flooding event would take about 20 hours, which means formidable computational cost and impractical solution if using a naïve approach.

To overcome this issue, we separated the 3-D simulation sampling and the stochastic component failures into two different "layers" for analysis. 3-D simulation sampling for an LIP event (namely, the precipitation rate of gallon per minute, or gpm) is conducted first. After the sampling, we repeatedly sampled for the random component failures using the same results from the 3-D simulation and evaluated the system. If the system fails "N times" in the stochastic loop, the conditional failure probability of the sequence for the sampled rainfall event equals to (N/Stochastic runs). Upon completing the full range LIP precipitation rates sampling, the total failure rate for each sequence is the summed rate from each run divided by the total number of sampling events.

6.6.2 Quantification Results and Comparison

The revised state-based PRA model was run on five clustered Windows-based PC servers named from Minion 1 to Minion 5, which took about 10 seconds computation time for 1 second simulation time and about 1 day to simulation a 2-hr flooding event. Each server had run eight 3-D flood simulations with various flooding rates that were generated by sampling the pre-defined precipitation rates and their frequencies. Six of the 40 flood simulation runs have had particles disappeared during the simulations and thus were discarded (this issue was later fixed in the Neutrino software). For the remaining 34 flood simulations, each of them was linked to the EMRALD PRA model, which evaluated both flood-induced failures from the 3-D simulation and non-flood induced failures by sampling for random component failures and human failures. Table 6-1 shows the 3-D flood simulations and EMRALD model results. The "3-D Sim. Run" column lists thirty-four 3-D simulation runs with the run number representing the Minion computer number and the run number on that computer. The flood rate, in gallons per minute, sampled in each 3-D simulation run is provided. The conditional failure probability results for Sequence 3 and Sequence 18 of the EMRALD model are provided along with the components that failed in the simulations.

To compare the EMRALD model results with those of the corresponding SAPHIRE model, the thirty-four simulation runs in Table 6-1 were firstly ordered by the flow rate, and then grouped into the same scenario if the simulation runs have the same flood-induced component failure list. The process generates a total of six scenarios. In Scenario 1, the flow rate is less than 609 gpm and there is no flood-induced component failure. In Scenario 2, the flow rate is in the range of 642 to 668 gpm, and the HPI Pump B fails. In Scenario 3, the flow rate is from 696 to 731 gpm and the HPI Pump B and CSR Pump B fail. In Scenario 4, the flow rate is from 737 to 824 gpm and the HPI Pump B, CSR Pump B, and LPI Pump B fail. In Scenario 5, the flow rate is from 827 to 992 gpm and all LPI and CSR pumps (Pump A and Pump B) and HPI Pump B fail. In Scenario 6, the flow rate is from 1010 to 1030 gpm and all HPI, LPI, and CSR pumps fail. Then for the corresponding SAPHIRE model, one change set was created for each scenario (except for Scenario 1 in which there is no flood-induced component failure) to represent the associated component failures in the scenario. The SAPHIRE model was then quantified with the related change set to obtain results for each scenario.

In a static PRA like the SAPHIRE model, an analyst will typically describe component failures with an overall failure probability or will decompose this probability into specific failure mode basic events (e.g., fails to start, fails to run, fails due to common-cause). In the dynamic analysis, we incorporated fails to start, fails to run, and dependent failure modes in the details of the model. However, note that these failure modes are not explicitly called out in the "Component Failure" column of Table 6-1. In a more detailed analysis, these results would be decomposed into more detailed outputs since they are readily obtained from the simulation results. Further, the dynamic simulation also provides additional details such as the time when components fail, the failure causes (random or flood-caused) for the components failed, the sequential order at which components fail, the depth of water at the time of component failure, etc. Consequently, the dynamic approach described in this report can provide both "static types" of results plus additional information beyond the cut set level results found in a static PRA.

Table 6-2 presents the comparison of the EMRALD model simulation results with the corresponding SAPHIRE PRA model results from the traditional event tree/fault tree approach. A summary of the comparison is provided below.

- For Scenario 1 (flow rate less than 609 gpm), there is no flood-induced failures occurred and the SAPHIRE and EMRALD model results are similar with the base case in Section 5.4 where the EMRALD model does not include 3-D simulation elements in the state diagrams, i.e., 2.3E-7 of SAPHIRE versus 2.0E-7 of EMRALD for Sequence 18, and 5.0E-10 of SAPHIRE versus 0 of EMRALD in which the failure is not detectable due to very low probability for Sequence 3.
- For Scenarios 2 to 5, the SAPHIRE model estimates that the conditional failure probabilities for Sequence 18 are the same 2.7E-7, slightly higher than the base case of 2.3E-7. In these scenarios, one or more pumps, but not all of them, in the High-Pressure Injection, Low Pressure Injection, and Containment Spray Recirculation systems fail. At least one injection pump (high pressure or low pressure) is available to provide coolant to the core. In comparison, the EMRALD model predicts a failure probability of around 4E-7 for Sequence 18 (with a range of 3.8E-7 to 4.5E-7).
- For Scenario 6, in which all HPI, LPI, and CSR pumps fail, the SAPHIRE model estimates that the conditional failure probability for Sequence 18 is 8.6E-6, while the EMRALD model has a slightly higher estimation of 1.3E-5.
- For Sequence 3 in Scenarios 2 to 4, in which Pump B of HPI, CSR, or LPI system fails, the SAPHIRE model estimates a conditional failure probability of about 1E-9. The EMRALD model could not detect the failure in millions of simulation runs.
- For Sequence 3 in Scenario 5, in which all LPI pumps plus Pump B of HPI and CSR systems fail, the SAPHIRE model estimates a conditional failure probability of 1.3E-7. The sequence failure probability is elevated from the previous scenarios as all LPI pumps fail and could not provide shutdown cooling, which is a key function for the sequence. The EMRALD model estimates the sequence failure probability of 2.0E-7.
- For Sequence 3 in Scenario 6, in which all HPI, LPI, and CSR pumps fail, the SAPHIRE model estimated a conditional failure probability of 3.2E-6 while the EMRALD model has a slightly higher estimation of 3.8E-6.

Table 6-1. 3-D flood simulations and EMRALD model results.

3-D Sim. Run	Flood Rate (gpm)	Precipitation Rate (in/hr)	Seq. 18 Prob.	Seq. 3 Prob.	Component Failure
1-2	1010	6.48	1.1E-05	3.5E-06	CSR_MDP_1A_Failed, CSR_MDP_1B_Failed, HPI_MDP_1A_Failed, HPI_MDP_1B_Failed, LPI_MDP_1A_Failed, LPI_MDP_1B_Failed
1-3	919	5.90	2.0E-07	2.0E-07	CSR_MDP_1A_Failed, CSR_MDP_1B_Failed, HPI_MDP_1B_Failed, LPI_MDP_1A_Failed, LPI_MDP_1B_Failed
1-4	731	4.69	7.0E-07	0.0E+00	CSR_MDP_1B_Failed, HPI_MDP_1B_Failed
1-5	737	4.73	4.0E-07	0.0E+00	CSR_MDP_1B_Failed, HPI_MDP_1B_Failed, LPI_MDP_1B_Failed
1-7	702	4.51	4.0E-07	0.0E+00	CCW_HTX_1B_Failed, CSR_MDP_1B_Failed, HPI_MDP_1B_Failed
1-8	700	4.49	2.0E-07	0.0E+00	CSR_MDP_1B_Failed, HPI_MDP_1B_Failed
2-1	763	4.90	3.0E-07	0.0E+00	CSR_MDP_1B_Failed, HPI_MDP_1B_Failed, LPI_MDP_1B_Failed
2-2	839	5.38	1.0E-07	1.0E-07	CSR_MDP_1B_Failed, HPI_MDP_1B_Failed, HPI_XHE_FB_Failed, LPI_MDP_1A_Failed, LPI_MDP_1B_Failed
2-3	609	3.91	2.0E-07	0.0E+00	
2-5	873	5.61	5.0E-07	1.0E-07	CSR_MDP_1B_Failed, HPI_MDP_1B_Failed, LPI_MDP_1A_Failed, LPI_MDP_1B_Failed
2-6	772	4.96	4.0E-07	0.0E+00	CSR_MDP_1B_Failed, HPI_MDP_1B_Failed, LPI_MDP_1B_Failed
2-7	668	4.29	5.0E-07	0.0E+00	HPI_MDP_1B_Failed
2-8	992	6.37	5.0E-07	5.0E-07	CSR_MDP_1A_Failed, CSR_MDP_1B_Failed, HPI_MDP_1B_Failed, LPI_MDP_1A_Failed, LPI_MDP_1B_Failed
3-1	594	3.82	2.0E-07	0.0E+00	
3-2	696	4.47	4.0E-07	0.0E+00	CSR_MDP_1B_Failed, HPI_MDP_1B_Failed
3-3	785	5.04	5.0E-07	0.0E+00	CSR_MDP_1B_Failed, HPI_MDP_1B_Failed, LPI_MDP_1B_Failed
3-4	642	4.12	3.0E-07	0.0E+00	CSR_MDP_1B_Failed, HPI_MDP_1A_Failed, HPI_MDP_1B_Failed
3-5	802	5.15	6.0E-07	0.0E+00	CSR_MDP_1B_Failed, HPI_MDP_1B_Failed, LPI_MDP_1B_Failed
3-6	820	5.26	2.0E-07	0.0E+00	CSR_MDP_1B_Failed, HPI_MDP_1B_Failed, LPI_MDP_1B_Failed
3-7	656	4.21	4.0E-07	0.0E+00	HPI_MDP_1B_Failed
3-8	747	4.79	2.0E-07	0.0E+00	CSR_MDP_1B_Failed, HPI_MDP_1B_Failed, LPI_MDP_1B_Failed
4-1	824	5.29	5.0E-07	0.0E+00	CSR_MDP_1B_Failed, HPI_MDP_1B_Failed, LPI_MDP_1B_Failed
4-2	664	4.26	6.0E-07	0.0E+00	HPI_MDP_1B_Failed
4-4	710	4.56	1.0E-07	0.0E+00	CSR_MDP_1B_Failed, HPI_MDP_1B_Failed, LPI_MDP_1B_Failed

Table 6-1. (continued)

3-D Sim. Run	Flood Rate (gpm)	Precipitation Rate (in/hr)	Seq. 18 Prob.	Seq. 3 Prob.	Component Failure
4-5	869	5.58	5.0E-07	1.0E-07	CSR_MDP_1B_Failed, HPI_MDP_1B_Failed, LPI_MDP_1A_Failed, LPI_MDP_1B_Failed
4-6	823	5.28	8.0E-07	0.0E+00	CSR_MDP_1B_Failed, HPI_MDP_1B_Failed, LPI_MDP_1B_Failed
4-7	699	4.49	5.0E-07	0.0E+00	CSR_MDP_1B_Failed, HPI_MDP_1B_Failed
4-8	873	5.61	3.0E-07	4.0E-07	CSR_MDP_1B_Failed, CVC_PDP_1A_Failed, HPI_MDP_1B_Failed, LPI_MDP_1A_Failed, LPI_MDP_1B_Failed
5-1	801	5.14	1.0E-07	0.0E+00	CSR_MDP_1B_Failed, HPI_MDP_1B_Failed, LPI_MDP_1B_Failed
5-2	950	6.10	6.0E-07	2.0E-07	CSR_MDP_1A_Failed, CSR_MDP_1B_Failed, HPI_MDP_1B_Failed, LPI_MDP_1A_Failed, LPI_MDP_1B_Failed
5-4	1030	6.61	1.4E-05	4.1E-06	CSR_MDP_1A_Failed, CSR_MDP_1B_Failed, HPI_MDP_1A_Failed, HPI_MDP_1B_Failed, LPI_MDP_1A_Failed, LPI_MDP_1B_Failed
5-5	850	5.46	4.0E-07	1.0E-07	CSR_MDP_1B_Failed, HPI_MDP_1B_Failed, LPI_MDP_1A_Failed, LPI_MDP_1B_Failed
5-7	827	5.31	3.0E-07	1.0E-07	CSR_MDP_1B_Failed, HPI_MDP_1B_Failed, LPI_MDP_1A_Failed, LPI_MDP_1B_Failed
5-8	818	5.25	4.0E-07	0.0E+00	CSR_MDP_1B_Failed, HPI_MDP_1B_Failed, LPI_MDP_1B_Failed

Table 6-2. Comparison of EMRALD model and SAPHIRE model results.

Scenario Group	3-D Sim. Run	Flood Rate (gpm)	Precipitation Rate (in/hr)	Model	Component Failure	Seq. 18 Prob.	Seq. 3 Prob.
1	2-3 3-1	< 609	< 3.91	SAPHIRE	No Change Set	2.3E-07	5.0E-10
				EMRALD	None	2.0E-07	0.0E+00
2	2-7 3-4 3-7 4-2	642 - 668	4.12 - 4.29	SAPHIRE	Change Set FLOOD_HPI-B (HPI-B pump failed)	2.7E-07	7.7E-10
				EMRALD	HPI-B pump failed	4.5E-07	0.0E+00
3	1-4, 1-7 1-8, 3-2 4-4, 4-7	696 - 731	4.47 - 4.69	SAPHIRE	Change Set FLOOD_HPI-B_CSR-B (HPI-B, and CSR-B pumps failed)	2.7E-07	7.7E-10
				EMRALD	HPI-B, and CSR-B pumps failed	3.8E-07	0.0E+00
4	1-5, 2-1, 2-6 3-3, 3-5, 3-6 3-8, 4-1, 4-6 5-1, 5-8	737 - 824	4.73 - 5.29	SAPHIRE	Change Set FLOOD_LPI-B_HPI-B_CSR-B (LPI-B, HPI-B, and CSR-B pumps failed)	2.7E-07	1.9E-09
				EMRALD	LPI-B, HPI-B, and CSR-B pumps failed	4.0E-07	0.0E+00
5	1-3, 2-2, 2-5 2-8, 4-5, 4-8 5-2, 5-5, 5-7	827 - 992	5.31 - 6.37	SAPHIRE	Change Set FLOOD_LPI_HPI-B_CSR (All LPI and CSR pumps and HPI-B pump failed)	2.7E-07	1.3E-07
				EMRALD	All LPI and CSR pumps and HPI-B pump failed	3.8E-07	2.0E-07
6	1-2 5-4	1010-1030	6.48-6.61	SAPHIRE	Change Set FLOOD_LPI_HPI_CSR (All LPI, HPI, CSR pumps failed)	8.6E-06	3.2E-06
				EMRALD	All LPI, HPI, CSR pumps failed	1.3E-05	3.8E-06

In general, the EMRALD model predictions are very close to those from the SAPHIRE model. Different from using change sets in SAPHIRE for various component failure scenarios, the EMRALD model uses 3-D dynamic simulations to visually demonstrate which components would fail under which flooding scenarios and flood parameters and evaluate the impacts these failed components and flood event would have on the plant. The above example shows that for this specific case study (with the input and boundary conditions discussed later) when the flood rate is less than 609 gpm for 2 hours, there is no flood-induced component failures for those monitored components in the EMRALD model. When the flood rate increases to 642 gpm, the HPI Pump B will fail due to the flood as water accumulates in the pump room with large drain system from the above floor. When the flood rate increased to 696 gpm, CSR Pump B will also fail due to the water flow through the openings between the HPI Pump B room and the CSR Pump B room. When the flood rate increases to 737 gpm, LPI Pump B fails due to the water flow through the openings between the LPI Pump B room and the CSR Pump B room. When the flood rate increases to 827 gpm, LPI Pump A fails as the water accumulates in the pump room with smaller drain system from the above floor. Finally, when the flood rate increases to 1010 gpm, HPI Pump A and CSR Pump A fail with the water flow through the openings between the Pump A rooms.

Note that the above results are based on the specific EMRALD and SAPHIRE models discussed in Section 5 and Section 6. Important inputs and assumptions for this case study are presented below:

1. The SAPHIRE model in the case study represents a typical PWR PRA model, which includes the simplified external flood-induced transient event tree as shown in Figure 5-9, the associated fault trees, and the related data.
2. The EMRALD logic model in the case study is presented in Appendix A, which is based on the SAPHIRE model and revised as necessary.
3. Section 6.3 describes the flooding pathway and scenarios that are considered in this project.
4. The flood event in the case study is caused by heavy rainfall and degraded site drain system. Flooding occurred in three buildings/places: Building C, the tunnel between Building C and Auxiliary Building, and the Auxiliary Building (Underground Level 1 and Underground Level 2).
5. The water flows from Building C to the tunnel by an elevated 2 feet × 2 feet opening on the ground of Building C.
6. A 3-inch conduit between the tunnel and the Auxiliary Building is degraded and assumed to be fully open for water flow from the tunnel to the Auxiliary Building.
7. In the Auxiliary Building, there are three drains (two are 4 inch, one is 3 inch) from Underground Level 1 to the High-Pressure Injection Pump B room at Underground Level 2. There are two drains (one 4 inch and the other one 3 inch) from Underground Level 1 to the Low-Pressure Injection Pump A Room at Underground Level 2. All the drains can be manually closed by operators in order to protect these pumps from flood damage.
8. There are small openings (6 inch × 6 inch) between HPI Pump B Room and CSR Pump B Room, CSR Pump B Room and LPI Pump B Room, LPI Pump A Room and CSR Pump A Room, and CSR Pump A Room and HPI Pump A Room.
9. Besides the HPI, LPI, CSR pumps at Underground Level 2, CVC pumps, CSR heat exchangers, and AC cabinets at Underground Level 1 are also modeled and monitored in the 3-D dynamic simulations. It is assumed that these components have different fragilities for different flood heights (see Appendix A3 for different failure probabilities corresponding to various flood heights). However, for the case study in this report, only Flood Height 1 with failure probability of 1.0 is modeled in the EMRALD.
10. It is assumed that sump drain pumps located at the ECCS pump rooms are not available to drain the water out from the Auxiliary Building.

11. Since all risk-significant and flood vulnerable components in this case study are located at the Auxiliary Building, 3-D dynamic simulations are later focused on this building. The flooding at the Building C and the tunnel are modeled at early stage and used to verify the water flow rate to the Auxiliary Building.
12. The thirty-four 3-D dynamic simulation runs represent the sampled flood rate (constant for each run) that last for 2 hours. The simulations assume that operators failed to take action to close the drain valves. A couple of sensitivity runs are performed for the two runs in Scenario 6 (Run 1-2 with 1010 gpm and Run 5-4 with 1030 gpm flood rate) so that operators close the drain at 1 hour for Run 1-2 and 30 minutes for Run 5-4. There are no flood-induced component failures in both sensitivity runs.

Another assumption that has been used to convert the flood rates (in the unit of gallon per minute) for simulation scenarios in Tables Table 6-1 and Table 6-2 to the precipitation rate (in the unit of inch/hour) is that the precipitation effective area is 15,000 ft^2. It would be interesting if the flood rate/precipitation rate in the simulation scenarios could be connected to the GEV model-predicted precipitation frequency in Section 3. Table 6-3 shows the precipitation frequency ranges, estimated from the GEV model and Table 3-5 (as a 2-hour duration event), that would be corresponding to the flood simulation scenario groups by comparing the 2-hour precipitation amounts between the scenario and the GEV model. Note that this table does not account for the back flow from the degraded site drain system to the building. For Scenario Group 6, the precipitation amount in the simulations is from 12.96 to 13.22 inches, which could be a 2E-6 to 1E-6 per year LIP event if the back flow from the site drain system is not accounted for. However, depending on the contribution from the degraded site drain system, it could be a 1E-4 or 1E-3 per year LIP event.

Figure 6-11 shows a screenshot of 3-D simulation inside Building C and pipe tunnel. Figure 6-12 shows the 3-D simulation in Underground Level 1 of the Auxiliary Building.

Table 6-3. Precipitation frequency ranges for the flood simulation scenario groups (2-hour duration).

Scenario Group	Flood Simulations			GEV Model (from Table 3-5)		Component Failure
	Flood Rate (gpm)	Precipitation Rate (in/hr)	Precipitation Amount (in)	Precipitation Amount (in)	Precipitation Frequency (/yr)	
1	< 609	< 3.91	<7.82	7.31	1.0E-03	None
				7.88	5.0E-04	
2	642 - 668	4.12 - 4.29	8.24 - 8.58	8.62	2.0E-04	HPI-B pump failed
3	696 - 731	4.47 - 4.69	8.94 - 9.38	9.19	1.0E-04	HPI-B, and CSR-B pumps failed
4	737 - 824	4.73 - 5.29	9.46 - 10.58	9.77	5.0E-05	LPI-B, HPI-B, and CSR-B pumps failed
				10.56	2.0E-05	
5	827 - 992	5.31 - 6.37	10.62 - 12.74	11.17	1.0E-05	All LPI and CSR pumps and HPI-B pump failed
				11.79	5.0E-06	
6	1010-1030	6.48-6.61	12.96 - 13.22	12.63	2.0E-06	All LPI, HPI, CSR pumps failed
				13.28	1.0E-06	

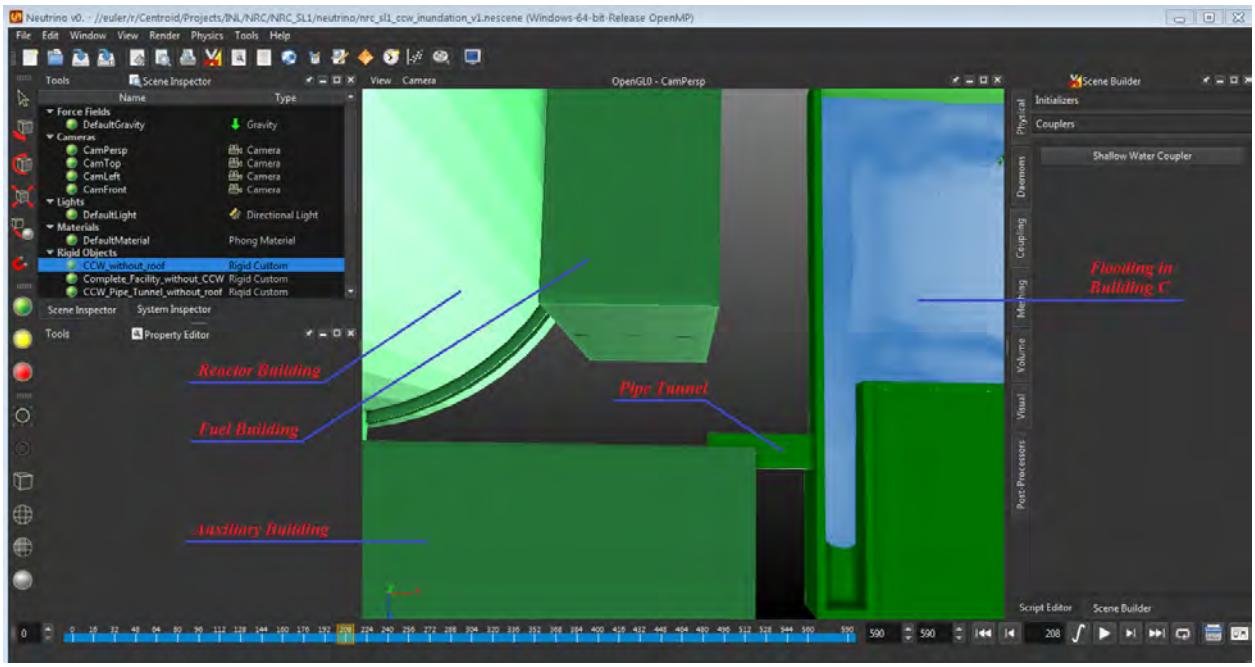

Figure 6-11. 3-D simulation – Building C and pipe tunnel.

Figure 6-12. 3-D simulation – Auxiliary Building Underground Level 1.

7. INSIGHTS AND LESSONS LEARNED

The objective of this project is to develop possible approaches to investigate plant response to flooding events. Dynamic analysis approaches that depict scenarios through simulation methods were investigated in the project. A framework to perform simulation-based flooding analysis was developed. A combination of margins analysis, mechanistic physics-based modeling, and probabilistic risk assessment approaches are considered in the project. A LIP event was used as a case study of this project for plant response. As an exploratory research activity, the project answered many questions, but leaves other questions for discussions and further investigation. The insights and lessons learned from the project and the discussion with the NRC staff are presented in this section.

1. The project investigates and applies the simulation-based dynamic approach in modeling plant response to external flooding events – this approach has several appealing features. Dynamic methods are useful when complexities such as time, space, and physical phenomena behavior drive the scenarios. It provides a natural framework to both represent and understand the problems and scenarios related to flooding. It can provide visual demonstration of component or system behavior during a highly spatial- and time-dependent flood event, including the potential of providing a design tool for flood mitigation investigations. It can provide important insights to risk-informed decision makers such as the direct relationship between the flow rate of a flood event and the impacted components shown in Table 6-1. The simulations could demonstrate the interactions among the SSCs that are impacted by the floods.
2. State-based PRA modeling tools such as EMRALD could be used as an integrated dynamic PRA tool for external flood and other hazard analysis. Note that nuclear PRA-oriented research and development on the use of state-transition models has been ongoing for a while. Insights and lessons learned from those activities (such as dynamic event tree approach, procedure-based operator actions, etc.) [24-28] could be useful in the future development of EMRALD.
3. The project is an exploratory research exercise, and the investigated dynamic approach is not intended to discount or replace the traditional event tree/fault tree or static approach for external flood analysis. It should be emphasized that traditional static PRA is an adequate tool for risk-informed decision making. For example, traditional static PRA can also accommodate multiple flooding levels and treat fragilities associated with different flood heights.
4. Under the current initial development phase, the difficulty to develop accurate terrain/plant layout model, and other issues, the simulation/dynamic approaches are not expected to be suitable for a completely stand-alone tool that could fully model all aspects of flooding in lieu of the traditional approach. Instead, it could rather play one of the following roles:
   - To support the development or enhancement of a static PRA with the insights from the evaluation with the dynamic approaches, which could appropriately account for physics-, spatial-, and time-dependent aspects of external and internal flood events.
   - To perform a stand-alone analysis that focuses on specific issues with limited sequences and components (e.g., FLEX).
   - To provide a design-type of tool that focuses on flood mitigation questions such as new or enhanced barriers and timing for human actions.

   It is believed that simulation/dynamic approaches could be very useful in a focused manner to validate (or challenge) some specific assumptions and inputs in the traditional static PRA models.
5. The project is a proof-of-concept with the purpose to investigate plant response to external flooding events. Various assumptions have been applied in the case study. External flood hazard analysis and fragility analysis were discussed briefly to show the picture of a complete external flood

analysis. However, there are aspects that need attentions and detailed discussions in a future study and pilot project. For example:

- Critical sources of uncertainty in the dynamic analysis as well as general external flood analysis should be identified and characterized (e.g., uncertainties existed in external flood hazard curves, especially for extrapolated longer return period part; uncertainties in external flood fragility evaluations, which may be supported either by existing operational or experimental data or by engineering judgment; uncertainties in plant responses such as flooding pathways, effective flow areas of as-designed and degraded doorways and penetrations, flooding event timelines including those of human interventions, sequence scenarios).
- The hazard curve evaluation extrapolates existing precipitation height data to long return period. Different flood hazard parameters such as flood event duration and those defining associated effects (e.g., debris loads, sedimentation) are not discussed in this report, but should be included in a full external flood hazard analysis. It should be noted that current data may not be able to support the approach and future data development is needed.
- The hazard curve evaluation is based upon a statistical model which relies on relatively recent observational data points. Enhancements to this approach such as using physics-based event models or paleo-data sources have not been considered.
- The effects of external flood on human performance should be considered in human reliability analysis. The effects include additional workload and stress, limited site accessibility, limited staffing and communications, different warning time, spurious and incorrect instrumentation indications, and other scenario-specific effects.
- The failure modes of interest in the external flood PRA model may be different from those in the internal event model for some SSCs (e.g., spurious actuations or instrument malfunctions caused by the external flood and the associated effects).
- The mission time in external flood analysis should be defined properly and be consistent with the flood event duration.
- The project does not couple the flooding-physics models to thermal-hydraulic codes, such as RELAP or MAAP, to determine the reactor core state for various scenario times. This type of integrated model could be a future effort to see whether it is computationally feasible and whether it could provide additional insights.
- The case study uses direct Monte Carlo sampling approach, which may not detect some very low probabilities events even with millions of simulation runs. Enhanced simulation approaches might be explored, such as importance sampling, using surrogate models, and using dynamic event trees.
- Multiple flood mechanisms, coexistent hazards (e.g., seismic, large storms, high winds), and multiple units are not considered in this project. They could be considered properly in a full external flood analysis.

6. When comparing the EMRALD and SAPHIRE model results in Sections 5.4 and 6.6, it is observed that with the EMRALD Monte Carlo simulation method does not force the results to detect a failure event for systems or sequences with extremely low probabilities (e.g., 1E-9 or lower). There are three observations related to this point:
    a. Scenarios with very low probability (e.g., < 1E-9) should be evaluated critically due to uncertainties that might dominate these low probability events regardless of the quantitative approach (i.e., simulation or minimal cut sets). Having realistic and accurate results in the 1E-7 to 1E-4 range is much more important than having any results in the

1E-10 to 1E-7 range. The dynamic simulation approach helps to enhance the realism in these higher-frequency scenarios.

b. The events with extremely low probabilities can still be captured in the dynamic approach:

    i. If the number of simulations is increased, this will increase the realization of low-probability combinations. Increasing the number of simulations is a matter of analysis time, computational power, or both.

    ii. If advanced simulation methods are utilized, this enhancement will force low-probability combinations to be produced. Some examples of advanced Monte Carlo simulation methods are the cross-entropy method and the subset simulation method [29]. With the advanced simulation methods, scenarios with low flooding IE frequency can be simulated directly and repeatedly because the sequence results are determined by multiplying the simulation results (after the start of the scenario) with the IE frequency.

c. Specific component failures that are not captured via the simulation approach have, by definition, low risk significance as measured by the Fussell-Vesely importance measure. For example, if a component failure does not appear in the results, even though scenarios down to the 1E-7 range have been simulated, then the risk contribution from that component failure would be bounded to be lower than 1E-7.

8. SUMMARY

All nuclear power plants must consider external flooding risks, such as LIP, riverine flooding, flooding due to upstream dam failure, and coastal flooding due to storm surge or tsunami. These events have the potential to challenge offsite power, threaten plant systems and components, challenge the integrity of plant structures, and limit plant access. Detailed risk assessments of external flood hazard are often needed to provide significant insights to risk informed decision makers. Many unique challenges exist in modeling the complete plant response to the flooding event. SSCs, flood protection features, and flood mitigation measures to external flood may be highly spatial- and time-dependent and subject to the hydrometeorological, hydrological, and hydraulic characteristics of the flood event (antecedent soil moisture, precipitation duration and rate, infiltration rate, surface water flow velocities, inundation levels and duration, hydrostatic and hydrodynamic forces, debris impact forces, etc.). Simulation based methods and dynamic analysis approaches can be a valuable tool to model the performance of SSC and operator actions during an external flooding event. In support of the NRC PFHA research plan, INL was tasked to develop new approaches and demonstrate a proof of concept for the advanced representation of external flooding analysis.

This report presents the INL efforts to conduct the exploratory research to develop possible approaches to investigate plant response to flooding events. Dynamic analysis approaches that depict scenarios through simulation methods were investigated in the project. A framework to perform a simulation-based dynamic flooding analysis was developed. There are four main tasks under the framework to conduct the flooding analysis. (1) Flood hazard analysis evaluates the frequency of occurrence of external floods as a function of magnitude based on site-specific, up-to-date information, with the output of the task being a hazard curve (or a family of hazard curves) giving occurrence frequency versus hazard intensity. (2) Flood fragility analysis evaluates the fragility of plant SSCs as a function of the magnitude of the external flood using proper engineering method for the postulated failure, with the output of the task being a table or tables of SSCs that are included in the plant response model, as well as their failure probabilities as a function of the magnitude of the external floods (e.g., fragility tables, failure models based upon flooding characteristics, or probabilistic curves). (3) Plant response modeling develops a plant response model that addresses the initiating events and failures caused by the effects of external flooding that can lead to core damage or large early release. (4) Create a 3-D external flood simulation model, revise the state-based PRA model from a previous task to incorporate the 3-D simulation elements, and perform 3-D simulations and plant response model quantification. As a proof-of-concept demonstration, this project focuses on the plant response modeling with the 3-D simulation-based dynamic analysis approach. The flood hazard analysis and flood fragility analysis are included but are not analyzed in detail for this project.

A previous LIP event that occurred in a PWR plant was reviewed and used as the case study in this project. A Generalized Extreme Value model was used in this report to estimate precipitation rates for return periods longer than the ones from NOAA, which provides precipitation magnitude estimates for up to 1 in 1,000 years based on historical precipitation data and modeling. An approach to approximate the uncertainty associated with the precipitation estimates for long return periods in the GEV model is proposed. The NOAA 5% or 95% precipitation values are used to estimate respective uncertainty for the GEV estimates in this approach.

General plant responses to an external flood are discussed in this report. The plant response is divided into two stages: external plant response and internal plant response. During the external plant response stage, the plant flood protection features, including both as-designed features (site drain system, water-tight doors and penetration seals, drain systems within buildings, etc.) and temporary features (portable pumps, sandbag barriers, etc.), would perform their functions and prevent risk-significant SSCs from flood damages. If the flood protection features fail to perform the functions and the manual actions (e.g., installation of portable pumps and floodgates, construction of barriers) are not effective, the plant is in undesirable conditions of flood damage state and enters the internal plant response stage in which plant

mitigation measures along with the manual actions are maintaining key safety functions and preventing core damage and large early release. An external flooding event tree is developed to assess the flood damages states due to the external flood event for the external plant response stage, while an internal event, at-power PRA model, usually exists prior to the external flood analysis, is used as the base to model the internal plant response stage.

EMRALD was used in this project to incorporate time-related interactions from both 3-D physical simulations and stochastic failures into traditional PRA logic models. An example state-based PRA model (including component state diagrams, CCF state diagrams, system state diagrams, and plant state diagrams) was developed by converting a simplified traditional transient event tree and the associated fault trees and basic events. This EMRALD model represents two accident sequences, seven system logics, and about seventy components (human action is treated as a component in the model). It was tested against the corresponding SAPHIRE model. The results for both the system failure probabilities and the sequence failure frequencies from the EMRALD model (in which 3-D flood simulation elements have not been incorporated at this stage) are very close to those from the SAPHIRE model, although the simulation runs of the state-based system model were stopped prior to all failures scenarios being considered.

The initial EMRALD model was then revised to incorporate 3-D simulation elements (flood initiating event, flood-caused failure events, and simulation related state/event) into the logic so that the PRA model could communicate with the 3-D simulation models. To develop 3-D simulation models, a 3-D site terrain model was obtained for the interested plant/site with a web-based application that interacts with the Google's Elevation API, a 3-D plant model was developed for a typical PWR plant, and flooding scenarios and pathways were identified. Then, the 3-D simulation software Neutrino was used to integrate these pieces into 3-D simulation models which can represent the flooding scenarios physics and communicate with the state-based PRA model. The integrated 3-D simulation models and the EMRALD model were run with 34 3-D dynamic simulations and millions of Monte Carlo simulations. The EMRALD model results were compared with the corresponding SAPHIRE model results. It was shown that the EMRALD model predictions are very close to those from the SAPHIRE model. In addition to providing conditional core damage probabilities in various flooding scenarios, the EMRALD model can use 3-D dynamic simulations to visually demonstrate which components would fail under which flooding scenarios and flood parameters and evaluate the overall impacts these failed components and flood events would have on the plant. The EMRALD model results can also show the cliff edge effect from a flood event by covering a spectrum of scenarios ranging from small to large floods and the corresponding failure behavior of the plant and SSCs.

Insights and lessons learned from the project are documented for future research and applications. The project shows that dynamic approaches could be used as an important tool to investigate plant response to external flooding events. It can provide visual demonstration of component or system behavior during a highly spatial and time dependent flood event. It could provide important insights to risk informed decision makers. The dynamic approaches could also play a supplemental role by supporting the development or enhancement of a static PRA with the insights from the dynamic analysis or performing a standalone analysis that focuses on specific issues with targeted sequences and components (e.g., FLEX). Improvement as well as custom modifications to the 3-D Neutrino code has also been conducted to satisfy the specific requirements of the project.

9. REFERENCES

[1] F. Ferrante, "External Flooding in Regulatory Risk-Informed Decision-Making for Operating Nuclear Reactors in the United States," *PSA2015, Sun Valley, Idaho, USA, 2015*.

[2] C. Miller, A. Cubbage, D. Dorman, J. Grobe, and G. Holahan, *Enhancing Reactor Safety in the 21st Century: The Near-Term Task Force Review Of Insights from the Fukushima Dai-Ichi Accident*, U.S. Nuclear Regulatory Commission, 2011.

[3] Title 10, Code of Federal Regulations, Part 50, "Domestic Licensing of Production and Utilization Facilities."

[4] Title 10, Code of Federal Regulations, Part 52, "Licenses, Certifications, and Approvals for Nuclear Power Plants."

[5] Title 10, Code of Federal Regulations, Part 100, "Reactor Site Criteria."

[6] U.S. Nuclear Regulatory Commission, "Proceedings of the Workshop on Probabilistic Flood Hazard Assessment (PFHA)," U.S. Nuclear Regulatory Commission, January 29–31, 2013.

[7] T. J. Nicholson and W. A. Reed, *Probabilistic Flood Hazard Assessment Research Plan*, U.S. Nuclear Regulatory Commission, ML14296A442, 2014.

[8] C. L. Smith, S. T. Wood, *Systems Analysis Programs for Hands-on Integrated Reliability Evaluations (SAPHIRE) Version 8*, U.S. Nuclear Regulatory Commission, NUREG/CR-7039, 2011.

[9] ASME and ANS, "Addenda to ASME/ANS RA-S-2008 Standard for Level 1/Large Early Release Frequency Probabilistic Risk Assessment for Nuclear Power Plant Applications," ASME/ANS RA-Sb-2013 (2013).

[10] A. Alfonsi, C. Rabiti, D. Mandelli, J. Cogliati, and R. Kinoshita, "Raven as a tool for dynamic probabilistic risk assessment: Software overview," in *Proceeding of M&C2013 International Topical Meeting on Mathematics and Computation*, CD-ROM, American Nuclear Society, LaGrange Park, IL (2013).

[11] C. Rabiti, A. Alfonsi, D. Mandelli, J. Cogliati, R. Martinueau, C. Smith, "Deployment and Overview of RAVEN Capabilities for a Probabilistic Risk Assessment Demo for a PWR Station Blackout," Idaho National Laboratory report INL/EXT-13-29510 (2013).

[12] A. David, R. Berry, D. Gaston, R. Martineau, J. Peterson, H. Zhang, H. Zhao, L. Zou, "RELAP-7 Level 2 Milestone Report: Demonstration of a Steady State Single Phase PWR Simulation with RELAP-7," Idaho National Laboratory: INL/EXT-12-25924 (2012).

[13] NOAA Atlas 14, *Precipitation-Frequency Atlas of the United States*, National Oceanic and Atmospheric Administration, 2013.

[14] NOAA, "NOAA Precipitation Frequency Data Server," NOAA's National Weather Service, http://hdsc.nws.noaa.gov/hdsc/pfds/index.html, 2016.

[15] D. Kelly and C. Smith, *Bayesian Inference for Probabilistic Risk Assessment: A Practitioner's Guidebook*, Springer, 2011.

[16] D. Lunn, D. Spiegelhalter, A. Thomas, and N. Best, "The BUGS Project: Evolution, Critique and Future Directions," *Statistics in Medicine*, Vol. 28, 2009.

[17] S. Prescott, R. Sampath, C. Smith, and T. Koonce, *Prototype Development Capabilities of 3D Spatial Interactions and Failures during Scenario Simulation*, Idaho National Laboratory, INL/EXT-14-33211, 2014.

[18] S. Prescott, C. Smith, T. Koonce, and T. Yang, *Case Study for Enhanced Accident Tolerance Design Changes*, Idaho National Laboratory, INL/EXT-14-32355, Rev. 1, 2014.

[19] C. Smith, D. Mandelli, S. Prescott, A. Alfonsi, C. Rabiti, J. Cogliati, and R. Kinoshita, *Analysis of Pressurized Water Reactor Station Blackout Caused by External Flooding Using the RISMC Toolkit*, Idaho National Laboratory, INL/EXT-14-32906, 2014.

[20] Z. Ma, *SPAR-ICM Model Maker's Guideline (MMG)*, Idaho National Laboratory, INL/LTD-12-27650, 2012.

[21] Tutorials Point, "C# Programming, object-oriented programming," Tutorials Point (I) Pvt. Ltd, 2014.

[22] Google Developers, "Google Maps Elevation API," https://developers.google.com/maps/documentation/elevation/intro#Introduction, Google, 2015.

[23] N. Akinci, M. Ihmsen, G. Akinci, B. Solenthaler and M. Teschner, "Versatile Rigid-Fluid Coupling for Incompressible SPH," *ACM Transactions on Graphics Proc.*, SIGGRAPH 2012, Vol. 31, No. 4 2014.

[24] C. Acosta and N. Siu, *Dynamic Event Tree Analysis Method (DETAM) for Accident Sequence Analysis*, Massachusetts Institute of Technology, MITNE-295, 1991.

[25] N. Siu, "Risk Assessment for Dynamic Systems: an Overview," *Reliability Engineering and System Safety*, 41, pp. 43–73, 1994.

[26] K. Hsueh and A. Mosleh, "The Development and Application of the Accident Dynamic Simulator for Dynamic Probabilistic Risk Assessment of Nuclear Power Plants," *Reliability Engineering and System Safety*, 52, pp. 297–314, 1996.

[27] D. Kunsman, S. Dunagan, et. al., *Development and Application of the Dynamic System Doctor to Nuclear Reactor Probabilistic Risk Assessments*, Sandia National Laboratories, SAND2008-4746, 2008.

[28] D. Helton, *Scoping Study on Advancing Modeling Techniques for Level 2/3 PRA*, U.S. Nuclear Regulatory Commission, ML091320447, 2009.

[29] E. Zio, *The Monte Carlo Simulation Method for System Reliability and Risk Analysis*, Chapter 6, Springer, Verlag, London (2013).

Appendix A

An Example State-Based PRA Model

Appendix A
An Example State-Based PRA Model

A1. Simplified External Flood-Induced Transient Event Tree

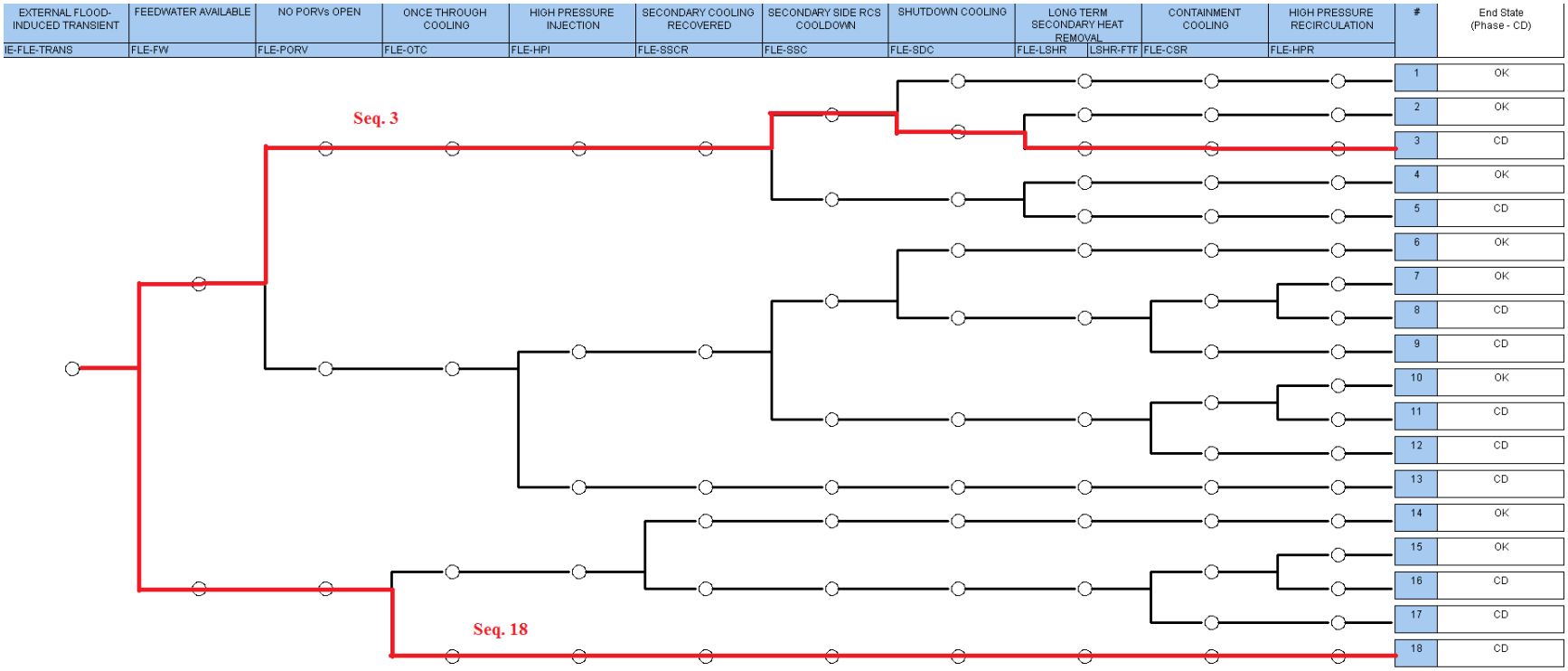

Figure A-1. A simplified external flood-induced transient event tree.

A2. SSCs Modeled in the Example State-Based PRA Model

Table A-1. Components, systems, and human actions included in the example state-based PRA model.

Component	System/Fault Tree						
	AFW	OTC	SDC	LSHR	HPR (1)	CSR (1)	CCS (1)
1	AFW-TDP-1C	HPI-MDP-1A (2,3)	LPI-MDP-1A (2)	CST	HPI-MDP-1A (2,3)	CSR-MDP-1A (2)	CCS-FAN-1A
2	AFW-MDP-1A	HPI-MDP-1B (2,3)	LPI-MDP-1B (2)	CST-XHE-U2	HPI-MDP-1B (2,3)	CSR-MDP-1B (2)	CCS-FAN-1B
3	AFW-MDP-1B	HPI-MOV-INJ	CVC-PDP-1A (2)	CST-XHE-LTMAKEUP	HPI-MOV-CF-SUMP	LPI-AOV-14-3A	CCS-FAN-1C
4	AFW-MOV-09-9	PORV1	CVC-PDP-1B (2)	SDC (1)	CCW-HTX-1A (3)	LPI-AOV-14-3B	CCS-FAN-1D
5	AFW-MOV-09-10	PORV2	CVC-PDP-1C (2)	OTC (1)	CCW-HTX-1B (3)	CSR-XHE-ERROR	CCW-HTX-1A (3)
6	AFW-MOV-09-11	RWST	LPI-MOV-3452	HPR (1)	HPI-MDP-CF-STRT (3, 4)	CCS (1)	CCW-HTX-1B (3)
7	AFW-MOV-09-12	HPI-XHE-FB	LPI-MOV-3453	CSR (1)	HPI-MDP-CF-RUN (3, 4)	CSR-MDP-CF-STRT (4)	CCW-TNK-SURGE
8	AFW-CKV-9119	HPI-MDP-CF-STRT (3, 4)	LPI-MOV-03-2			CSR-MDP-CF-RUN (4)	CCS-XHE-SIAS
9	AFW-CKV-9151	HPI-MDP-CF-RUN (3, 4)	CVC-MOV-2501			LPI-AOV-CF-143AB (4)	CCS-FAN-CF-START (4)
10	AFW-CKV-9135		CVC-MOV-2504				CCS-FAN-CF-RUN (4)
11	AFW-CKV-9157		CSR-HTX-1A (2)				
12	AFW-CKV-SG-A		CSR-HTX-1B (2)				
13	AFW-CKV-SG-B		CCW-HTX-1A (3)				
14	ACP-MCC-1A5		CCW-HTX-1B (3)				
15	ACP-MCC-1B5		CVC-HTX-RGHX				
16	AFW-PMP-CF-ALL (4)		LPI-XHE-SDC				
17	AFW-MOV-CF-SGS (4)		LPI-MDP-CF-STRT (4)				
18	AFW-CKV-CF-SGALL (4)		LPI-MDP-CF-RUN (4)				
19	AFW-CKV-CF-SGS (4)		CVC-PDP-CF-RUN (4)				
20			LPI-MOV-CF-HTX (4)				
21			CSR-HTX-CF-ALL (4)				

Notes:
(1) This is a transfer fault tree.
(2) This component subjects to flooding failure.
(3) This component is used in multiple fault trees.

A3. SSCs Modeled in 3-D Dynamic Simulations

Table A-2. Components modeled and monitored in 3-D dynamic simulations.

Component Name	ID	Location (Underground Level)	Failure Prob. = 1.0		Failure Prob. = 0.1	Failure Prob. = 0.01
			Flood Height 1 (in)	Flood Height 1 (cm)	Flood Height 2 (cm)	Flood Height 3 (cm)
LPI-MDP-1A	101	Level 1	27	68.58	60	20
LPI-MDP-1B	102	Level 1	27	68.58	60	20
CSR-MDP-1A	103	Level 1	24	60.96	50	20
CSR-MDP-1B	104	Level 1	24	60.96	50	20
HPI-MDP-1A	105	Level 1	24	60.96	50	20
HPI-MDP-1B	106	Level 1	24	60.96	50	20
CVC-PDP-1A	201	Level 2	24	60.96	50	20
CVC-PDP-1B	202	Level 2	24	60.96	50	20
CVC-PDP-1C	203	Level 2	24	60.96	50	20
CSR-HTX-1A	204	Level 2	40	101.6	90	30
CSR-HTX-1B	205	Level 2	40	101.6	90	30
ACP-MCC-1A2	206	Level 2	18	45.72	35	10
ACP-MCC-1B2	207	Level 2	18	45.72	35	10

A4. Revised Fault Trees for Example State-Based PRA Model

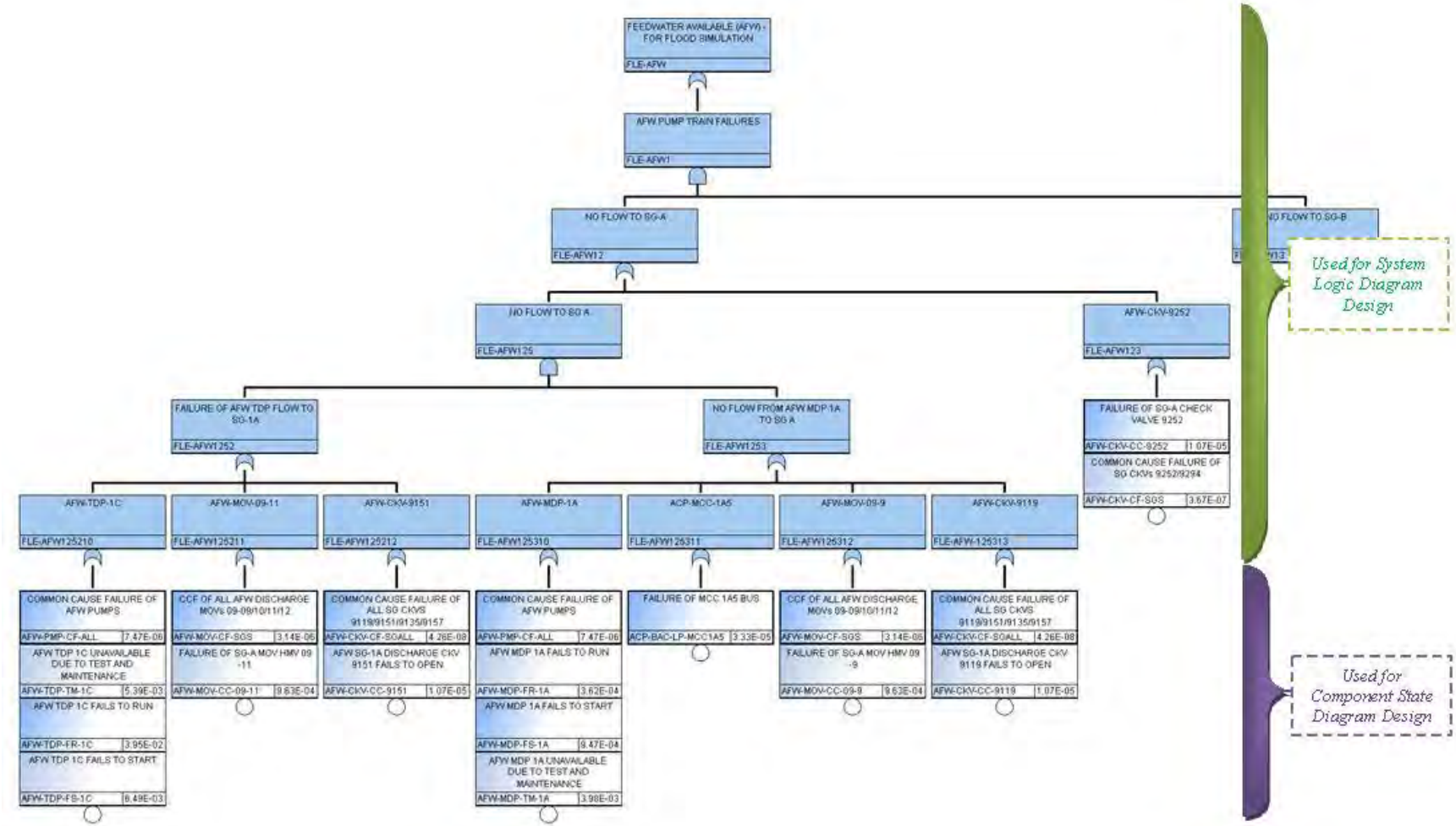

Figure A-2. Revised Auxiliary Feedwater fault tree (FLE-AFW), Part 1.

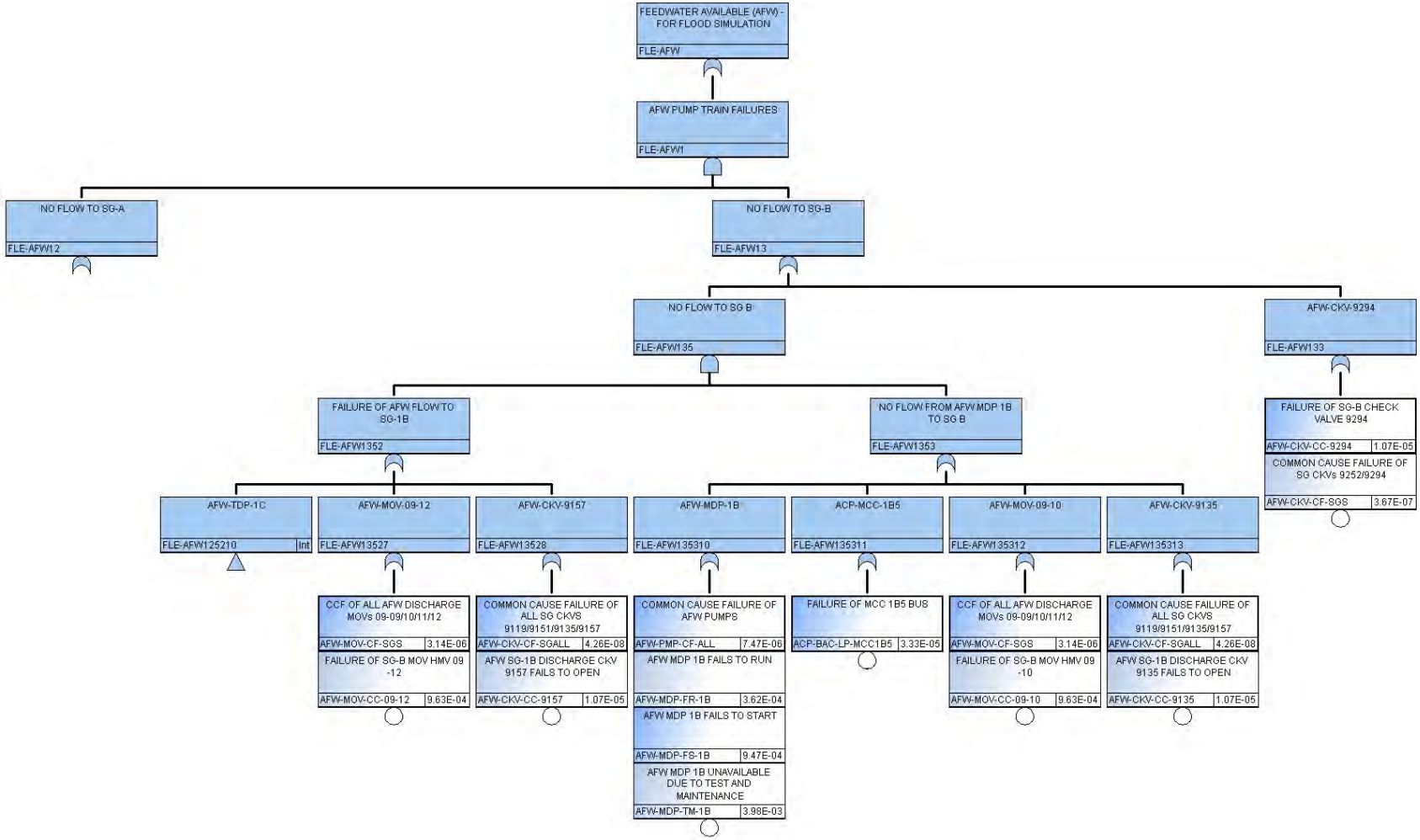

Figure A-3. Revised Auxiliary Feedwater fault tree (FLE-AFW), Part 2.

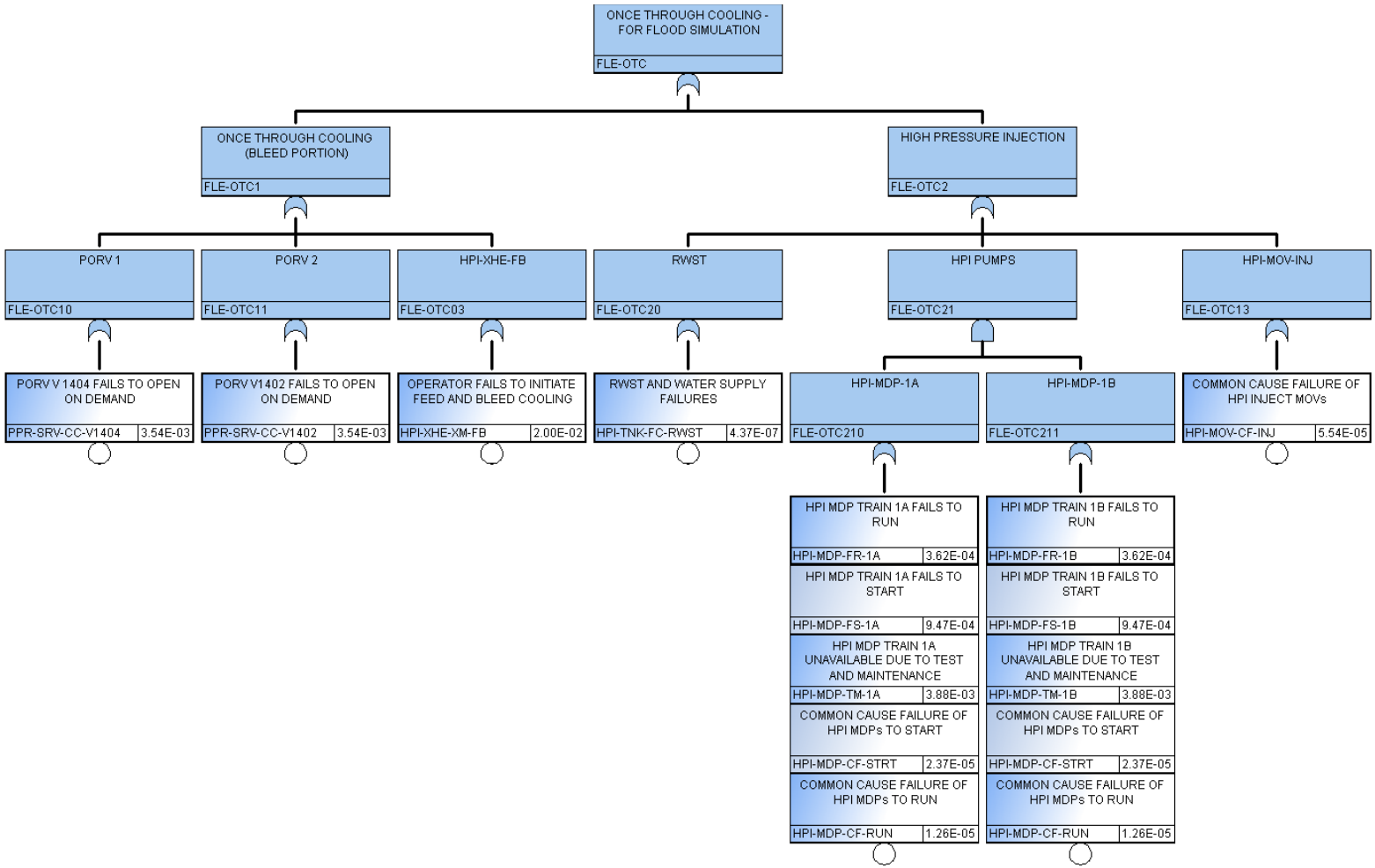

Figure A-4. Revised Once Through Cooling fault tree (FLE-OTC).

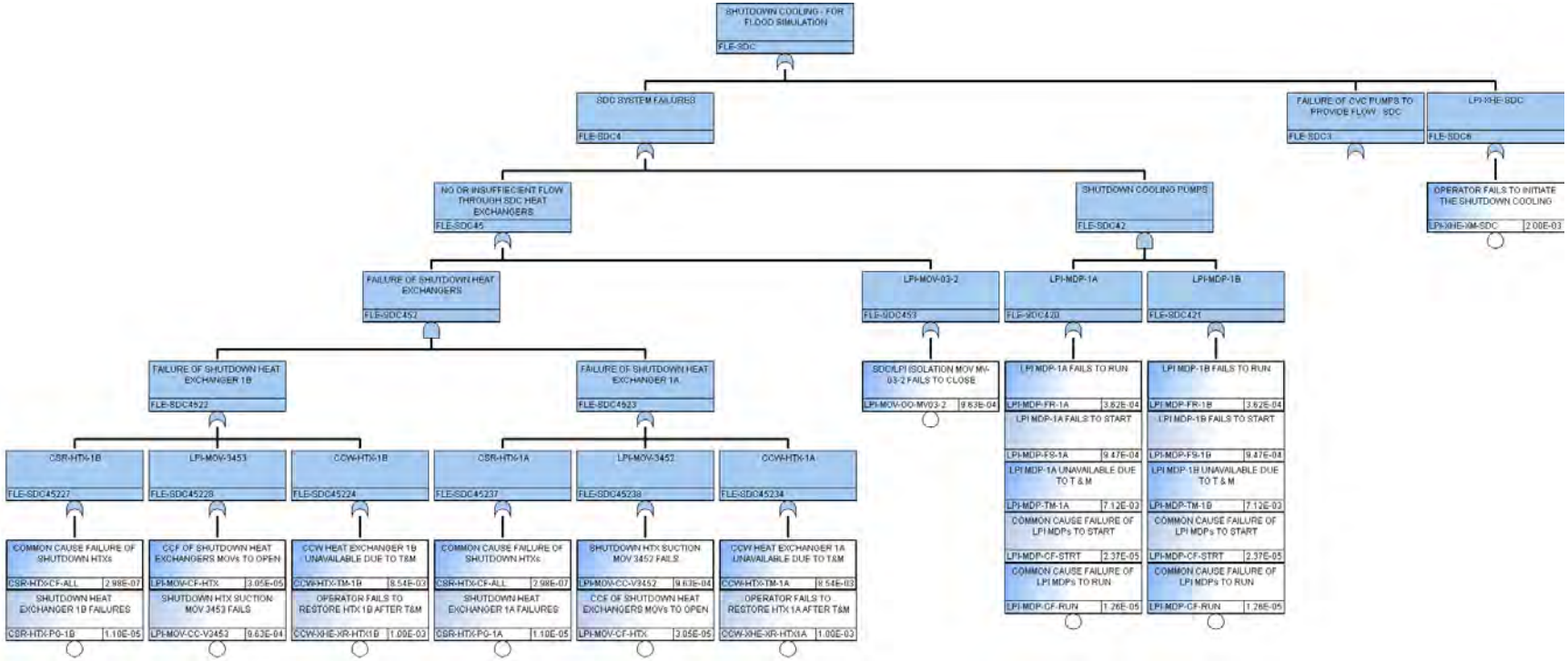

Figure A-5. Revised Shutdown Cooling fault tree (FLE-SDC), Part 1.

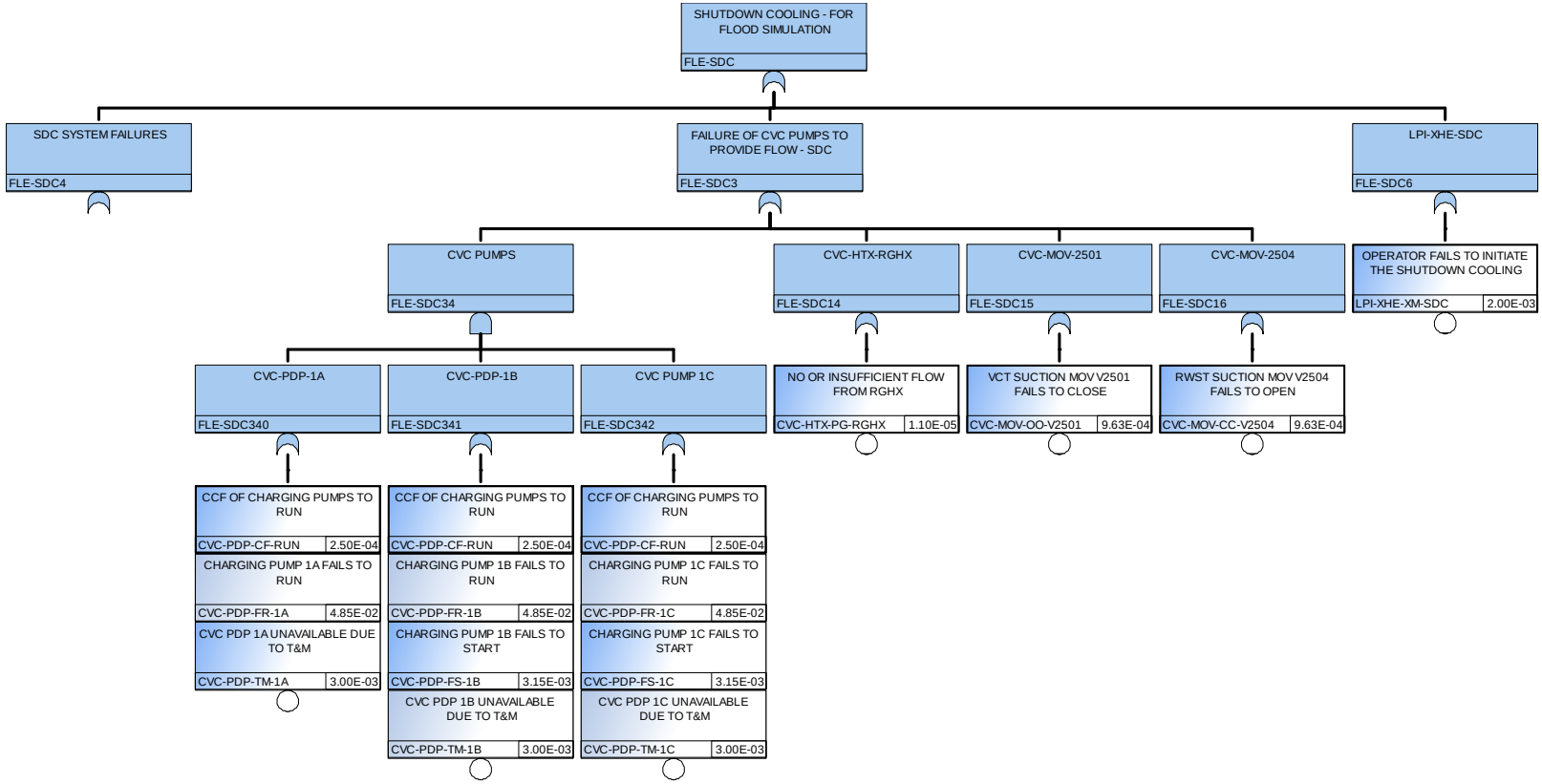

Figure A-6. Revised Shutdown Cooling fault tree (FLE-SDC), Part 2.

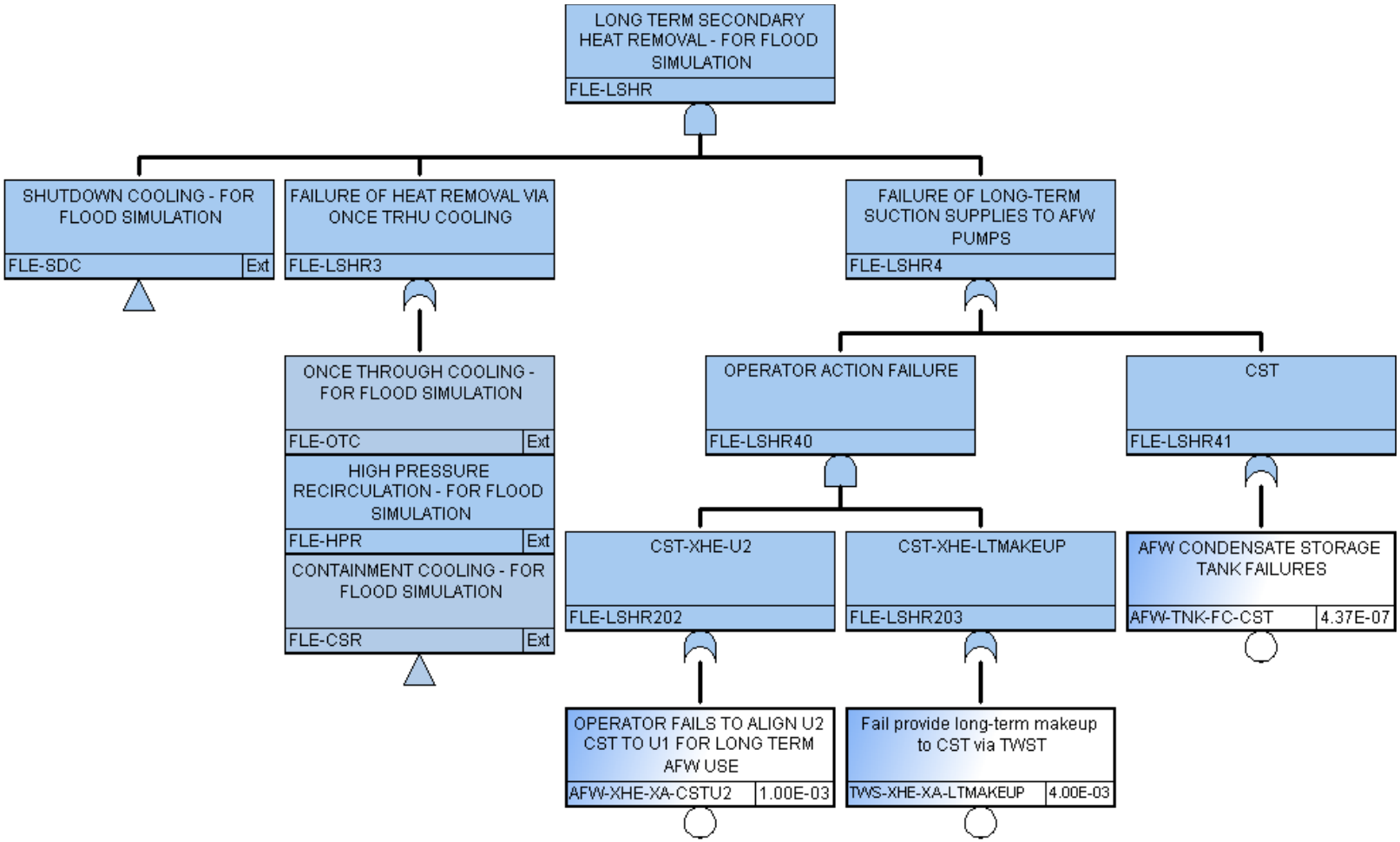

Figure A-7. Revised Long Term Secondary Heat Removal fault tree (FLE-LSHR).

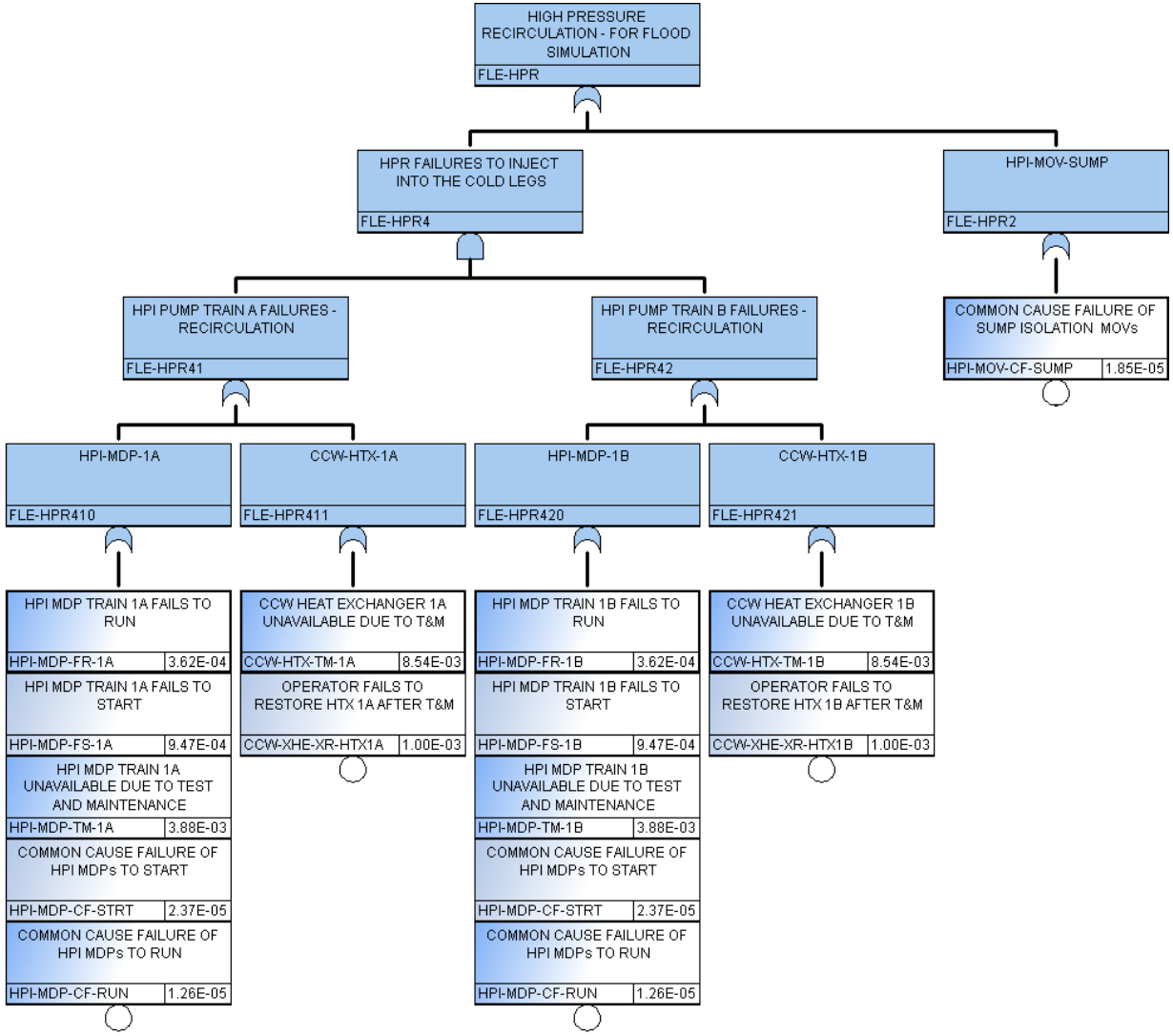

Figure A-8. Revised High Pressure Recirculation fault tree (FLE-HPR).

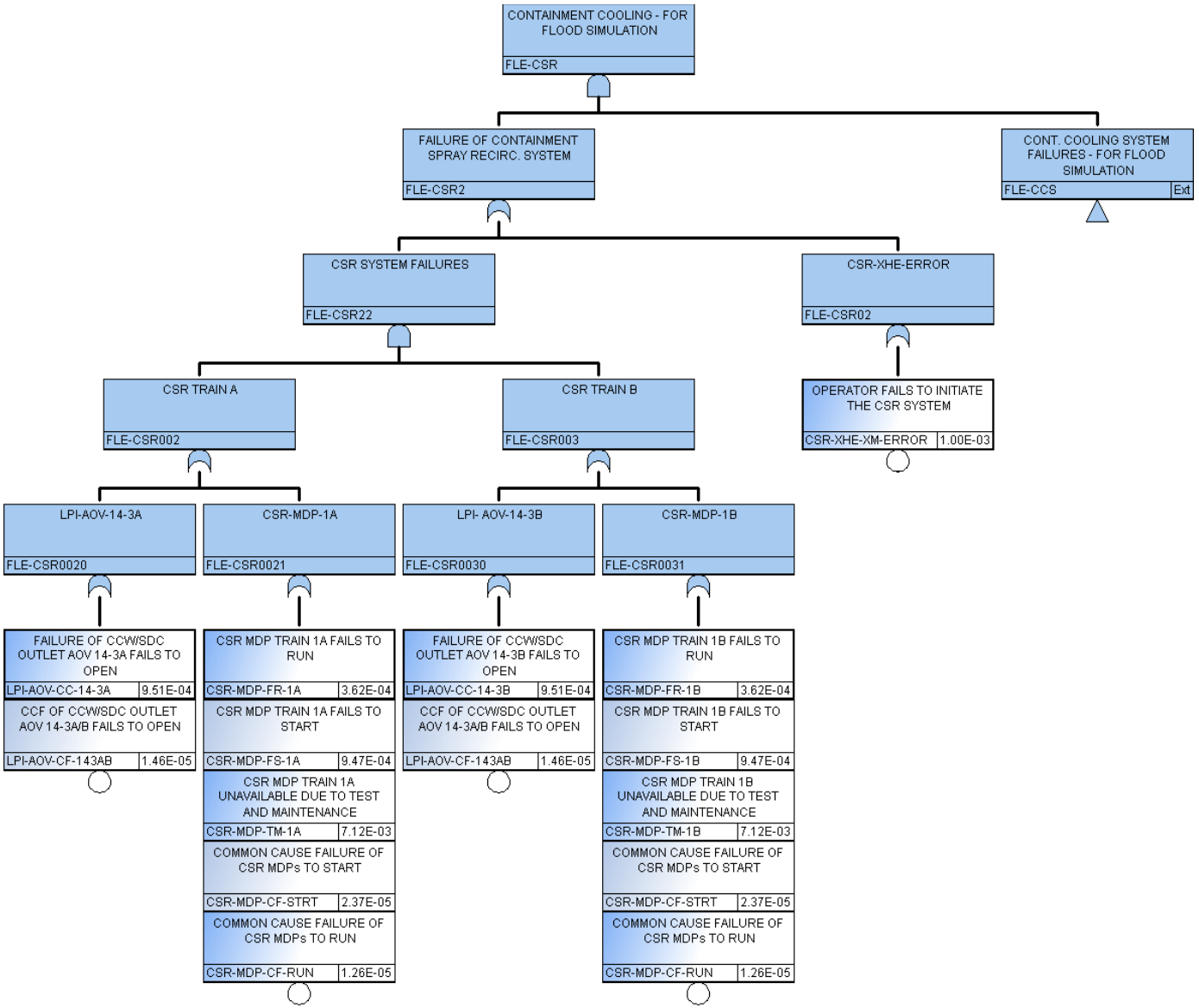

Figure A-9. Revised Containment Spray Recirculation fault tree (FLE-CSR).

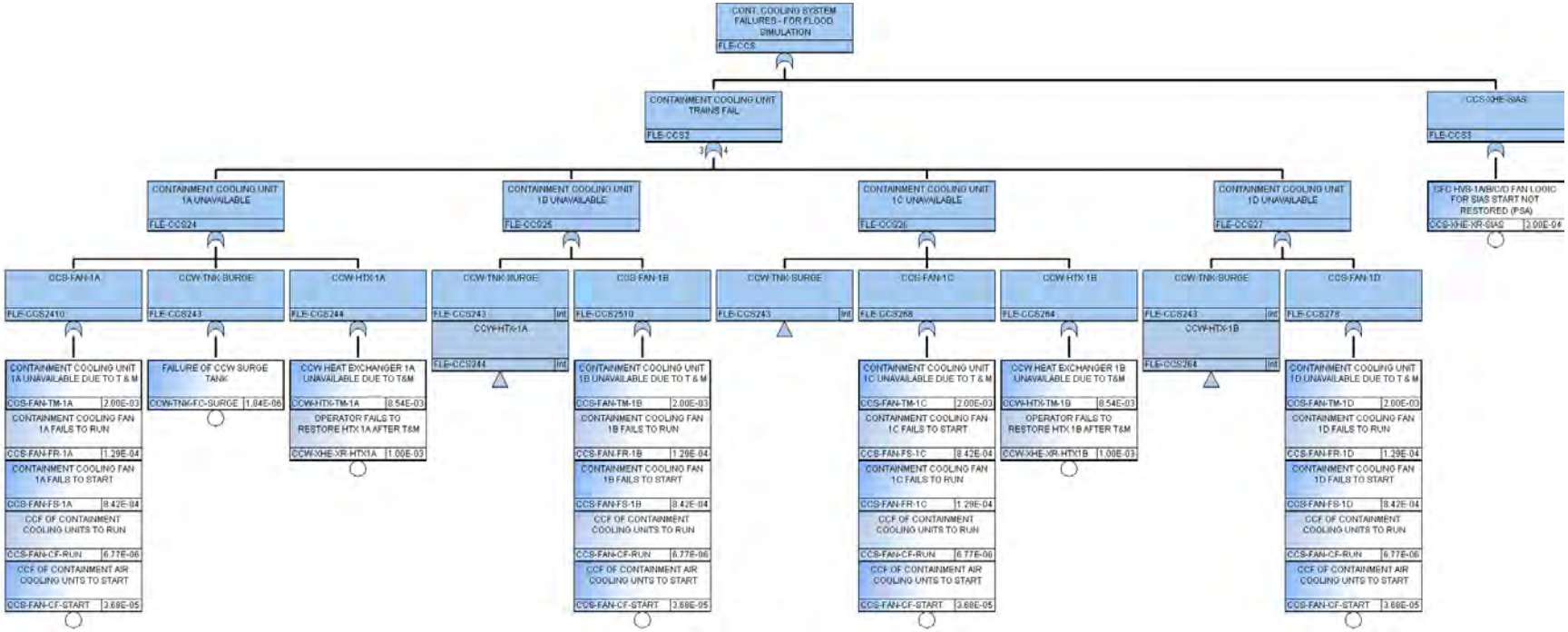

Figure A-10. Revised Containment Cooling System fault tree (FLE-CCS).

Appendix B

Torricelli Emitter Implementation in Neutrino

Appendix B
Torricelli Emitter Implementation in Neutrino

B.1 Mass Conservation

Considering mass inflow and outflow rates Fr_{in}^{m} and Fr_{out}^{m}, respectively, the variation of mass m over time t is expressed by the mass conservation equation:

$$\frac{dm}{dt} = Fr_{in}^{m}(t) - Fr_{out}^{m}(t) \tag{B-1}$$

Assuming the incompressibility condition satisfied, it can be transformed into the following volume conservation equation, stating the variation of volume V over time:

$$\frac{dV}{dt} = Fr_{in}(t) - Fr_{out}(t) \tag{B-2}$$

Where Fr_{in}^{m} and Fr_{out}^{m} are the volumetric flow rates. If supposed uniform along the vertical direction, V can be decomposed as the product of the accumulation area A and accumulating fluid height h. Assuming A to be constant over time, the variation of h over time is represented by the following differential equation:

$$\frac{dh}{dt} = \frac{Fr_{in}(t) - Fr_{out}(t)}{A} \tag{B-3}$$

A numerical time integration can be done to solve the equation, such as with the explicit Euler scheme:

$$h(t + \Delta t) = h(t) + \Delta t\left(\frac{Fr_{in}(t) - Fr_{out}(t)}{A}\right) \tag{B-4}$$

with Δt denoting the time step. The initial accumulating fluid height h_0 must be given to initialize the procedure.

B.2 Flow Rate

It is observed that a contraction of the outflow section could occur due to convergence of the streamlines. A discharge coefficient $C \in]0,1]$ is employed to take into account of this contraction effect, and also to incorporate any related velocity decrease of the outflow jet. The volumetric outflow rate Fr_{out} can thus be expressed as:

$$Fr_{out}(t) = C(t)A_{out}(t)\,|\,\mathbf{v}_{out}(t)\,| \tag{B-5}$$

with A_{out} the outflow section area, and $\boldsymbol{V}_{out}$ the velocity of the outflow jet. For a rectangular emitter for which the edges are along the horizontal and vertical directions, A_{out} can be simply expressed as:

$$A_{out}(t) = W_{emit}H_{out}(t) \tag{B-6}$$

where W_{emit} is the emitter width and H_{out} is the outflow section height. In the case of a circular emitter, its expression can be derived using a reasoning on semi-ellipsoids:

$$A_{out}(t) = \begin{cases} \frac{\pi}{2} H_{out}(t)\sqrt{r^2 - (H_{out}(t) - r)^2} & \text{if } H_{out}(t) \le r \\ \pi(r^2 - \frac{1}{2}(2r - H_{out}(t))\sqrt{r^2 - (H_{out}(t) - r)^2}) & \text{if } H_{out}(t) \ge r \end{cases} \quad \text{(B-7)}$$

where r is the emitter radius. In the following, r and $H_{emit}/2$ can be conflated. Three situations are to be considered for estimating the values of H_{out} and C, depending on if the emitter is: (1) non-submerged, (2) partially-submerged, or (3) completely-submerged by the fluid. By noting the emitter height H_{emit}, the vertical coordinate z and z_0 of the emitter center and accumulation floor, respectively, these situations correspond to:

(1) $$h(t) \le z - z_0 - \frac{H_{emit}}{2}$$

(2) $$z - z_0 - \frac{H_{emit}}{2} \le h(t) \le z - z_0 + \frac{H_{emit}}{2}$$

(3) $$h(t) \ge z - z_0 + \frac{H_{emit}}{2}$$

For H_{out} ,we have:

$$H_{out}(t) = \begin{cases} 0 & \text{if (1)} \\ h(t) - z + z_0 + \frac{H_{emit}}{2} & \text{if (2)} \\ H_{emit} & \text{if (3)} \end{cases} \quad \text{(B-8)}$$

Denoting as C_d the discharge coefficient corresponding to the completely submerged case, we can suppose a lesser contraction of the cross section of the jet along the vertical direction and reasonably consider a value $\sqrt{C_d}$ at the non- and partially-submerged borderline. Continuity and a smooth variation of C can be realized with a linear interpolation:

$$C(t) = \begin{cases} \sqrt{C_d} & \text{if (1)} \\ \sqrt{C_d} + \frac{H_{out}(t)}{H_{emit}}(C_d - \sqrt{C_d}) & \text{if (2)} \\ C_d & \text{if (3)} \end{cases} \quad \text{(B-9)}$$

B.3 Torricelli's Law

Supposing a steady, incompressible, inviscid flow and neglecting any work done by or heat transfer into the fluid, the following formulation of Bernoulli's principle can be applied:

$$\frac{|\mathbf{v}_{top}|^2}{2} + |\mathbf{g}|(z_0 + h(t)) + \frac{P_{top}}{\rho_0} = \frac{|\mathbf{v}_{out}(t)|^2}{2} + |\mathbf{g}| z_{out}(t) + \frac{P_{out}}{\rho_0} \quad \text{(B-10)}$$

where $\boldsymbol{V}_{top}$ and P_{top} are the velocity and pressure of the fluid at the top, respectively, z_{out} and P_{out} are the vertical coordinate (defined just after) and pressure at the outflow jet, respectively, and **g** is the

gravitational acceleration. Further assumptions are done by considering a free jet (i.e., surrounded by a fluid of much smaller density, null velocity of the fluid at the top, and same atmospheric pressure at the top and jet locations). We then obtain an expression for $|\boldsymbol{V}_{out}|$ (i.e., a Torricelli's law):

$$|\mathbf{v}_{out}(t)| = \sqrt{2|\mathbf{g}|(z_0 + h(t) - z_{out}(t))} \tag{B-11}$$

Taking z_{out} at the middle vertical position of the outflow section, we obtain:

$$z_{out}(t) = \begin{cases} z_0 + h(t) & \text{if (1)} \\ \frac{1}{2}(z_0 + h(t) + z - \frac{H_{emit}}{2}) & \text{if (2)} \\ z & \text{if (3)} \end{cases} \tag{B-12}$$

Finally, Torricelli's law becomes:

$$|\mathbf{v}_{out}(t)| = \begin{cases} 0 & \text{if (1)} \\ \sqrt{|\mathbf{g}| H_{out}(t)} & \text{if (2)} \\ \sqrt{2|\mathbf{g}|(z_0 + h(t) - z)} & \text{if (3)} \end{cases} \tag{B-13}$$

B.4 Steady State

In the specific case of Fr_{in} constant over time, or more generally an inflow rate converging to a value Fr_{in}^{lim}, a steady state is eventually reached, at which $Fr_{out} = Fr_{in}^{lim}$. An accumulating fluid height h^{lim} and outflow velocity $|\boldsymbol{V}_{out}^{lim}|$ can then be determined. Their calculation varies depending on if the emitter is completely or partially submerged at equilibrium.

Formally, the former occurs when $Fr_{in}^{lim} \geq C_d A_{emit}\sqrt{|\mathrm{g}|H_{emit}}$, while this is the later otherwise; A_{emit} denotes the emitter area:

$$A_{emit} = \begin{cases} W_{emit} H_{emit} & \text{if rectangular emitter} \\ \pi r & \text{if circular emitter} \end{cases} \tag{B-14}$$

In the case of a steady state with the emitter completely submerged, h^{lim} and $|\boldsymbol{V}_{out}^{lim}|$ can be easily calculated:

$$h^{lim} = z - z_0 + \frac{1}{2|\mathbf{g}|}\left(\frac{Fr_{in}^{lim}}{C_d A_{emit}}\right)^2 \tag{B-15}$$

$$|\mathbf{v}_{out}^{lim}| = \frac{Fr_{in}^{lim}}{C_d A_{emit}} \tag{B-16}$$

In the other situation, for which the emitter is only partially submerged at equilibrium, numerical calculus is necessary. Furthermore, differentiation between rectangular and circular shapes must be done, and also the case $C_d = 1$ has to be treated separately. First, let us assume a rectangular emitter. The expression for h^{lim} and $|\boldsymbol{V}_{out}^{lim}|$ can be analytically derived when $C_d = 1$:

$$h^{lim} = z - z_0 - \frac{H_{emit}}{2} + \left(\frac{Fr_{in}^{lim}}{\sqrt{|\mathbf{g}|}W_{emit}}\right)^{\frac{2}{3}} \tag{B-17}$$

$$|\mathbf{v}_{out}^{lim}| = \left(\frac{Fr_{in}^{lim}}{|\mathbf{g}|W_{emit}}\right)^{\frac{1}{3}} \tag{B-18}$$

Otherwise, we have:

$$h^{lim} = z - z_0 - \frac{H_{emit}}{2} + X^2 \tag{B-19}$$

$$|\mathbf{v}_{out}^{lim}| = \sqrt{|\mathbf{g}|}X \tag{B-20}$$

where X is defined as root of the following polynomial function:

$$f : X \mapsto X^5 + \frac{\sqrt{C_d}H_{emit}}{C_d - \sqrt{C_d}}X^3 - \frac{H_{emit}Fr_{in}^{lim}}{(C_d - \sqrt{C_d})\sqrt{|\mathbf{g}|}W_{emit}} \tag{B-21}$$

for which the derivative reads:

$$f' : X \mapsto X^2\left(5X^2 + 3\frac{\sqrt{C_d}H_{emit}}{C_d - \sqrt{C_d}}\right) \tag{B-22}$$

Newton's method for root-finding can be employed to estimate X. Choosing $X_0 = \sqrt{H_{emit}/2}$ as a first guess value is optimal, and until $|f(X_n)| < \varepsilon$ or a maximum iteration number l_{max} is reached, the method iterates as following:

$$X_{n+1} = X_n - \frac{f(X_n)}{f'(X_n)} \tag{23}$$

Lastly, let us assume a circular emitter. The computations are more technical, and an additional distinction has to be made, that is if the fluid height level at the steady state is below or above the emitter center. In the former case, we have $Fr_{in}^{lim} \leq \frac{\pi}{4}\left(\sqrt{C_d} + C_d\right)\sqrt{|\mathrm{g}|}r^{\frac{3}{2}}$, and the opposite otherwise. In all cases, then h^{lim} and $\left|\boldsymbol{V}_{out}^{lim}\right|$ are computed as:

$$h^{lim} = z - z_0 - \frac{H_{emit}}{2} + X^2 \tag{B-24}$$

$$|\mathbf{v}_{out}^{lim}| = \sqrt{|\mathbf{g}|}X \tag{B-25}$$

With root X of a given function f which is specific to each case. Once again, Newton's method for root-finding can be employed for evaluating X. Let us start by considering the situation for which the fluid height level at equilibrium is below the emitter center. If $C_d = 1$, then we obtain:

$$f : X \mapsto \sqrt{r - X}\, X^2 - \frac{\sqrt{2} F r_{in}^{lim}}{\pi C_d \sqrt{|\mathbf{g}|}} \tag{B-26}$$

$$f' : X \mapsto -\frac{1}{2} \frac{X^2}{\sqrt{r - X}} + 2\sqrt{r - X}\, X \tag{B-27}$$

Otherwise, we have:

$$f : X \mapsto \sqrt{r - X}\, X^3 + \frac{2\sqrt{C_d} r}{C_d - \sqrt{C_d}} \sqrt{r - X}\, X^2 - \frac{\sqrt{2} F r_{in}^{lim}}{\pi (C_d - \sqrt{C_d}) \sqrt{|\mathbf{g}|}} \tag{B-28}$$

$$f' : X \mapsto -\frac{1}{2} \frac{X^3}{\sqrt{r - X}} + 3\sqrt{r - X}\, X^2 - \frac{\sqrt{C_d} r}{C_d - \sqrt{C_d}} \frac{X^2}{\sqrt{r - X}} + \frac{4\sqrt{C_d} r}{C_d - \sqrt{C_d}} \sqrt{r - X}\, X \tag{B-29}$$

Let us now deal with the situation with the fluid height level above the emitter center when at equilibrium. In the case $C_d = 1$, the function and its derivative are:

$$f : X \mapsto \sqrt{r - X}\, X^2 - 2r\sqrt{r - X}\, X + \sqrt{2} r^2 \sqrt{X} - \frac{\sqrt{2} F r_{in}^{lim}}{\pi C_d \sqrt{|\mathbf{g}|}} \tag{B-30}$$

$$f' : X \mapsto -\frac{1}{2} \frac{X^2}{\sqrt{r - X}} + 2\sqrt{r - X}\, X + r \frac{X}{\sqrt{r - X}} - 2r\sqrt{r - X} + \frac{r^2}{\sqrt{2}} \frac{1}{\sqrt{X}} \tag{B-31}$$

Lastly, if $C_d < 1$, then we have:

$$f : X \mapsto \sqrt{r - X}\, X^3 + \frac{2(2\sqrt{C_d} - C_d) r}{C_d - \sqrt{C_d}} \sqrt{r - X}\, X^2 + \sqrt{2} r^2 X^{\frac{3}{2}} \tag{B-32}$$

$$- \frac{4\sqrt{C_d} r^2}{C_d - \sqrt{C_d}} \sqrt{r - X}\, X + \frac{2\sqrt{2}\sqrt{C_d} r^3}{C_d - \sqrt{C_d}} \sqrt{X} - \frac{2\sqrt{2} r F r_{in}^{lim}}{\pi (C_d - \sqrt{C_d}) \sqrt{|\mathbf{g}|}} \tag{B-33}$$

$$\begin{aligned} f' : X \mapsto & -\frac{1}{2} \frac{X^3}{\sqrt{r - X}} + 3\sqrt{r - X}\, X^2 - \frac{(2\sqrt{C_d} - C_d) r}{C_d - \sqrt{C_d}} \frac{X^2}{\sqrt{r - X}} + \frac{4(2\sqrt{C_d} - C_d) r}{C_d - \sqrt{C_d}} \sqrt{r - X}\, X \\ & + \frac{2\sqrt{C_d} r^2}{C_d - \sqrt{C_d}} \frac{X}{\sqrt{r - X}} + \frac{3r}{\sqrt{2}} \sqrt{X} - \frac{4\sqrt{C_d} r^2}{C_d - \sqrt{C_d}} \sqrt{r - X} + \frac{\sqrt{2}\sqrt{C_d} r^3}{C_d - \sqrt{C_d}} \frac{1}{\sqrt{X}} \end{aligned} \tag{B-34}$$

Appendix C

Lessons Learned From 3-D Simulations

Appendix C
Lessons Learned From 3-D Simulations

With the investigation of the simulation-based dynamic flooding analysis that involves several different fields, including 3-D plant modeling, 3-D simulations, software development, and PRA analysis, there were multiple lessons we have learned from the process, which are presented in this section to benefit the research and the applications with this approach in the future.

C.1 3-D Modeling

Many different 3-D modeling software packages exist, and each uses its own method for modeling and converting into other formats. The Neutrino simulation code can import several different 3-D file types such as OBJ, STL, 3DS, and BLEND, but the ways how different applications save those formats could cause problems in the simulation. Furthermore, the process on which how polygons are determined in 3-D software could also cause other issues. Preprocessing and "clean up" of these types of models is important.

C.1.1 Normals

A normal is the direction a polygon is facing in the model. Normal in a 3-D model must be correct for the simulation calculations to work correctly. There are several ways a normal can be stored and interpreted depending on the 3-D file format. It was discovered that the OBJ 3-D file format did not work well with saving and interpreting normals between different applications. Figure C-1 and Figure C-2 show the difference in models with "good" versus "bad" normals, respectively. The sharp lines and consistent shadings in Figure C-1 are indications of correct normals. The blurred edges and variation in shading in Figure C-2 are indications of incorrect normals. The STL 3-D file format seems doing better for storing normals and being more compatible between different applications.

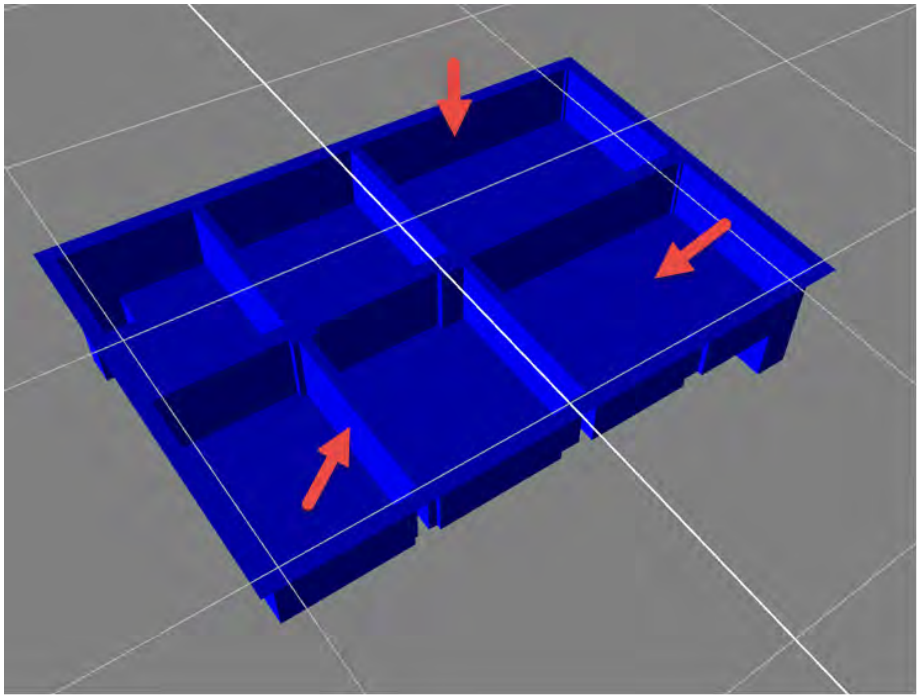

Figure C-1. 3-D Model with proper normal assigned.

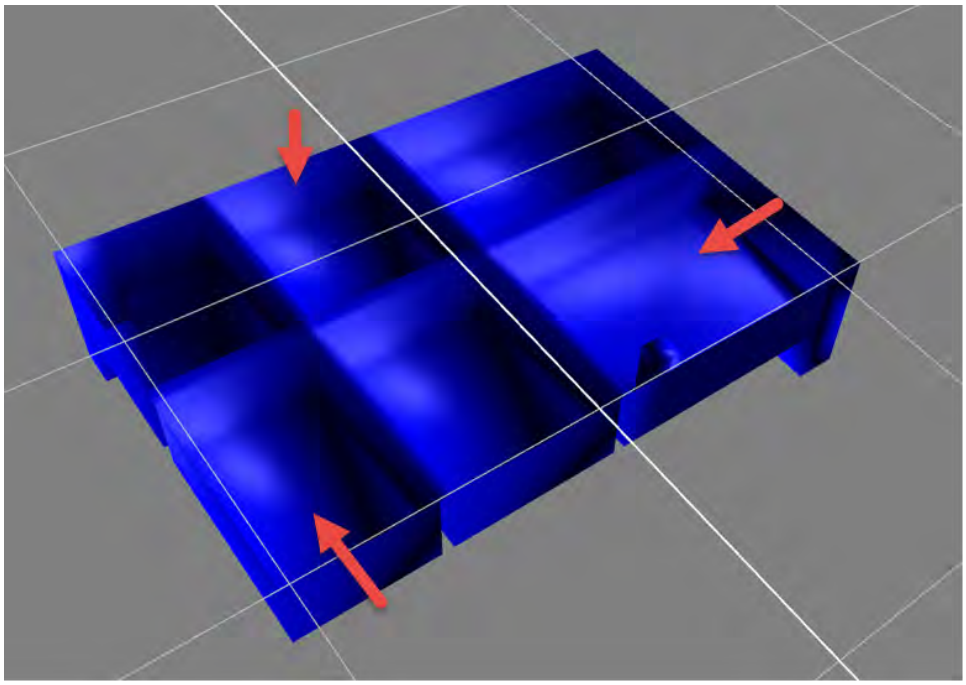

Figure C-2. 3-D Model with incorrectly interpreted normal.

C.1.2 Overlapping Faces

Some 3-D software packages tend to produce overlapping faces when saving to non-native formats. Overlapping faces are where two different polygons cover some of the same area on a plane (Figure C-3). This causes problems for the simulation because it creates overlapping particles when constructing the rigid body shell.

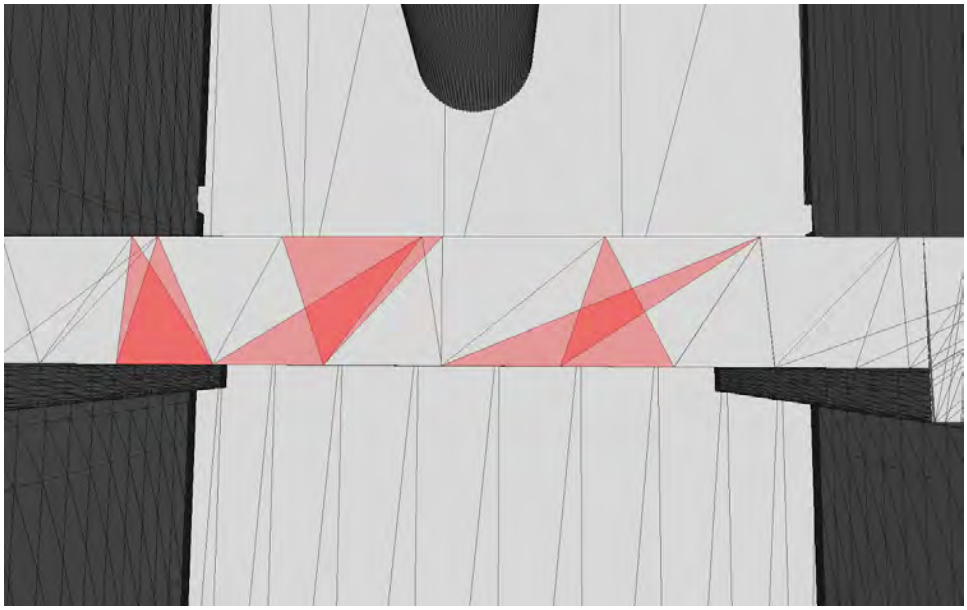

Figure C-3 Example of a 3-D model with overlapping faces.

C.1.3 Extreme Acute Polygons

Different applications use different methods to generate polygons for a 3-D model. Some of those methods take a vertex and construct a polygon to all the surrounding vertices in a circular pattern. If the modeler does not take steps to prevent it, an overabundance of polygons can be created and many of them forming very acute angles. In addition, some methods tend to use a single vertex for a large number of polygons (Figure C-4). The simulation code uses the polygons to construct a rigid shell of particles for boundary conditions. Very thin polygons or a single vertex used for many polygons, causes overlapping particles in the rigid body shell. Multiple overlapping particles can cause the simulation math to return incorrect results, causing particles to "push through" the containment boundary. Adjustments to the simulation methods are being made to fix the problem. In either case, appropriate modeling methods should be used to minimize this condition.

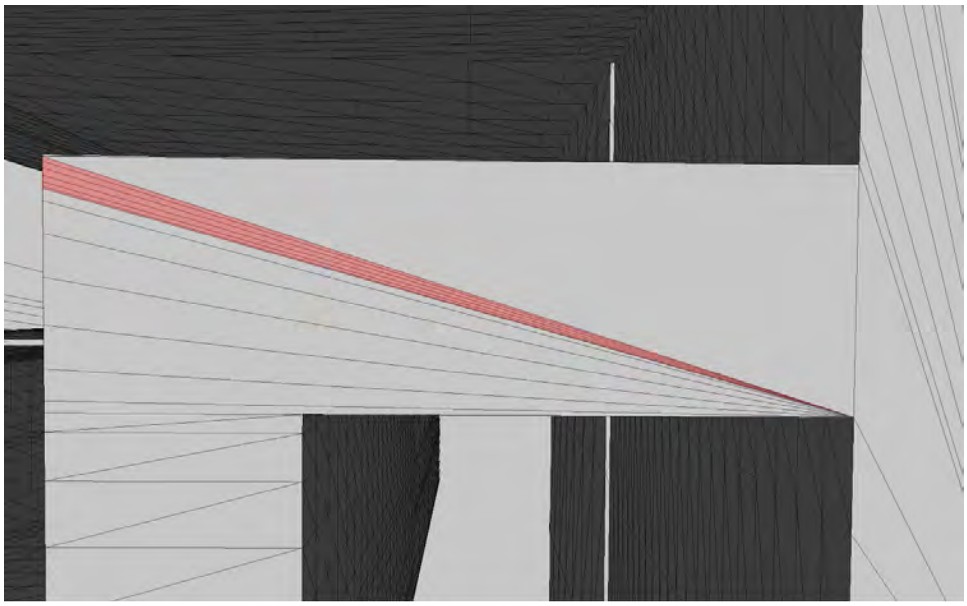

Figure C-4. Example of acute polygons and overuse of single vertex.

C.2 Simulation Issues

In developing and running a flooding model, several issues needed to be addressed. To maximize the number of simulations in minimal time, optimization methods needed to be added. Several tools to minimize the number of particles needed for the simulations were developed.

C.2.1 Torricelli Emitter

As described in Section 1.1, the rainfall and subsequent flow into an area can be mathematically computed over time. Developing a Torricelli emitter allowed us to eliminate any particles for the rain accumulation on the Building C and the connecting tunnel allowing the simulation to only produce particles inside the Auxiliary Building (Figure C-5).

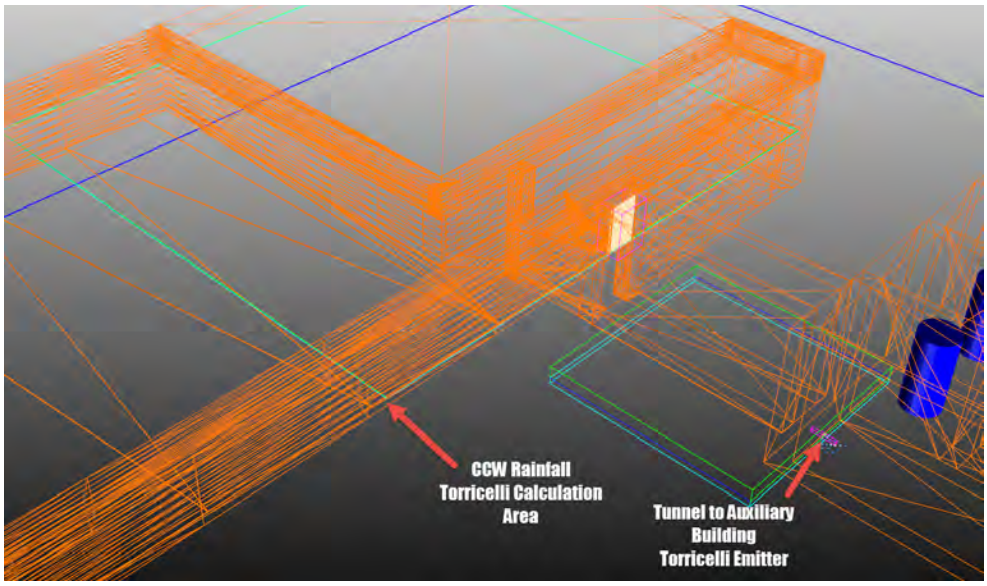

Figure C-5. Torricelli emitters used to calculate the flow into the Auxiliary Building from the rain fall.

C.2.2 Particle Killer-Emitter Pair

Simulation runtime can be reduced by using larger particles. However, if large particles are used, they may not be able to flow through the openings smaller than the particle size. To overcome this and make it possible to mimic piped drains, a particle killer-emitter pairing was used. This pairing removes particles from the "killer" area (a drain or a hole) and transports them to corresponding "emitter" area (for example, a sump or the lower-level side of the hole). The rate of flow (killing and emitting) is determined by the properties of the particles near the drain and the configuration of the drain. Drains from Underground Level 1 of the Auxiliary Building to the sumps of Underground Level 2 were modeled using this method (Figure C-6).

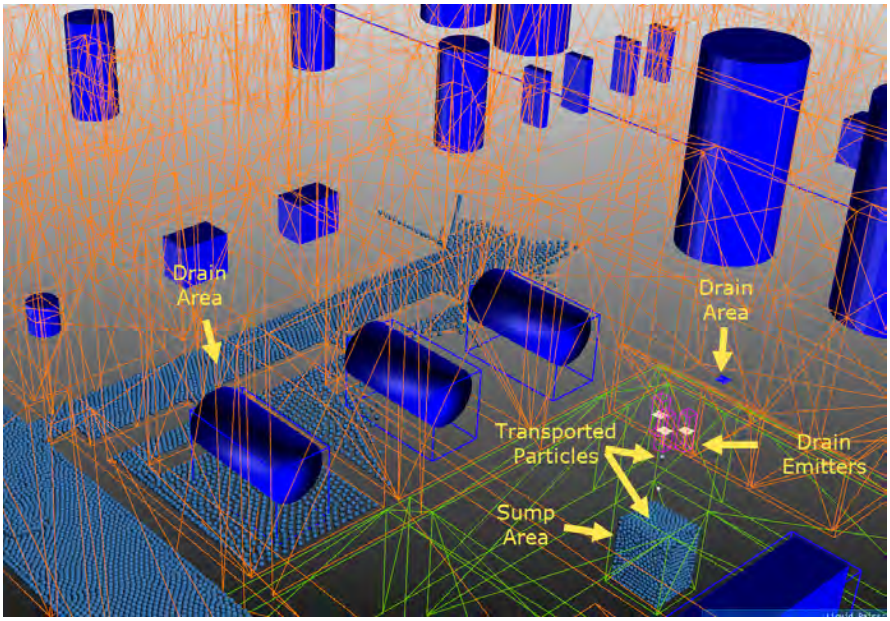

Figure C-6. Drains in the Auxiliary Building model.